NASA Contractor Report 4293

Optical Properties Monitor

Experiment Definition Phase

Donald R. Wilkes, Jean M. Bennett,
Leigh L. Hummer, Russell A. Chipman,
James B. Hadaway, and Larry Pezzaniti

19980819 166

NASA

U2371

NASA Contractor Report 4293

Optical Properties Monitor

Experiment Definition Phase

Donald R. Wilkes, Jean M. Bennett,
Leigh L. Hummer, Russell A. Chipman,
James B. Hadaway, and Larry Pezzaniti
John M. Cockerham & Associates, Inc.
Huntsville, Alabama

NASA

National Aeronautics and
Space Administration

Office of Management

Scientific and Technical
Information Division

1990

TABLE OF CONTENTS

LIST OF EXHIBITS

OPTICAL PROPERTIES MONITOR
LIST OF ACRONYMS

A-D   - Analog to Digital
ADP   - Acceptance Data Package
AO   - Atomic Oxygen
APAE   - Attached Payload Accommodation Experiment
ARS   - Angle-Resolved Scattering
A/RR   - Acceptance / Readiness Review
ASTM   - American Society of Testing and Materials
ATM   - Apollo Telescope Mount
CAD   - Computer Aided Design
CAO   - Center for Applied Optics
CAP   - Complex Autonomous Payload
CDR   - Critical Design Review
CERL   - Corps of Engineers Research Laboratory
CG   - Center of Gravity
CIR   - Cargo Integration Review
CMOS   - Complementary Metal-Oxide Semiconductor
COQ   - Certificate of Qualification
DACS   - Data Acquisition and Control System
DC   - Direct Current
DOD   - Department Of Defense
DTL   - Diode-Transistor Logic
ELV   - Expendable Launch Vehicle
EMI   - Electromagnetic Interference
EOIM   - Evaluation of Oxygen Interactions with Materials Experiment
FAT   - First Article Test
FEU   - Flight Electronics Unit
FOR   - Flight Operations Review
FRR   - Flight Readiness Review
GAS   - Get Away Special
GSE   - Ground Support Equipment
GSFC   - Goddard Space Flight Center
HHG   - Hitchhiker G
HHM   - Hitchhiker M

HST   – Hubble Space Telescope
ICD   – Interface Control Document
IECM   – Induced Environment Contamination Monitor
IITRI   – Illinois Institute of Technology Research Institute
IR   – Infrared
JMCA   – John M. Cockerham & Associates, Inc.
JPL   – Jet Propulsion Laboratory
JSC   – Johnson Space Center
KSC   – Kennedy Space Center
LaRC   – Langley Research Center
LDEF   – Long Duration Exposure Facility
LEO   – Low Earth Orbit
LeRC   – Lewis Research Center
LM1P   – Long Module – 1 Pallet
M&P   – Materials and Processes
MOSFET – Metal-Oxide Semiconductor Field Effect Transistor
MSFC   – Marshall Space Flight Center
MTA   – Multiple Time Averaging
NASA   – National Aeronautics and Space Administration
NHB   – NASA Handbook
NWC   – Naval Weapons Center
OAST   – Office of Aeronautics and Space Technology
OPM   – Optical Properties Monitor
OSR   – Optical Solar Reflector
PDR   – Preliminary Design Review
PIP   – Payload Integration Plan
PROM   – Programmable Read Only Memory
PRR   – Payload Readiness Review
PRT   – Platinum Resistance Thermometer
PSD   – Phase Sensitive Detector
RAM   – Random Access Memory
RE   – Reaction Efficiency
RF   – Radio Frequency
rms   – Root Mean Square
RMS   – Remote Manipulator System
RSS   – Root Sum Square

SARR   – Small and Rapid Response
SDC   – Strategic Defense Command
SDI   – Strategic Defense Initiative
SDP   – Safety Data Package
SFP   – Single Failure Point
SPOC   – Special Payload Opportunity Carrier
SRB   – Solid Rocket Booster
SRR   – Systems Requirements Review
STS   – Space Transportation System
TBD   – To Be Determined
TCSE   – Thermal Control Surfaces Experiment
TDP   – Technical Data Package
TIS   – Total Integrated Scatter
TQCM   – Temperature-controlled Quartz Crystal Microbalance
TTL   – Transistor-Transistor Logic
UAH   – University of Alabama in Huntsville
UV   – Ultraviolet
VCM   – Vacuum Condensable Material
VEM   – Viscoelastic Materials
VUV   – Vacuum Ultraviolet
XUV   – Extreme Ultraviolet

1.0 INTRODUCTION

The Optical Properties Monitor (OPM) Experiment was selected for definition as part of the National Aeronautics and Space Administration (NASA) and the Office of Aeronautics and Space Technology (OAST) In-Space Technology Experiment Program. The OPM Experiment is one of 36 experiments selected for the definition phase. The Definition Phase was a joint effort between John M. Cockerham & Associates (JMCA) and the University of Alabama (UAH) Center for Applied Optics (CAO) under contract NAS8-37755, and was administered through the Materials and Processes (M&P) Laboratory; Science and Engineering Directorate, George C. Marshall Space Flight Center (MSFC). James M. Zwiener of the M&P Laboratory was the technical monitor and provided valuable assistance and guidance in the performance of this effort. Roger C. Linton, Palmer Peters, Robert DeHaye and Billy H. Nerren provided additional assistance in instrument conception and sample preparation.

This Final Report describes the results of the OPM Definition Phase. In Section 2, the problem addressed by the OPM and the impact of the problem are discussed. In Sections 3, 4, and 5, the objectives, the experimental approach, and flight opportunities are described. A detailed discussion of the design of the OPM hardware systems and capabilities are provided in Section 6. Section 7 describes the application of the OPM hardware capabilities to the OPM Experiment mission. An Implementation Plan is presented in Section 8 for the Development Phase where the OPM hardware is built, tested, and flown on its initial mission.

2.0 BACKGROUND

It has been demonstrated that the natural and induced space environment can cause optical, mechanical and thermal damage to exposed surfaces.[1-13] This materials damage can seriously affect the performance of critical spacecraft systems, including solar arrays, optical instruments, and thermal control systems. The space environment is a complex combination of mostly independent constituents, including atomic oxygen, particulate radiation (electrons, protons, etc.), thermal vacuum, micrometeoroid/debris bombardment and contamination (see Exhibit 1). These constituents vary in composition and quantity with orbital parameters, solar activity, season, and time of day. The complex nature of the space environment makes it difficult—if not impossible—to simulate an individual constituent accurately and certainly not the combined environment. The synergistic effects of the combined environment also add to the difficulty in simulating the environment.

Atomic Oxygen (AO) effects are currently the major concern. These effects can damage not only the optical properties, but the mechanical integrity of materials.[5,6] This is particularly important for flexible solar arrays, such as the Hubble Space Telescope (HST) solar array, where long-term AO exposure of unprotected Kapton used as the flexible substrate could cause physical failure of the array.

The damaging effects of the space environment are critically important for spacecraft thermal control. The increasing size and complexity of spacecraft and the longer-duration mission requirements increase the difficulty of maintaining spacecraft thermal control. Even in an era of highly complex active thermal control systems utilizing fluid loops and heat pipes, the ultimate regulation of absorbed solar energy and radiated thermal energy remains dependent on the optical and thermal properties of thermal control surfaces.

The stability of materials in the space environment is not well understood. To compensate for this uncertainty, spacecraft and instrument designers frequently overdesign systems at greater cost and weight—sometimes with reduced performance. For the large, long-duration missions of the future (such as the space station) overdesign of systems is extremely undesirable[7], and in some cases, impossible.

The impact of materials degradation in the space environment extends across the aerospace community, including NASA, the Department of Defense (DOD), and

2

Sun

Particulate Radiation
$(e^-, p^+, \propto, \beta, \gamma)$

Direct
solar
(including UV radiation)

Residual Atmosphere
$(0, O_2, N, N_2, H, ...)$

Spacecraft Induced Environment
(molecular, particles)

Space Debris
(micrometeoroid, spacecraft)

Spacecraft
emission
ε

Earth
Albedo

Earth
emitted

Earth
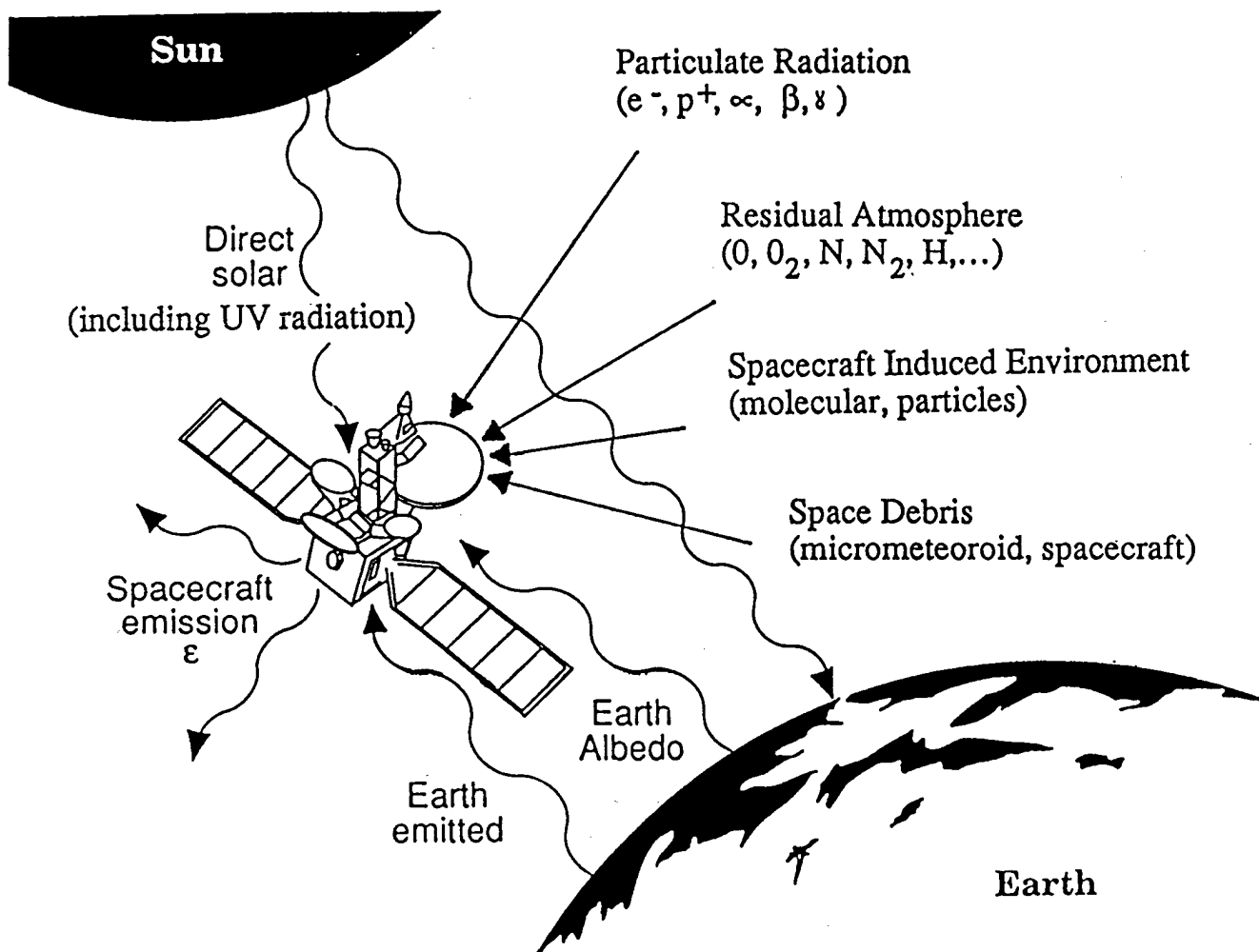
EXHIBIT 1 - The Spacecraft Environment

the Strategic Defense Initiative (SDI). The 20-year lifetime requirements for Space Station Freedom and its various payloads offer many additional challenges for materials performance in space. The SDI missions will see similar problems, but will have additional problems with survivability during an armed conflict.

Extensive effort has gone into developing space stable materials and testing their stability in different environments. Because we cannot accurately simulate the space environment, in-space experiments are required to determine the stability of materials and validate ground test methods and procedures. The measurement of optical properties in-situ is particularly important because some environmental damage is bleachable when the test material is returned to the laboratory environment.[1]

3

Much of the early data on the performance of materials in space were derived from operational data where the materials property could be calculated or inferred. This was particularly true where systems failed or their performance degraded, and the degradation could be attributed to material changes. A limited number of experiments have been performed in space to measure the effects of the environment on optical and thermal control materials.[14] Most previous flight tests used calorimetric methods to calculate solar absorptance and total emittance of thermal control surfaces from temperature data.[8-12] Other experiments exposed passive samples to the space environment and returned them to the laboratory to determine the effects of the exposure. The Induced Environment Contamination Monitor (IECM) measured in-situ transmittance and scatter at a single wavelength in the ultra-violet to assess the induced environment in the Shuttle cargo bay.[6,13] Of these past experiments, only the Thermal Control Surfaces Experiment (TCSE) on the Long Duration Exposure Facility (LDEF) offered a comprehensive materials test program of detailed in-situ optical measurements combined with pre- and post-flight analyses.[15] The LDEF was placed in earth orbit in April, 1984, by the Shuttle. The LDEF with the TCSE onboard was originally scheduled to remain in space for nine months to one year. However, due to Shuttle schedule conflicts and the Solid Rocket Booster (SRB) redesign, it is not scheduled for retrieval until late 1989. Even if the LDEF is recovered, there is some concern whether the data stored on the TCSE flight recorder have survived the extended space exposure.

The OPM experiment is designed to provide the investigative plan and flight instrumentation to perform needed in-space materials testing. More than one OPM mission in different orbits and for different exposure periods will be required to address the problem adequately.

Longer duration and increasingly complex missions will require improved materials and better characterization of the performance of these materials. Improved materials and better performance characterization will lead to more cost effective space systems designs with lower weight and greater performance.

An understanding of materials exposure effects and the damage mechanisms will lead to more stable materials and coatings and more accurate ground simulation testing.

3.0 OPM EXPERIMENT OBJECTIVES

The primary objectives of the OPM Experiment are to study the natural and induced effects of the space environment on optical, thermal control, and other materials, and to develop a multifunction, reusable flight instrument to measure these effects. Specific objectives are:

o **To determine the effects of the space environment on materials** - The effects of the space environment on materials are not well understood. This experiment will provide detailed in-situ optical measurements of these effects to enhance the understanding of the damage mechanisms caused by the synergistic constituents of the space environment. This understanding will enhance the efforts to develop space stable materials.

o **To provide flight testing of critical spacecraft and optical materials** - The constituents of the space environment—and certainly the combined environment—cannot be simulated exactly. For this reason, the only sure test of materials—particularly newly developed materials—is to test the material in space, eliminating the uncertainties of simulation testing.

The materials to be tested include, but are not limited to:

Thermal control surfaces

- sprayable coatings
- conversion coatings (anodize, alodine, etc.)
- Optical Solar Reflectors (OSR)
- second surface teflon mirrors

Solar power materials

- flexible substrates
- protective coatings
- interconnects
- coverglasses
- solar dynamic mirrors

Optical materials and coatings

- mirrors
- windows
- gratings
- filters
- lenses

o **To validate ground test facilities and techniques** - The current generation of laboratory space simulation facilities is extremely complex and well-designed. However, because of

the inability to simulate the space environment exactly, these facilities provide only relative performance of test materials in these limited conditions. Past flight measurements (although limited in scope) show significant disagreement between flight and laboratory data. An important objective of this experiment is to provide a "calibration" for ground test facilities and techniques with in-space measurements of the same properties measured in ground tests.

o **To develop a multifunction, reusable flight instrument for optical studies** - There is a need to test many different materials in space and under different conditions of environment, orientation, temperature, duration, etc. More than one space experiment will be required to satisfy the many requirements. The OPM flight instrument will be designed to be reflown with minimum refurbishment and will allow easy reprogramming to meet varied mission requirements. The qualified OPM instrument can be repackaged—or the proven design used—for a Space Station module or free flyer spacecraft at a lower cost than a new design.

4.0 EXPERIMENTAL APPROACH

To accomplish the experimental objectives, the OPM will expose selected materials to the space environment and measure the effects with in-space optical measurements. The in-space measurements will be augmented with extensive pre- and post-flight sample measurements to determine other optical, mechanical, electrical, chemical or surface effects of space exposure. Environmental monitors will provide the amount and time history of the sample exposure to solar irradiation, atomic oxygen and molecular contamination.

The materials to be studied fall into three major classes: optical materials and coatings, thermal control surfaces, and solar power materials. While all of these materials may degrade when exposed to the space environment, the specific properties of concern range widely including optical, thermal, mechanical and electrical. Sections 4.1 though 4.3 discuss these classes of materials, the expected environmental effects, and the measurements needed to study these materials.

The environmental monitors are described in Section 4.4 followed by a summary of all of the OPM measurement capabilities in Section 4.5. The sample selection process and a list of candidate flight sample materials are presented in Section 4.6.

4.1 Optical Materials

Optical payloads are increasing in size, complexity and mission duration. Optical materials and coatings are required to maintain stable properties in the spacecraft environment. This environment can be considered in two components—the spacecraft induced (or contamination) environment and the natural environment. The contamination environment of concern consists of molecular and particle constituents. The molecular contamination from outgassing and other spacecraft effluents can cause reduced reflectance and transmission due to increased surface absorption. The contaminant layer can also cause increased surface scattering, which, for some optical applications, is more important than the degradation of optical properties. On the other hand, particle contamination (dust) causes mainly increased light scattering at the surface. The area coverage of the particles is normally insufficient to affect transmittance or reflectance.

7

The natural environment, including atomic oxygen, solar Ultra Violet (UV), thermal vacuum and particulate radiation, can also cause degradation of optical properties and increased scatter due to physical changes at the surface or in the bulk of materials.

The effects of the natural environment on optically black coatings are a good example of the diversity of these effects. AO exposure can cause an undesirable increase in the reflectance of black coatings such as Chemglaze Z306 and Z302 while also causing an equally undesirable decrease in the specularity (glossiness) of the Z302 glossy black.[5]

Properties the OPM needs to measure are reflectance, transmission and scatter. All these materials properties must be well understood to design and build suitable optical systems and to develop new optical materials. The scatter measurements, as will be discussed, are very sensitive to surface changes. They can provide valuable data on the cause of any change and indicate the on-set of environmental damage.

With the wide range of optical space experiments to be performed, the measurement of material optical properties is desirable across the entire optical spectrum--from the extreme ultraviolet (XUV) through longwave infrared (IR). However, for a small multi-purpose optical studies experiment, this is clearly not feasible. For example, longwave IR measurements would require cooled detectors with the appropriate dewar systems; and scanning spectrometers for the XUV are generally large, relatively heavy units.

The range of spectral measurements for the OPM must be limited to ranges of specific interest and where the instrumentation can be reasonably packaged in size and accommodated easily on standard payload carriers. The wavelength range from the near UV (250 nm) to the near IR (2500 nm) is a range of much interest not only for thermal control surfaces (see Section 4.2) but for many optical instruments. This region covers a significant portion of stellar, solar, and earth sciences studies, as well as many of the operational instruments and sensors for DOD and SDI applications.

There is also significant interest in the Vacuum Ultra Violet (VUV) range from 110 to 200 nm. The Hubble Space Telescope wavelength range extends down to 115 nm. Upper atmospheric and solar studies extend into this range. The importance of this spectral range is compounded because of the observed sensitivity of the optics and coatings to environmental damage. High

8

performance VUV coatings of osmium have completely eroded away due to AO exposure[5,6]. The MSFC M&P Laboratory routinely uses VUV measurements of test articles or witness samples for contamination monitoring.

In the laboratory there are qualitative and quantitative instruments to measure the properties and condition of optical materials and coatings. The basic properties of transmission and reflectance are easily and routinely measured with spectrometers available commercially. Flight versions of these laboratory instruments can be built for the desired spectral range. The TCSE integrating sphere reflectometer proved that a small flight instrument can provide comparable performance to the laboratory version for the 250 to 2500 nm spectral range.

Instruments for the VUV spectral range can also be accommodated in a relatively small flight package. The compact Optical Effects Module on the IECM provided valuable data on the effects of environmental exposure on optics and coatings.[13]

The reasons for any changes in these properties and the surface scatter are not determined so easily. One of the most sensitive laboratory instruments for detecting changes on optical surfaces is the Nomarski microscope.[16,17] This microscope is sensitive to surface structure and defects on surfaces, particularly high-reflecting ones like optical mirrors. Dust, scratches, polishing marks, fingerprints, diamond turning marks, and other surface imperfections can be seen easily. The microscope is particularly useful for observing contamination effects, such as a liquid residue from a solvent (e.g.) acetone on a surface, dried liquid droplets from a vapor degreaser, scratches from cleaning with an abrasive cloth, or a water residue covering a dirt or grease spot[19]. The key to the usefulness of the Nomarski microscope is skilled operators and observers who can interpret what they see in the microscope correctly.

In a surface characterization laboratory, there are other instruments to quantify the effects that are observed visually in the Nomarski microscope. These include optical and mechanical profilers that can measure the actual topography of the surface[18,19] and scatter-measuring instruments to show the effect of the surface topography on light scattered from the surface.[18] For the scatter-measuring instruments, a theory is needed that can interpret the

9

scattered light measurements and relate them to statistical properties of the surfaces. Theories are available that work reasonably well under some conditions.[18]

With a mechanical surface profiler and a Nomarski microscope, it is possible to document changes quantitatively in surface topography. No theories are needed, and excellent statistics for the surface topography can be obtained.[18] Unfortunately, the mechanical surface profile is far too sensitive for the space environment and also requires a skilled operator.

There are two types of scatter measurements—Angle Resolved Scatter (ARS) and Total Integrated Scatter (TIS). ARS instruments measure the scatter from a surface as a function of angle; TIS instruments measure the scatter integrated over all angles. A TIS instrument is simpler to build and operate than an instrument to measure ARS. A TIS instrument can be made small and rugged without sacrificing sensitivity, and can be made to operate remotely without a skilled operator. A TIS instrument is certainly a viable candidate for a flight surface characterization instrument.

The theory relating TIS to surface topography is simple when the topography consists of microirregularities remaining from the polishing process. This should also be true for surface roughness caused by AO erosion or molecular contamination. In contrast, the theory relating ARS to surface topography is much more complicated. Although it gives more information about the surface spatial wavelengths doing the scattering and other surface statistical information, there are some predictions of the theory that do not agree with experimental measurements.[18] The drawback to the TIS and ARS theories is that they do not consider scattering from isolated surface features, such as dust, scratches, tiny pits or material defects which have dimensions comparable to—or larger than—the wavelength of the measurement.

The interpretation of the scattering measurement data is a potential problem for a TIS flight instrument. A solution is offered by measuring the TIS at two wavelengths, as explained in the following discussion of TIS theory.

The theory of TIS that relates microirregularity scattering to the surface roughness is[18]

$$TIS = \frac{R_d}{R_0} = \frac{(R_0 - R)}{R_0} = 1 - e^{-(4\pi\delta/\lambda)^2} \approx (4\pi\delta/\lambda)^2 . \tag{1}$$

In this equation, R_d is the diffuse reflectance (scattering), R_0 is the total reflectance (specular reflectance plus scattering), R is the specular reflectance, δ is the root-mean-square (rms) surface roughness, and λ is the wavelength of light illuminating the surface. This equation holds when the surface heights, (i.e., the surface roughness δ) are small compared to the wavelength. Note that the TIS is inversely proportional to the square of the wavelength. If a surface is roughened uniformly under exposure to atomic oxygen or molecular contamination, the effect would be to increase the surface roughness and increase the scattering at all wavelengths in proportion to the inverse square of the wavelength.

In contrast, if isolated particles were present on a surface, they would have a different effect on the scattering. The effect would depend on the number and sizes of the particles, their shapes, optical constants, the polarization of the light beam, and other factors. Thus, it is not possible to predict the wavelength dependence of light scattered by particles because the mathematics are too complicated and too little information is known about the actual particles. However, it is possible to separate "dust effects" from microroughening effects by choosing two suitable wavelengths for the TIS measurements. It has been shown previously that there is a resonance effect for TIS at a wavelength close to the average size of scattering particles.[19] Exhibit 2 shows the results of a TIS measurement on an aluminized polished flint sample. The scattering and wavelength are both plotted on log scales, so that the theory curve from Eq. (1) is a straight line with a slope of -2. The measured data points (circles) follow the predictions of the scattering theory (for microirregularities) very well between the shortest wavelength measured and 1.15 micrometers. At longer wavelengths in the infrared, the scattering remains relatively constant and does not decrease according to the theoretical predictions. In this region, particulate scattering dominates. The square data points represent the difference between the average scattering level and minimum scattering level for the approximately 20 data points taken at each wavelength. The square data points are believed related to scattering from dust particles on the surface. Note that this scattering is relatively independent of wavelength except at wavelengths close to the size of the particles, where a resonance occurs. The particles were approximately 1 micrometer in diameter (as determined independently by multiple-beam interferometry) and the resonance in the scattering occurs in the dashed curve at 1.15 micrometers.

11
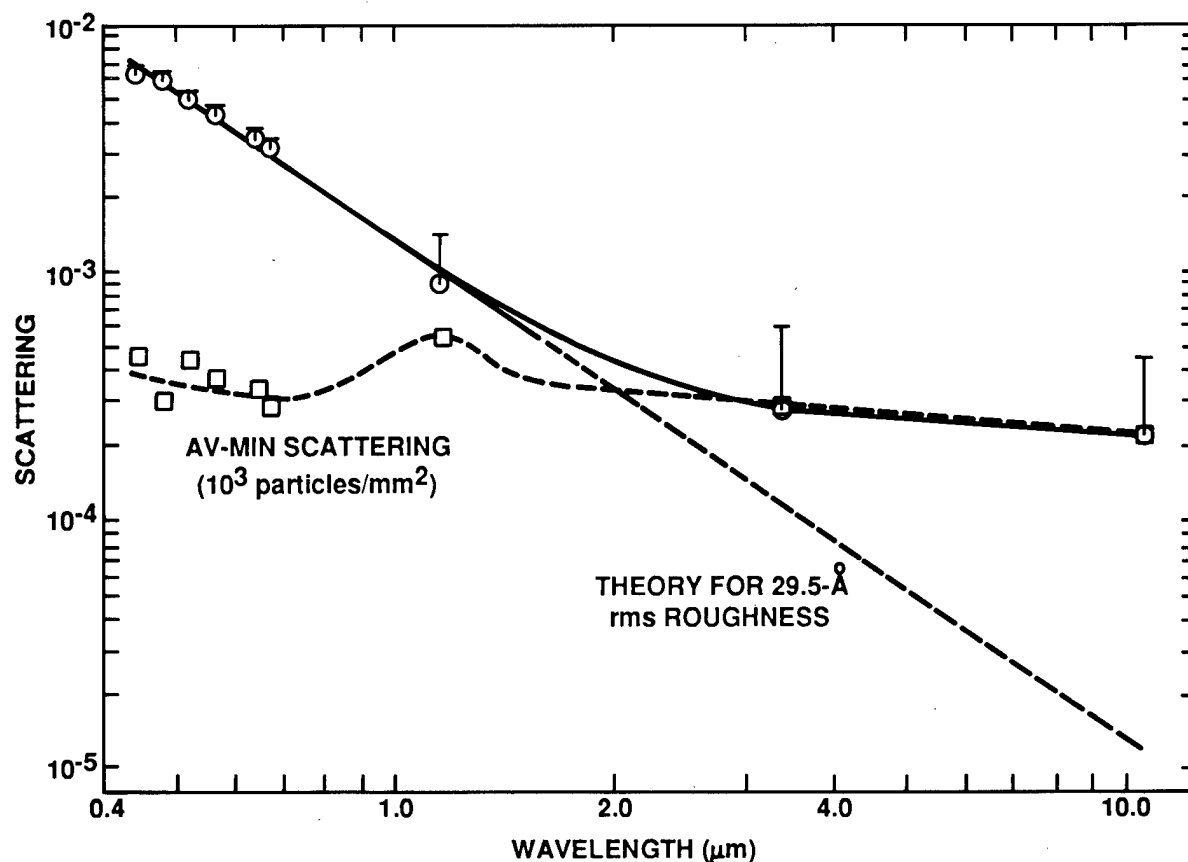
EXHIBIT 2 – Scattering from Aluminized Polished Dense Flint Glass

Based on the results of this experiment, we have chosen to use an infrared wavelength around 1 micrometer and a convenient visible wavelength to differentiate between scattering from dust particles and from overall roughening of the surface by atomic oxygen or other causes. Experiments are described in Section 6.2.4.5 that verify the predicted effects of dust particles on the measured TIS. A breadboard of a flight TIS instrument has been built under this effort to verify the suitability for inclusion in the OPM flight instrument package. Details of the instrument, and experiments that have been performed, are described Section 6.2.

4.2 Thermal Control Surfaces

Spacecraft thermal control is dependent on the optical and thermal properties of external surfaces. The primary engineering properties of interest are solar absorptance (α_s) and total emittance (ε_t).

The solar absorptance of a surface is the portion (or percent) of the direct solar irradiance that the surface will absorb. Typically, degradation of the solar absorptance has been the major environmental problem for thermal control surfaces.[7,20]

Solar absorptance is not a basic optical property, but is normally calculated from the measured basic property of spectral total hemispherical reflectance.[21] Solar absorptance is defined as:

$$\alpha_s = \frac{1}{E_s} \int\limits_0^\infty \alpha\, S_s(\lambda)\, d\lambda \simeq \frac{1}{E_s} \sum_{\lambda=0}^\infty \alpha\, S_s(\lambda)\Delta\lambda$$

where

α_s = total solar absorptance

α = spectral absorptance

$S_s(\lambda)$ = spectral solar energy distribution

E_s = total solar energy

λ = wavelength

Spectral absorptance (α) for the solar region of the spectrum is most easily determined[21] from the measured spectral total hemispherical reflectance (ρ), where for opaque samples:

$$\alpha = 1-\rho$$

Therefore

$$\alpha = \sum_{\lambda=0}^\infty (1-\rho)\, S_s(\lambda)\, \Delta\lambda$$

Because over 97%[22] of the solar energy is in the spectral range from 250 to 2500 nm, this reduces to

$$\alpha = \sum_{\lambda=250}^{2500} (1-\rho)\, S_s(\lambda)\, \Delta\lambda$$

If the total hemispherical reflectance is measured from 250 to 2500 nm, then α_S can be calculated.

Total hemispherical reflectance in the laboratory is measured using an integrating sphere reflectometer. This is the primary measurement used in all ground test chambers for materials development and space simulation testing.

While the measurement of spectral reflectance of test samples is important for determination of solar absorptance for engineering design and analysis, these measurements are even more important for understanding the damage mechanism of environmental exposure. Change of reflectance in one region of the spectrum and/or lack of change in another region can offer important evidence toward the cause of the damage and lead to a potential material improvement.

The total emittance (ε_t) of materials is the relative efficiency of the energy emitted by the material to that emitted by an ideal black body at the same temperature. The total emittance of spacecraft surfaces and the temperature of the surface control the amount of energy radiated to space. This radiative transfer is the only way to dissipate excess heat from a spacecraft and maintain thermal control.

Laboratory tests and short-term space exposure tests indicate that total emittance is not as sensitive to environmental effects as solar absorptance. Atomic oxygen, contamination and long-term UV exposure can, however, cause degradation of this critical property. Due to its importance, total emittance should be measured as part of a comprehensive test program.

4.3 Solar Power and Other Materials

Solar power materials are another class of materials that are susceptible to damage by the space environment. These materials include those used on solar cell arrays and solar concentrator power systems. Current solar array designs utilize polymetric materials, such as Kapton, as a flexible substrate for mounting the solar cells. The cells are interconnected with current carrying materials, such as silver. Both Kapton and silver have been shown to be particularly susceptible to damage by the atomic oxygen present in low earth orbit.[5,6] The optical coverglass over the solar cells can also be degraded by the exposure to the space environment.

The stability of solar dynamic mirrors used in solar concentrator power systems is also a concern for spacecraft designers. Even small changes in these

14

mirrors or coatings can result in significant degradation of power system performance.

Protection for these critical materials can be provided by protective overcoatings. These overcoatings, however, can themselves be susceptible to environmental damage, including cracking and pinhole formation.

The optical measurements used to study the space environmental effects on optical and thermal control materials can also be utilized to study solar power materials. Because over 97%[22] of the solar energy is in the spectral range from 250 to 2500 nm, the in-space measurement of material reflectance over this range is a direct measure of performance for many materials and coatings. The TIS measurements discussed in Section 4.1 offer a very sensitive method to characterize the surfaces of critical materials and to be able to study the early stages of surface damage.

The range of spacecraft materials that can be damaged by the space environment is not limited to those that have been discussed in this report. As space environment exposure times increase, more problems with materials performance will be found. The optical instruments proposed for the OPM will provide an excellent set of diagnostic tools to study these materials even, in some cases, where the critical damage is not optical.

4.4 Environmental Monitors

As discussed in Section 2.0, the space environment is a complex combination of constituents. To evaluate the effects of this environment on materials and to permit application of these results, the rate and total dose of the exposure must be known. Some of these constituents are well-defined for this application and need not be measured (e.g., the vacuum level). However, others should be measured where their makeup is transient or varies with the attitude of the spacecraft. The OPM will monitor three of these environmental constituents— Atomic Oxygen (AO), molecular contamination, and solar and earth irradiance. The AO monitor is a simple design using an exposed carbon film as a sensing element. The resistivity of the film rises as the carbon is eroded away by the AO environment. The molecular contamination monitor is a set of Temperature-Controlled Quartz Crystal Microbalance (TQCM) sensors. TQCM's have been used successfully for this purpose on a number of flights and have performed well.

Sample exposure to solar irradiance, earth albedo and earth IR is monitored using two radiometers. Each radiometer consists of a thermopile detector with optics to provide a field-of-view similar to that of the test samples. One radiometer will have quartz optics providing a bandpass of .2 to 3 micrometers. The second radiometer will have germanium window with a bandpass of 2 to 20 micrometers. Data from the radiometers will be used to determine the actual exposure of the test samples to solar UV. Additionally, the radiometer data are required to evaluate the sample calorimeter data to calculate solar absorptance and total emittance.

4.5 OPM Flight Measurements

To address the materials problems with space exposure, the OPM is designed to be a multipurpose optical properties monitor testbed for performing in-space optical studies. The OPM instruments will measure total hemispherical reflectance, TIS and VUV reflectance and transmission. Flight versions of laboratory instruments will be used to perform in-space measurements. A summary of the OPM measurements is presented below with the detailed design and performance of the instrumentation presented in Section 6.

- o Spectral Total Hemispherical Reflectance
    1. Spectral Range - 0.25 To 2.5 Micrometers
    2. Accuracy - $\pm2\%$
    3. Repeatability - $\pm1\%$
    4. Spectral Resolution - 5% or better

- o Total Integrated Scatter
    1. Wavelengths
        a. 0.532 Micrometers
        b. 1.064 Micrometers
    2. Scatter Collection Angle - 2.5 To 80 Degrees from Specular
    3. Accuracy - $\pm10\%$
    4. Repeatability - $\pm2\%$
    5. Surface rms Measurement Range - 5-500 Å

- o VUV Transmittance/Reflectance
    1. Wavelengths
        a. 0.1216 Micrometers
        b. 0.1606 Micrometers
        c. 0.1700 Micrometers

        d. 0.1800 Micrometers

        e. 0.200 Micrometers

        f. 0.250 Micrometers

    2. Accuracy – $\pm5\%$

    3. Repeatability – $\pm1\%$

o Calorimetric Measurements

    1. Total Emittance

        a. Accuracy – $\pm5\%$

    2. Solar Absorptance

        a. Accuracy – $\pm5\%$

o Environmental Monitors

    1. Molecular Contamination

        a. Temperature-controlled Quartz Crystal Microbalance (TQCM)

           – Sensitivity – 1.6×10^{-9} g/cm^2 Hz at 25 C, 15 MHz

           – Repeatability – 2 Hz at Beat Frequency

        b. Specialized Samples for Post Flight Analysis

    2. Atomic Oxygen Monitor

        a. Sensitivity – 1×10^{16} atoms/cm^2

        b. Resistance Measurement Accuracy – 1%

        c. Fluence Range – 1×10^{18} to 5×10^{20} atoms/cm^2

    3. Irradiance

        a. Direct Solar

           – Measurement Accuracy – 5%

           – Instrument Accuracy – 1%

        b. Earth Albedo

           – Measurement Accuracy – 5%

           – Instrument Accuracy – 1%

        c. Earth IR Emittance

           – Measurement Accuracy – 5%

           – Instrument Accuracy – 1%

4.6 Flight Sample Selection

There are many candidate materials for study by the OPM experiment. The selection of test materials for an OPM mission must be carefully considered to include the materials of the most current interest to the aerospace materials community.

17

When an OPM mission is approved, a sample selection committee, chaired by the OPM Principle Investigator, will be formed with representatives from NASA, DOD, Industry and Universities. This committee will develop the detailed objectives for that mission based on the expected environmental exposure and mission duration. A preliminary sample list will be defined based on these objectives. To assure a wide participation in this process and that all suitable candidate materials are considered, a sample announcement of opportunity will be issued to the materials community. The selection committee will consider all candidate materials and select the materials that provide the most benefit to current and future programs.

Most of the OPM samples will be provided by a researcher or project at little or no cost to the OPM program. The selected samples will be exposed on the OPM mission. Pre- and post-flight measurements will be performed as part of the OPM program. The samples will then be returned to the original researcher for his further evaluation.

A preliminary list of candidate materials for OPM missions was collected from the participants in the OPM design reviews. The following list is certainly not complete but demonstrates the diverse range of test materials to be tested in the space environment. Contributors to this list are NASA/MSFC, NASA/Lewis Research Center (LeRC), NASA/Langley Research Center (LaRC), NASA/Goddard Space Flight Center (GSFC), the Jet Propulsion Laboratory (JPL), the Army Strategic Defense Command (SDC) and the U.S. Army Corps of Engineers Research Laboratory (CERL).

Potential OPM Test Materials

Thermal Control Surfaces

o   IITRI YB-71 zinc orthotitanate white paint
o   IITRI S-13G LO white paint
o   Chemglaze Z302 glossy black paint
o   Chemglaze Z306 flat black paint
o   Pigmented transparent polyimide
o   Metalized transparent polyimide
o   Paints over composite materials with pinholes
o   Sulfuric acid anodize
o   Chromic acid anodize
o   Anodize coatings with pinholes
o   3M 401-C10 black paint
o   Metalized FEP Teflon
o   Titanium Nitrite
o   Aluminum epoxy
o   Aluminum molybdenum
o   A276 white paint

Optical Materials

o   Metallic first surface mirrors
o   Metallic coatings over composite substrates
o   Enhanced low scatter metallic coatings
o   Baffle Materials
    –Textured aluminum
    –Textured beryllium
    –Etched carbon fiber surfaces (some with protective coatings of
        silicon carbide, boron carbide, boron nitrate, boron nitrites, or
        diamond)
    –Etched beryllium film
    –Etched boron film

Protective Coatings

o   RTV-560
o   RTV-615
o   RTV-670
o   RTV-5695
o   RTV-3124
o   OI-650
o   DC1-2577
o   DC1-2755
o   DC1-2775
o   DC6-1104
o   Electrochromic coatings

Solar Power Materials

o Solar dynamic concentrator mirrors
   -zero distortion graphite fiber epoxy composites
   -microsheet glass laminates
   -leveling overcoatings
   -protective thin films
o High emittance radiator materials for the SP100 Power System
o Kapton H, F and other improved versions
o Cell interconnect materials such as silver

Special Materials

o The five materials circulated in the NASA Atomic Oxygen Effects Test
   Program: Kapton HN polyimide, low oxygen content polyethylene, FEP
   Teflon, pyrolytic graphite, and highly oriented pyrolytic graphite.
o Mylar
o Tedlar
o Graphite thermoplastics
o Other thermoplastic composites
o Graphite aluminum
o Graphite magnesium
o Other graphite-metal composites
o Viscoelastic Materials (VEM)
o Carbon-carbon composites

5.0 FLIGHT OPPORTUNITIES

The OPM is a multipurpose reflyable instrument for in-space optical studies serving the broad needs of the aerospace and defense community. To provide this capability, the OPM is designed to fly on multiple payload carriers and in various orbital configurations. A generic mounting design for payload accommodation and a reconfigurable spacecraft electrical interface permit this flexibility.

There are a number of payload carriers capable of supporting an OPM mission, while the limitations imposed by the OPM are few. The payload carriers that can accommodate the OPM experiment and their constraints have been considered.

5.1 OPM Constraints

The only constraint the OPM will place on the spacecraft and payload carrier (other than the power and data utilities) is to provide the desired environmental exposure. This requires that the OPM mounting provide an almost unrestricted view of the space environment for the OPM samples and monitors. This may also restrict the placement of other hardware near the OPM. For a Shuttle mission, the OPM mounting should be in the +Z direction (looking out of the cargo bay).

Providing the required environmental exposure may also necessitate the spacecraft maintain a specific attitude. For example, an OPM mission to study the effects of atomic oxygen would require a spacecraft orientation providing significant exposure of the OPM samples into the RAM direction (orbital velocity vector) where the AO fluence is maximum.

5.2 Payload Carriers

The available payload carriers have been investigated for their suitability to accommodate the OPM experiment. The payload carriers investigated include those for the Shuttle and the Space Station. Exhibit 3 summarizes the payload accommodations available for the OPM experiment. The Shuttle offers short-term (seven-to-ten days) test capability; the Space Station offers long-term (months or years) testing. Unmanned carriers, such as the Expendable Launch Vehicle (ELV), may provide another means to fly the OPM experiment.

21

<u>OPM REQUIREMENTS</u>

Preliminary Dimensions : 36 x 41 x 12 inches $\cong$ 10 ft^3
Preliminary Weight : 170 pounds
Average Power Requirements: < 25 watts
Peak Power Requirement: 200 watts

Payload Carrier	Maximum Power	Maximum Experiment Weight	Area/ Volume	Data Link
SHUTTLE				
• HITCHHIKER G (Large) Plate Mount	1400w*	250 lb	50x60in**	yes
• HITCHHIKER M	1400w* individual	1200 lb 380 lb	112 (4 x 28) x 36 in 28 x 36	yes
• SPACELAB PALLET	1700w	12275 lb	11.37M^2 (32.4M^3)	yes
SPACE STATION				
Small and Rapid Response (SARR) Payload				
• SARR: T/K	≤900w	≤900kg (1980 lb)	<10M^3 (325 ft^3)	yes
• SARR: GEN	≤300w	≤300kg (660 lb)	≤2M^3 (65 ft^3)	yes
• SARR: JEM EF Japanese Experiment Module Exposed Facility***	≤6000w	≤500kg (1100 lb)	≤2M^3 (65 ft^3)	yes

Notes:
* Includes 100w for Avionics package, 28 VDC nominal rating. Power is for dedicated customer - prorated for multiple customer payloads, 500 W for single payload.
** Volume is dependent on CG restrictions - about 10 inches.
*** Limited probability of use.

EXHIBIT 3 - Payload Accommodation

5.2.1 Shuttle

The Shuttle offers several payload carriers for short-term experiments, such as the Complex Autonomous Payload (CAP), the Hitchhiker series, and the Spacelab pallet. The OPM experiment can be accommodated by the Hitchhiker series or the Spacelab pallet. Either carrier provides sufficient power and energy, as well as a data link to the ground. The CAP is too small for the OPM experiment.

The Hitchhiker series consists of the G and M carriers. The G carrier, referred to as Hitchhiker G (HHG), can include a mounting plate, a Get Away Special (GAS) beam adapter, a GAS-like container, and an avionics unit. The GAS-like container is not required for OPM. The HHG mounts to the starboard side of the shuttle to avoid interference from the Remote Manipulator System (RMS) which is normally carried on the port side. The HHG carrier has one significant restriction for the OPM; the Center of Gravity (CG) of the experiment must be within 254 mm (10 inches) at a weight of 113 kg (250 pounds). The Hitchhiker M (HHM) carrier consists of an avionics unit identical to the HHG unit, and a truss-type mounting bridge across the cargo bay to mount the experiments. The mounting bridge is normally located to the rear of the cargo bay. In contrast to the HHG carrier, there is no CG constraint. Exhibits 4-6 illustrate the Hitchhiker series carriers. The OPM experiment could fly on either of these carriers; however, HHM is preferred because of the mounting configuration. The HHG may be the most likely carrier because its smaller size and weight make it easier to manifest on the Shuttle.

The Spacelab pallet carrier will also accommodate the OPM experiment easily. It consists of various manned module and pallet combinations, with the chosen configuration mission specific. If the OPM experiment flies on the pallet, it should be mounted high on the pallet to maximize the exposure of the flight samples to the space environment. Exhibit 7 shows a typical Spacelab pallet configuration. Exhibit 8 illustrates a Long Module - 1 Pallet (LM1P) configuration.

5.2.2 Space Station

The Space Station would offer OPM an ideal platform for studying the long-term effects of space exposure. The Space Station control attitude would also enable the OPM to be mounted facing in the RAM direction to obtain long-term high fluence exposure to AO.

23
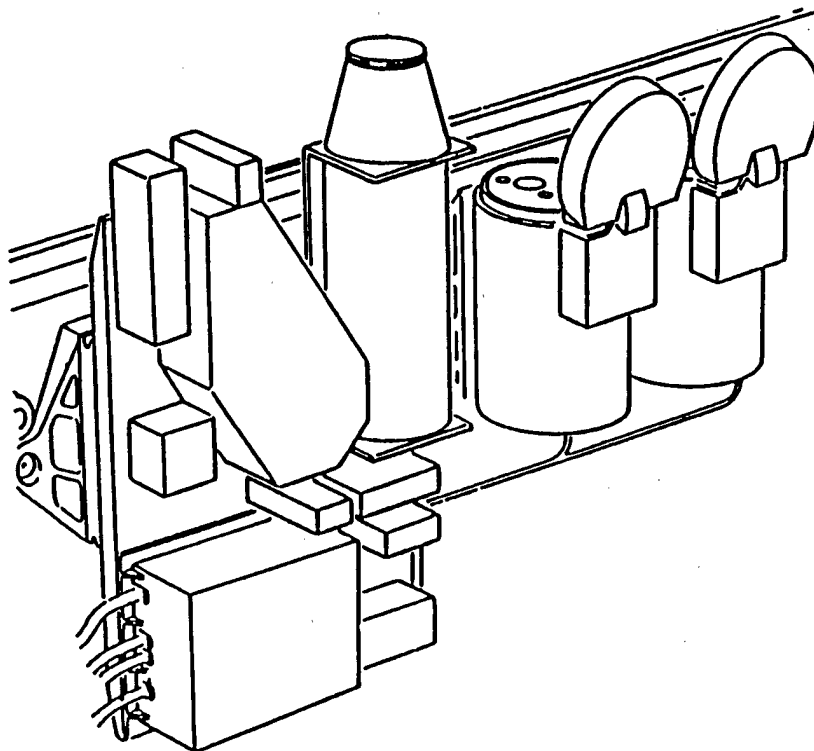
EXHIBIT 4 - Typical HHG Payload Mounting Example
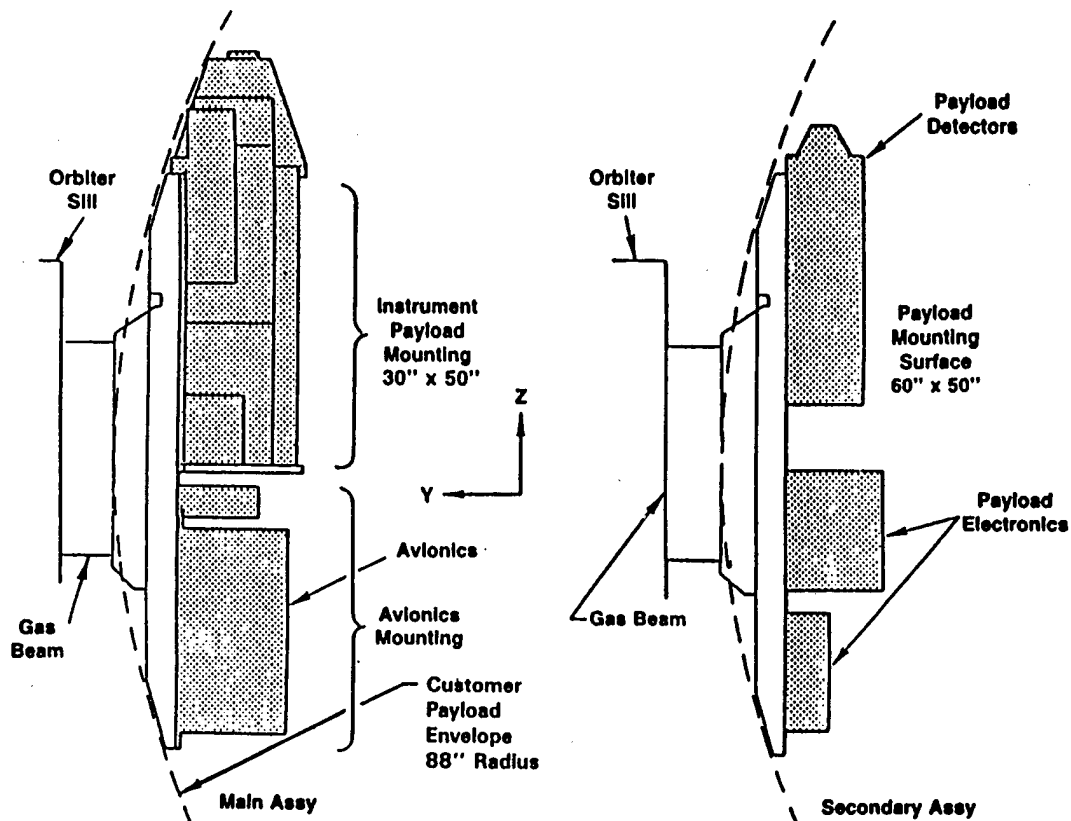
EXHIBIT 5 - HHG Payload Mounting Concept - Sideview

24

CENTER
LINE
OF BAY

28.20 — 28.20 — 28.20 — 28.20

VIEW L
TYP 8 PLCS

AVIONICS
UNIT

E

Z=414.0

Z=400.0

℄

E
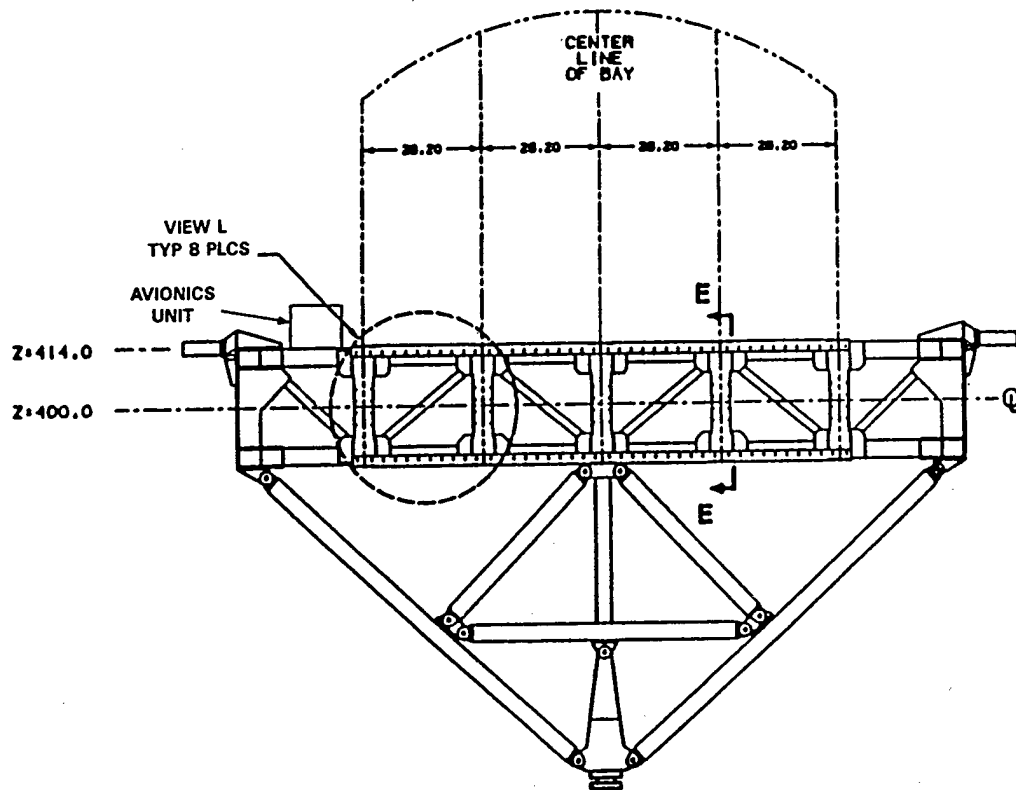
NOTE: ALL DIMENSIONS IN INCHES.

LOOKING AFT

EXHIBIT 6 - HHM Payload Mounting Interface

INSULATION

HIGH QUALITY
WINDOW

AIRLOCK

PALLET
SEGMENT

VIEWPORT

FORWARE ENDCONE
WITH THERMAL
INSULATION
TENT

PALLET/ORBITER
ATTACH FITTINGS

MODULE/ORBITER
ATTACH FITTINGS

EXPERIMENT SEGMENT

CORE SEGMENT
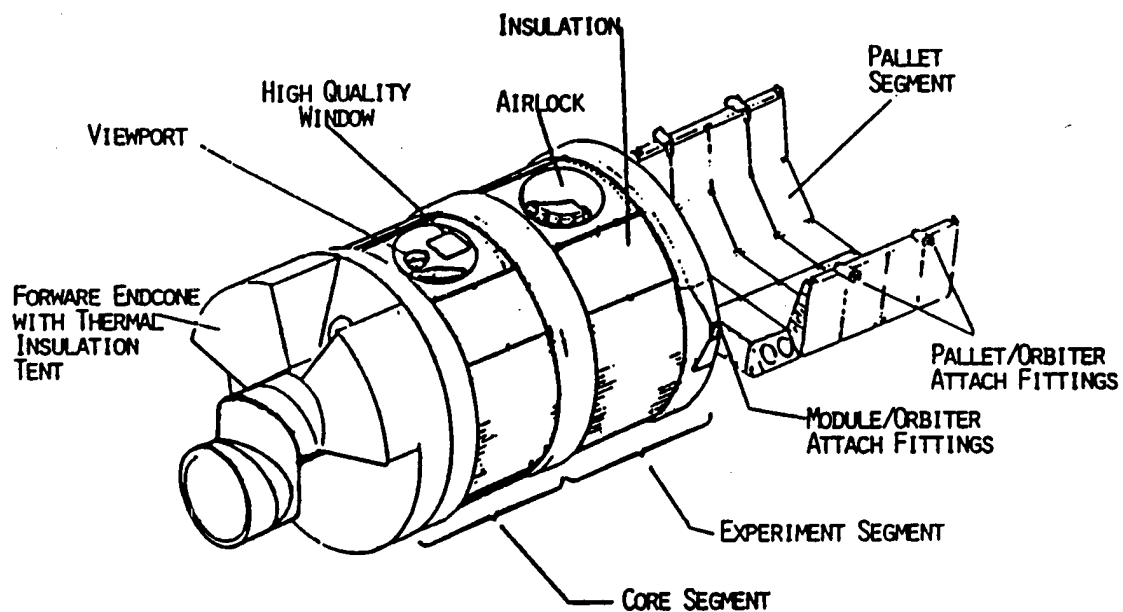
EXHIBIT 7 - Spacelab Pallet External Configuration

25
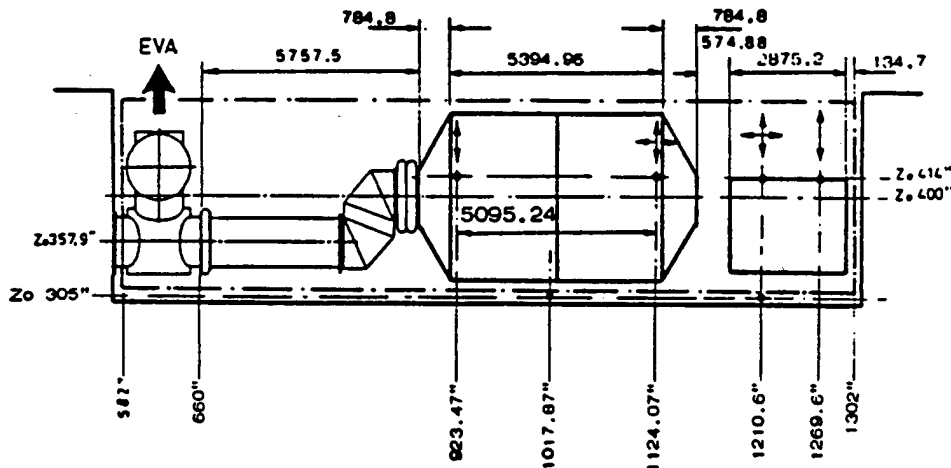
EXHIBIT 8 - Spacelab Pallet - LM1P Configuration

Currently, there are three types of planned payload accommodations available for experiments: the Attached Payload Accommodation Experiment (APAE), the Small and Rapid Response Payload (SARR), and the Distributed Sensor payload. The APAE mount is reserved for large experiments, therefore, its availability to small payloads is limited. The Distributed Sensor is envisioned for extremely small sensors directly attached to the Space Station structure. Therefore, the SARR is the most likely accommodator for the OPM. Based on the mounting of the experiment, the SARR offers three different payload accommodations; the Trunnion/Keel, the Generic, and the Japanese Module Exposure Facility. Any of these mounts is suitable for the OPM. However, due to foreign interests, the Japanese Module offers a limited probability of use. Therefore, either the Trunnion/Keel or the Generic payload accommodations would be suitable for the OPM experiment (see Exhibit 9). Exhibit 10 compares the SARR payload accommodations.

5.2.3 Specialized Missions

There are other missions that will provide the opportunity to fly the OPM. These will include ELV and Shuttle-launched missions to low earth orbit, geosynchronous orbit, polar orbit, elliptical orbit and planetary missions. There is no standard payload carrier defined for these missions. The OPM is designed with simple mechanical, thermal and electrical interfaces to permit easy accommodation on these missions.

26

• **TRUNNION/KEEL (T/K) SARR PAYLOAD:**

> **FIT INTO 4M X 1.25M X 2M ENVELOPE (MAX VOL <10M3)**
> **≤ 900 KG**
> **≤ 900 WATTS**
> **≤ 0.3 MBPS UPLINK/2.0 MBPS DOWNLINK**
> **≤ 100 MBYTES DATA STORAGE/ORBIT**
> **CAN ACCOMMODATE MORE THAN ONE PAYLOAD**
> **RMS GRAPPLE FIXTURE (ON T/K CARRIER)**
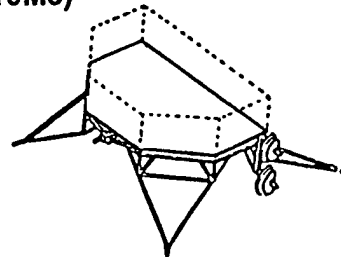
• **GENERIC (GEN) SARR PAYLOAD:**

> **FIT INTO 1.25 M X 1.25 M X 1.25 M ENVELOPE (MAX VOL ≤ 2 M3)**
> **≤ 300 KG**
> **≤ 300 WATTS**
> **≤ 0.3 MBPS UPLINK/2.0 MBPS DOWNLINK**
> **≤ 100 MBYTES DATA STORAGE/ORBIT**
> **ORU COMPATIBLE I/F (ORU TOOL)**
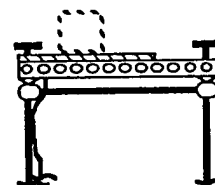
EXHIBIT 9 - Small and Rapid Response Payloads

Interface or Physical Constraint	PAYLOAD		
	SARR Trunnion Keel	SARR Generic	JEM Exposed Facility
Weight	≤ 1980 lbs ≤ 900 kg	≤ 660 lbs ≤ 300 kg	typically 1100 lbs or 500 kg
Volume Limitations Physical Dimensions	~ 10m3 1.25m x 2.0m x 4.0m	~ 2m3 1.25m x 1.25m x 1.25m	~ 2m3 0.8m x 1.0m x 1.85m (0.8m x 1.0m footprint)
Thermal Cooling	only passive	only passive	≤ 6kW active cooling
Power Constraint	≤1.5kW	≤0.3kW	≤6.0kW

Data Rates
  Downlink
  Uplink
	2.0 Mbps
	0.3 Mbps
		1.4 Mbps
		0.3 Mbps
			4 Mbps
			4 Mbps

Access to Pressurized Module	None	None	Possible thru JEM Airlock
Pointing Capability Provided	None	None	None

EXHIBIT 10 - SARR Payloads Interface Comparison Chart

5.3 Orbital Parameters

The OPM instrument will not be limited by orbital parameters. Instead, it will be reconfigurable to operate in any orbit monitoring the effects of the orbital environment on the test materials.

5.4 Mission Duration

The OPM is reconfigurable to accommodate short (seven-to-ten days) and long duration (months or years) missions. The OPM measurement timeline will be custom programmed for each mission to take full advantage of the space environment exposure offered by the mission's duration and orbital parameters. This OPM timeline can be adjusted to accommodate power and data limitations for a specific mission or payload carrier.

6.0 OPM SYSTEM DESIGN

The OPM flight hardware system is a fully integrated package consisting of a test sample array, optical measurement instruments, environmental monitors, and the support systems to accomplish OPM's experimental objectives. The overall design is simple, flexible and cost-effective. The design is simple because of the inherently simple sample handling mechanism minimizing the mechanical motions required to expose and measure the test samples. The design is flexible, allowing the OPM to be accommodated on many payload carriers and to be reprogrammed for different missions. The cost-effectiveness is provided by the use of previous proven flight designs and off-the-shelf components where possible. The design of the OPM is based on the Thermal Control Surfaces Experiment (TCSE) on the LDEF.

The OPM system is shown in Exhibit 11 and consists of measurement instruments and support systems positioned around the sample carousel. The configuration of the sample carousel was developed originally by Aerojet Electro-Systems for the TCSE flight hardware. The sample carousel is inclined at an 11° angle to allow a 150° field-of-view of space for each of the samples. Only a single rotation of the carousel is required to position each sample sequentially under its measuring station.

The test samples are arranged on one half of the circular carousel in four semicircular rows. The outside three rows of samples are called "active" samples because they are measured by the OPM optical instruments. The samples on the inner row of samples are called "passive" samples because these samples are not measured in-space, but are evaluated in pre- and post-flight testing. The outside row of 25 samples is measured by the VUV spectrometer. The VUV samples must be on the outside to allow for the detector calibration (as described in Section 6.3). The second row of 25 samples is measured by the integrating sphere reflectometer. These samples are mounted on calorimeter sample holders for the determination of solar absorptance and total emittance. The third row of 25 samples is measured by the TIS instrument. In the drawings, all the samples are shown as round. Only the calorimeter samples require round samples. The other rows of samples could be round, rectangular, or of mixed size.

The two radiometers for measuring solar and earth irradiance are also located on the carousel.

29

EXHIBIT 11 - OPM Assembly

DATA & CONTROL
SUBSYSTEM

12.0"

AO MONITOR

TOCM(2)

TIS
SUBSYSTEM

RADIOMETERS(2)

7" COBLENTZ
SPHERE

41.0"

REFLECTOMETER
SUBSYSTEM

SAMPLE
CAROUSEL

4.5" INTEGRATING
SPHERE

VUV
SAMPLES

36.0"

REFLECTANCE SAMPLES
(CALORIMETERS)

TIS SAMPLES

PASSIVE SAMPLES

VUV SPECTROMETER
SUBSYSTEM
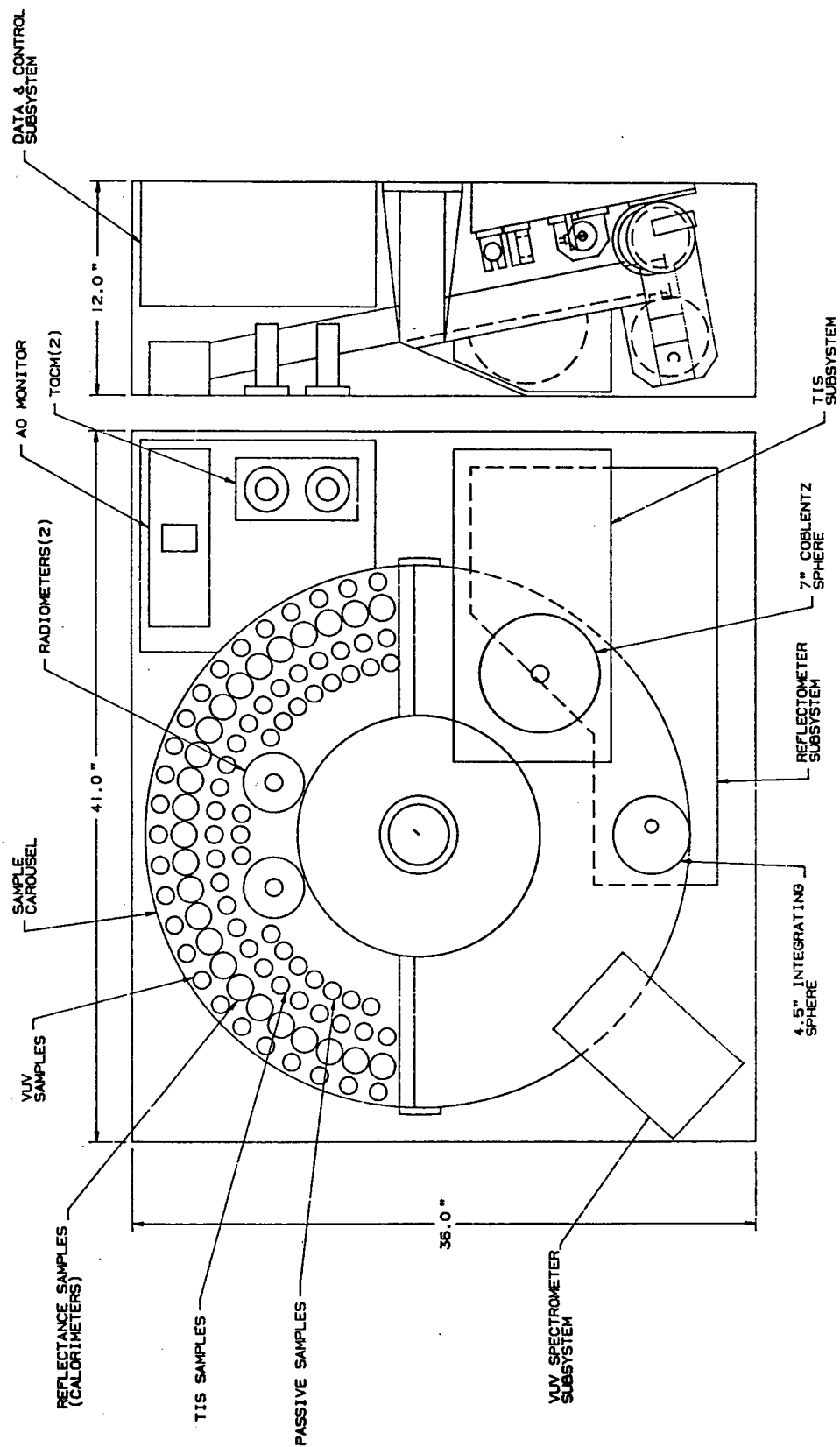
In addition to providing the capability to expose the samples and position them for measurement, the carousel provides two additional functions. The first is to provide protection of the samples during ground, launch, and deorbit operations. To achieve this protection, the half of the carousel containing the samples (and radiometers) is rotated 180° from the exposure position (see Exhibit 11) inside the OPM enclosure. In this position, the samples will face a thick metal emissivity plate that has a high emittance coating. This view of the emissivity plate provides the other function--determining the total emittance of the calorimeter samples. This process is further discussed in Section 6.4. The protected sample position of the carousel is defined as the IN position. The exposed position is defined as the OUT position.

The maximum rotation of the carousel for all its functions is about 300°. The carousel does not rotate continuously, but rotates 300° one way and then back. This feature eliminates the need for a complex and expensive wiring commutator to transfer the temperature sensor and radiometer analog data from the rotating carousel to the stationary baseplate. A simple service loop in the wiring cable will suffice.

The carousel is rotated by a stepper motor using an anti-backlash worm gear system under control of the Data Acquisition and Control System (DACS). An angular position encoder will be geared to the carousel to provide a positive position feedback to the DACS.

The 11° incline of the carousel provides the space above the samples (when they are rotated into measurement position) for the measurement instrumentation (see Exhibit 11). The integrating sphere, the TIS Coblentz sphere, and one of the two VUV detectors are positioned above the carousel and view the samples through holes in the emissivity plate.

The primary support structure for the OPM is an L-shaped baseplate allowing the OPM to be mounted on the various payload carriers—either to the bottom or to one side. The carousel, optical instruments, DACS, and the outside enclosure are mounted to the baseplate. The atomic oxygen monitor and TQCM molecular contamination monitors are mounted to the top panel.

The remainder of this Section discusses each of the optical instruments, the calorimeters, the environmental monitors, the DACS and other features of the system design in detail.

6.1 Reflectometer

The OPM reflectometer measures the total hemispherical reflectance of test materials over the spectral range from 250 to 2500 nm. The design of the OPM reflectometer is based on the reflectometer built for the TCSE.[15,23] The testing of the TCSE instrument verified that the required performance can be provided in a compact, rugged, and reliable flight configuration. The light source collection optics and the signal electronics will be improved, providing better performance. Critical optical components from the TCSE design are still available, including the monochromator, light sources, and detectors. The use of the TCSE design, coupled with hardware enhancements, will reduce costs significantly while providing state-of-the-art performance.

6.1.1 Design Objective

The design objective for the OPM reflectometer is to measure total hemispherical reflectance of OPM test materials with the following performance:

- o Accuracy – $\pm$ 2%
- o Repeatability – $\pm$ 1%
- o Wavelength range – 250 through 2500 nm
- o Spectral resolution – better than 5% of wavelength
- o Number of spectral measurements – 100 points for a full scan

The reflectometer design is integrated into the overall OPM design to work with the sample carousel and the DACS.

6.1.2 Optical Design

The OPM reflectometer is a standard optical design (see Exhibit 12) that is used routinely in the laboratory. Two light sources, tungsten and deuterium lamps, are used with a scanning prism monochromator with selectable slit widths to provide the monochromatic energy for the spectral measurement. A 115 mm (4.5 inch) diameter integrating sphere collects both the specularly- and diffusely-reflected light from a wall mounted sample providing the angularly integrated measurement capability. A UV enhanced silicon photodiode detector and a lead sulfide detector are used with the integrating sphere to cover the required 250 to 2500 nm spectral range.

Legend within the figure:

16 - Hz BEAM DIRECTOR

COMMON - PATH BEAM DIRECTOR MIRROR

115mm DIAMETER DIFFUSE INTEGRATING SPHERE

PbS PC DETECTOR

SILICON PV DETECTOR

SAMPLE UNDER TEST

0.4 μm TO 2.5 μm HIGH PASS DICHROIC FILTER

VARIABLE EXIT SLIT

ELLIPSOIDAL RELAY REFLECTOR

TUNGSTEN FILAMENT SOURCE

160 Hz TUNING FORK CHOPPER

COLLECTING OPTICS

VARIABLE ENTRANCE SLIT

28-3855-0989

f/6.5 PRISM MONOCHROMATOR FOR 0.25 - μm TO 2.50 - μm RANGE

DEUTERIUM SOURCE

EXHIBIT 12 - Reflectometer Optical Schematic

6.1.2.1 Monochromatic Light Source

Two light sources available commercially are used to provide adequate radiance over the wide 250 to 2500 nm spectral range. A Gilway model L2110 tungsten source is used for the majority of the spectral range from 400 to 2500 nm. A Hamamatsu deuterium arc lamp is used for the UV measurements. Optical lamp switching is accomplished with a dichroic high-pass filter that switches from transmitting to reflecting at 400 nm.

Collecting optics for each lamp focus the lamp image onto the entrance slit of an f/6.5 prism monochromator. This monochromator is the same design used on the TCSE and is manufactured by Research Support Instruments. A prism monochromator was chosen over a grating instrument because of the wide

wavelength coverage, relatively low wavelength resolution requirements, elimination of overlapping diffraction orders, lower inherent stray light, and operational simplicity.

The monochromator design uses a Littrow prism in a modified Ebert-Fastie monochromator mount. The broad spectrum beam from the entrance slit is dispersed by the prism. The prism is rotated to project the desired spectral component onto the exit slit. The total prism rotation to scan the 250 to 2500 nm range is 3.42 degrees.

The spectral bandpass of the monochromator is determined by the width of the exit slit. To provide a spectral resolution of 5%, three selectable entrance/exit slit pairs are provided. These are mounted on a slit wheel which is rotated into position by a stepping motor.

The monochromatic beam leaving the monochromator passes through a 160 Hz tuning fork chopper and is focused by an ellipsoidal reflector onto the 16 Hz beam director mirror at the integrating sphere entrance aperture.

6.1.2.2 Integrating Sphere

The heart of the reflectometer design is the integrating sphere (see Exhibit 13). A slowly diverging monochromatic beam enters the integrating sphere by being reflected by the common path beam director mirror. It is directed alternately onto the sample and the sphere wall. Integrating sphere theory states that, for an integrating sphere with no hole losses, a perfectly reflecting diffuse coating, and an ideal detector, the detector output is directly proportional to the radiance entering the sphere.[24,25] When the beam is directed alternately to the sphere wall and the test sample, the geometry of the two beams is identical—except for the absorptance of the sample material. The ratio of the detector readings for the sample and the sphere wall positions is the total hemispherical reflectance of the sample. The properties of the sphere cancel out, resulting in an absolute-type measurement.

In practice, sphere coatings are not perfect diffuse reflectors. Detectors are spatially and directionally nonuniform, and integrating spheres have hole losses. This is particularly important when measuring samples ranging from specular to diffuse. The most critical feature for non-ideal integrating sphere design is to maximize the detector field-of-view of the sphere wall while not permitting the detector to view the sample, the first specular reflection onto

34
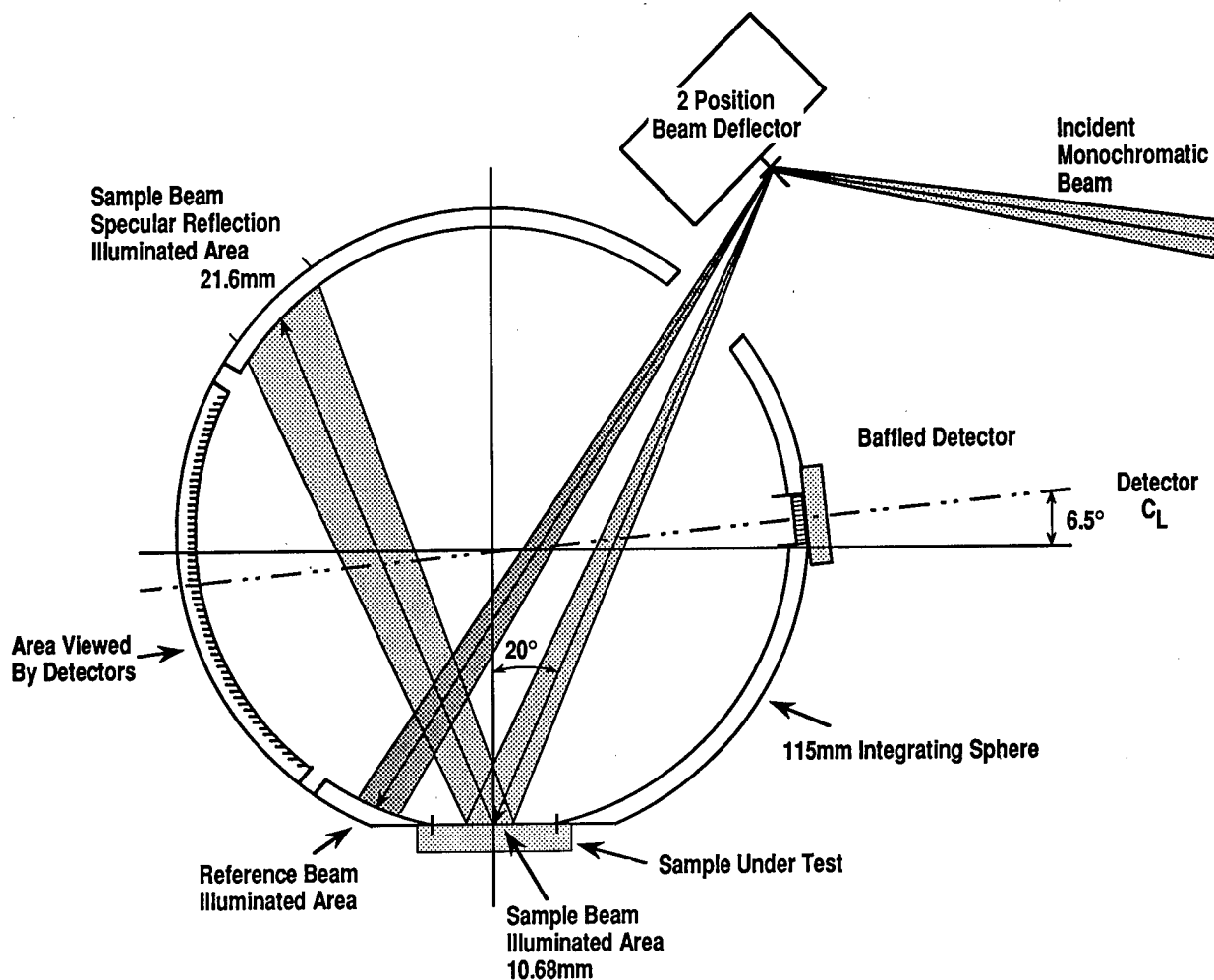
EXHIBIT 13 – OPM Integrating Sphere Geometry

the sphere wall, nor the direct illumination of sphere wall by the incident beam directly. This eliminates the major measurement differences between specular and nonspecular samples.

In addition to the integrating sphere geometry, the internal sphere coating is critical. The sphere coating, with the best optical properties, is a smoked magnesium oxide coating. Unfortunately, this coating, in the required thickness, is extremely delicate and cannot withstand the launch environment. Even in the laboratory, other coatings are used that are easier to apply and are more durable. $BaSO_4$ coatings such as the Eastman White Reflectance Paint[26], are widely used.

The coating selected for the TCSE reflectometer and for the OPM reflectometer is the MS-125 BaSO$_4$ coating developed by the NASA Goddard Space Flight Center. This coating is superior to the Eastman formulation in UV reflectance and durability. The MS-125 coating is applied over Z93 white paint manufactured by the Illinois Institute of Technology Research Institute (IITRI) to further improve uniformity and adhesion.

6.1.3 Mechanical Design

The OPM reflectometer is designed as an integrated unit that can be built and tested before integration into the OPM system. Exhibit 14 shows the reflectometer assembly. The light sources and monochromator are mounted to a baseplate that is inclined at an 11° angle to match the carousel tilt. A light baffle encloses the light beam from the monochromator to the integrating sphere.

The monochromator prism is rotated using a spring-loaded push rod and cam that is operated by a stepper motor under DACS control. The OPM design will include an improved position feedback sensor than that used in the TCSE design. The slit wheel is also rotated with a stepper motor but a geneva drive mechanism is used to provide the needed positional accuracy while maintaining a high degree of reliability.

6.1.4 Detector Signal Processing

The analog signal processor for the reflectometer is shown in Exhibit 15. The output from the detector is an AC signal modulated by the 160 Hz chopper and 16 Hz beam director (see Exhibit 16). This signal is amplified and the 160 Hz modulation is removed using a Phase Sensitive Detector (PSD). The sample and reference portions of the signal selected by the 16 Hz beam director are then separated into two separate channels. Each channel is further processed through active analog integrators providing Multiple Time Averaging (MTA). The output of the integrators is digitized by the system A-D converter and stored in the DACS where further digital MTA can be used as needed to obtain the desired precision. The detector selection, amplifier gain, and the analog integrators are controlled by the DACS (see Section 6.8). The use of phase sensitive detection techniques—combined with analog and digital multiple time averaging—provides an efficient method to minimize the effects of stray light, drift, offset, $^1/_f$ noise and white noise.[27]

DEUTERIUM LAMP

DICHROIC BEAM COMBINER

TUNGSTEN LAMP

MONOCHROMATOR

INTEGRATING SPHERE
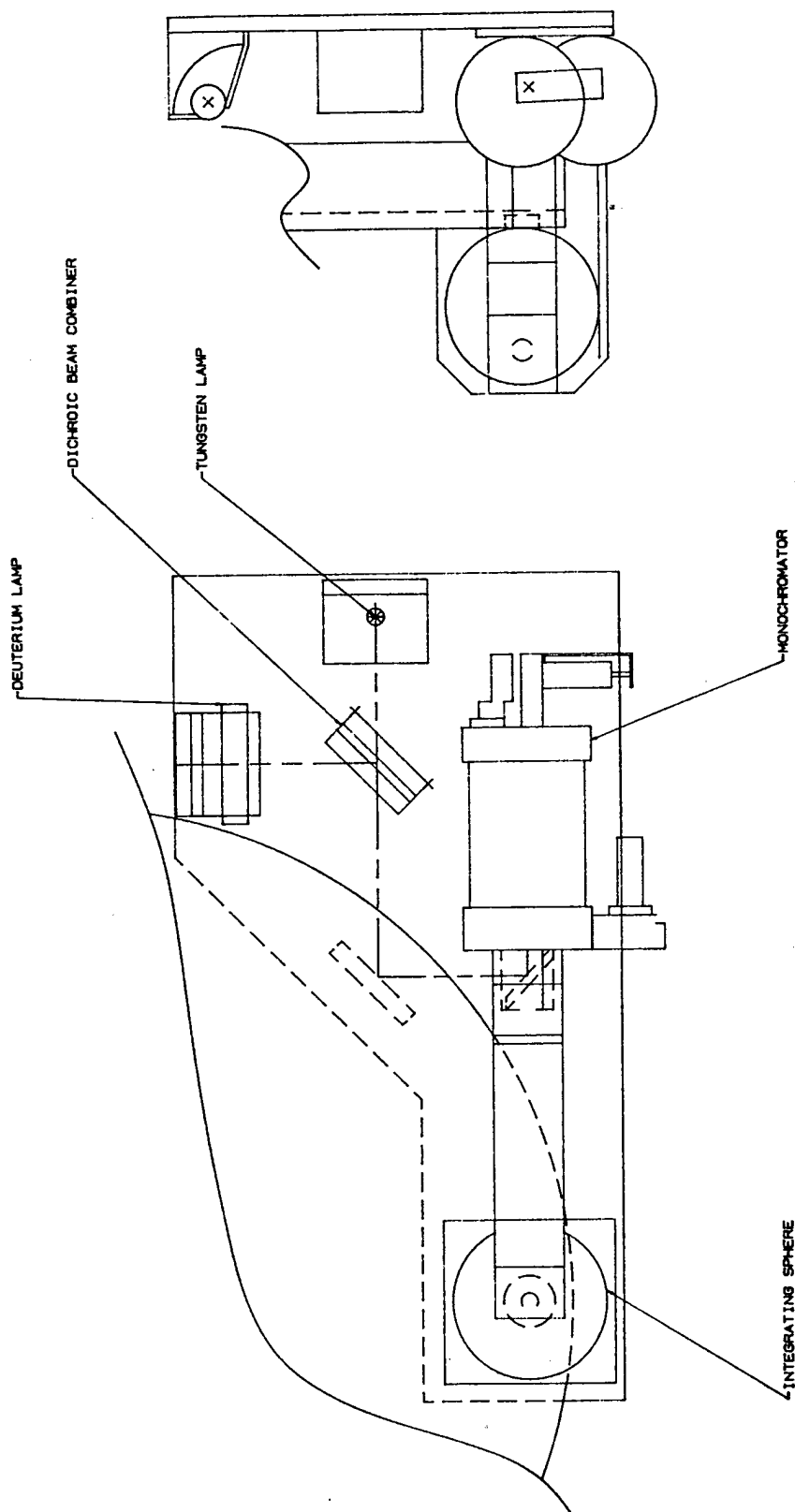
EXHIBIT 14 – Integrating Sphere Reflectometer Assembly

37
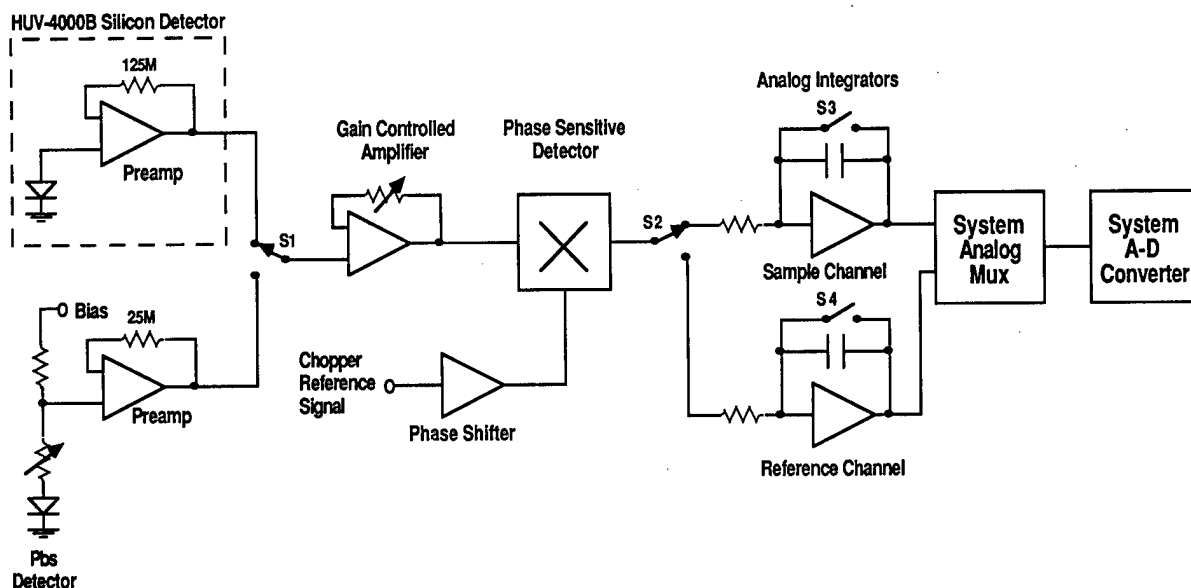
EXHIBIT 15 - Reflectometer Analog Signal Processor
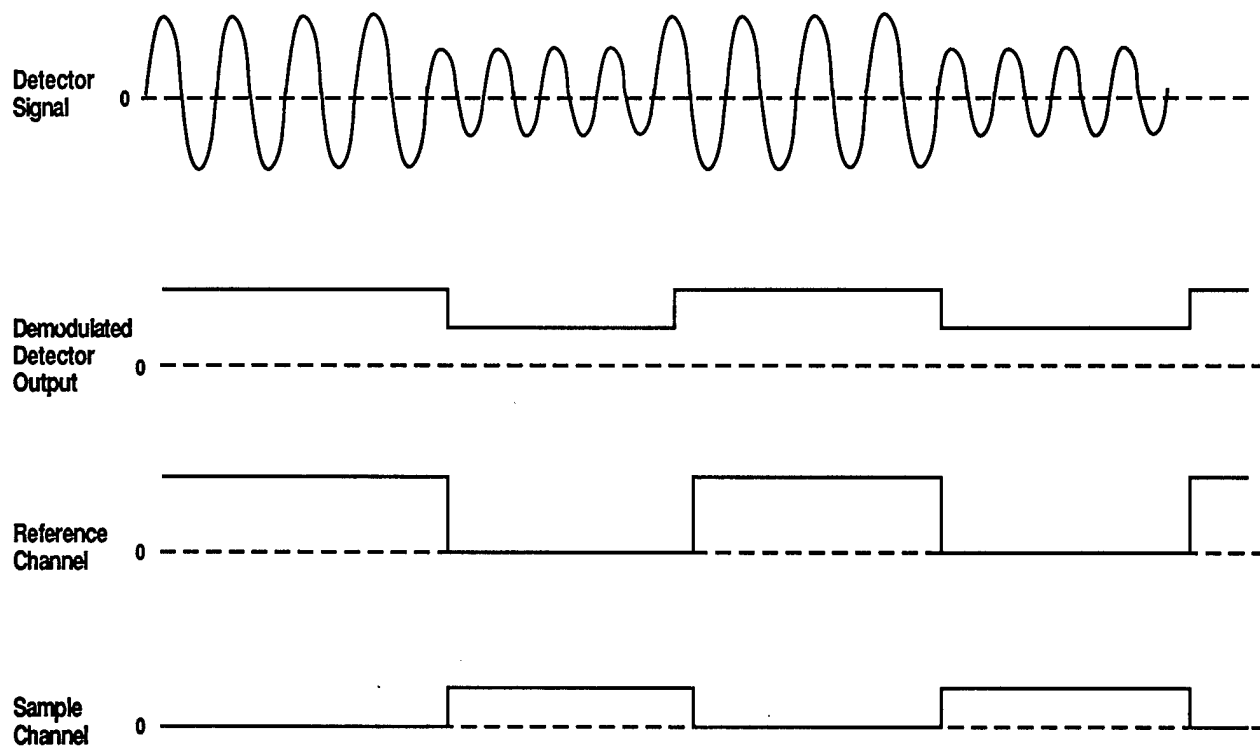
EXHIBIT 16 - Reflectometer Analog Signal

38

6.1.5 Reflectometer Performance

During the development of the TCSE reflectometer, an error analysis predicted that the design would meet the design requirements. The performance of the instrument verified this analysis. Exhibit 17 shows the results of the three separate measurements of S13G white paint by the TCSE reflectometer. This plot of the uncorrected instrument output verifies the precision and repeatability to be better than 1%.
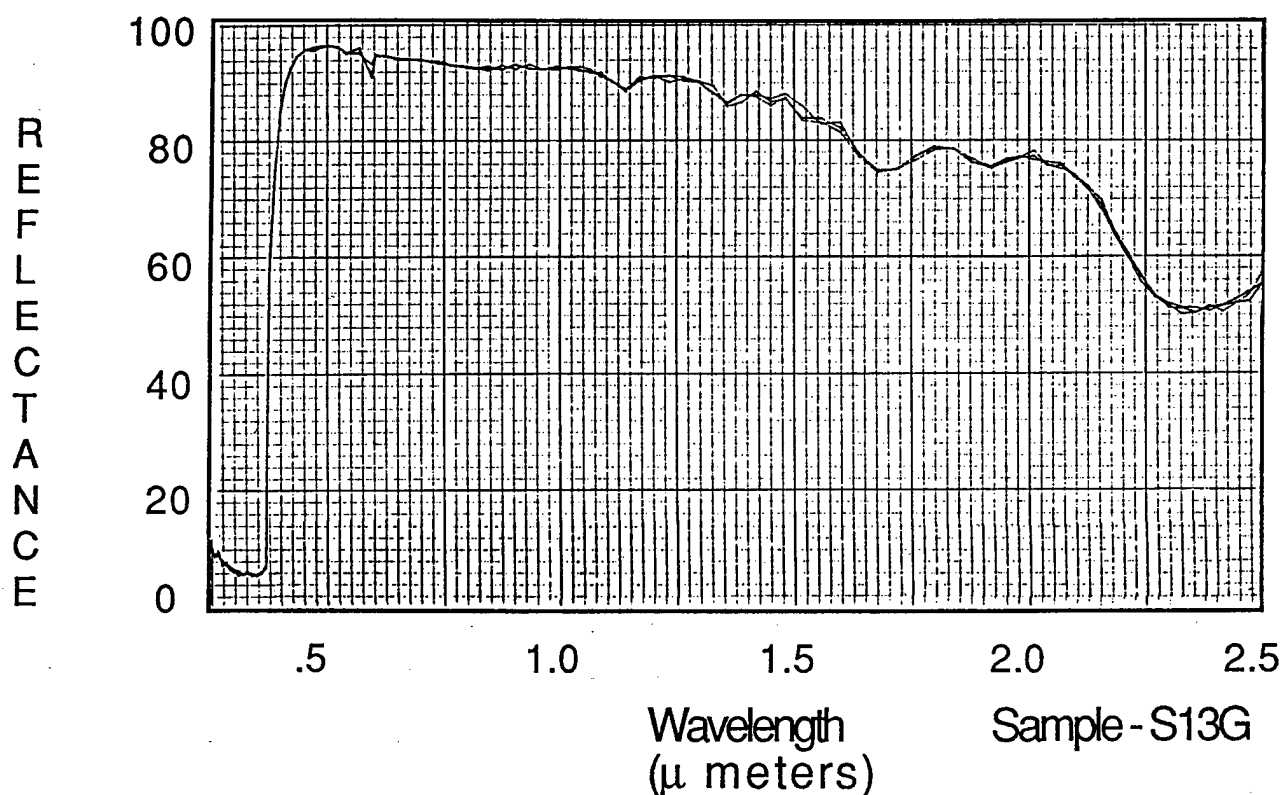
EXHIBIT 17 - TCSE Reflectometer Performance

6.2 Total Integrated Scatter (TIS) Instrument

6.2.1 Objective

The purpose of the TIS instrument is to monitor surface damage and/or contamination of optical and thermal control surfaces caused by the space environment. High-reflecting samples will work best in this apparatus (aluminum, gold, and platinum mirrors, for example). The resulting TIS value can be used to directly calculate the rms surface roughness of the sample as a function of exposure to atomic oxygen or contaminants. Semi-transparent polymer materials can also be measured as-is if they are fairly reflective, or they can be coated on the back surface with a reflector. For example, thin Kapton or Teflon with an aluminized back surface can be measured. In this case, the TIS values measured individually may not be directly convertible to rms surface roughnesses because of volume scattering. But, the change in TIS values during exposure can be directly related to changes in the sample caused by surface damage and/or contamination.

6.2.2 Performance Characteristics

The instrument will be capable of measuring TIS values in the range from 1×10^{-4} to 3.5×10^{-1}. For first surface reflectors, this corresponds to an rms surface roughness range of 5 to 500 Å. The accuracy of the measurements will be within $\pm$ 10%, which is comparable to the best laboratory instruments. More importantly for the OPM, the repeatability will be within $\pm$ 2%. This gives the instrument the required ability to measure small changes in the surface characteristics of the test samples caused by exposure to the space environment. Furthermore, through the use of two measurement wavelengths, the system will be able to distinguish between the effects of surface damage and particulate contamination.

6.2.3 Instrument Design

A schematic diagram of a typical TIS instrument is shown in Exhibit 18. Light from a laser source (shown here as a He-Ne laser) is chopped, and then strikes the sample surface. The specular beam returns at a small angle to the incident beam direction and can be measured by a detector. Light scattered by the sample is focused by the aluminized hemispherical collecting mirror (Coblentz sphere) onto a second detector. The illuminated spot on the sample surface and the scattered light detector are located at conjugate foci of the

40

HEMISPHERICAL
COLLECTING MIRROR

DETECTOR
(SCATTERED
RADIATION)

DETECTOR
(REFLECTED BEAM)

SAMPLE

CHOPPER

He-Ne LASER

FILTERS

DETECTOR
(INCIDENT BEAM)
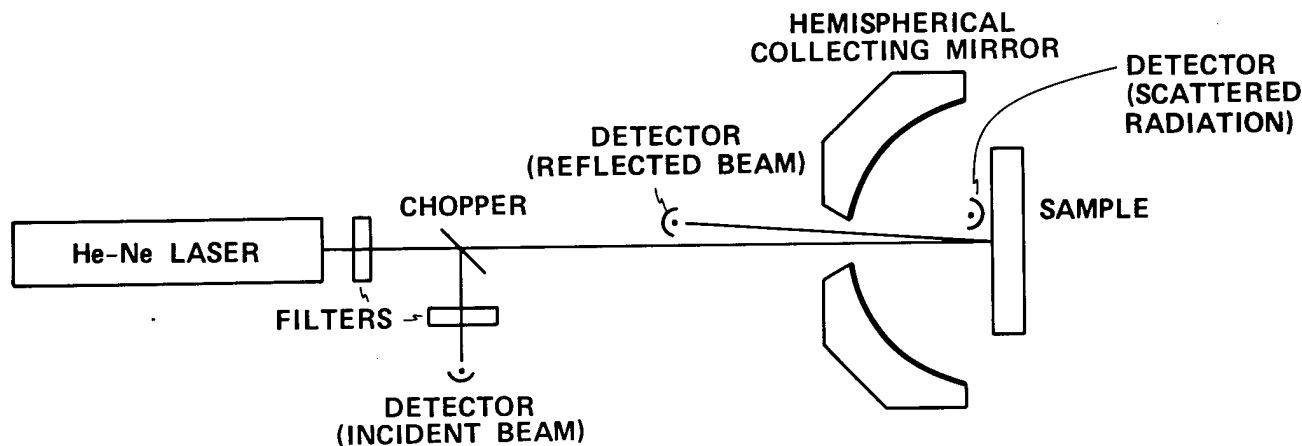
$$\text{TIS} = \frac{V_{\text{SAMPLE, SCATTERED}}}{V_{\text{SAMPLE, SPECULAR}}} = (4\pi\delta_{\text{rms}}/\lambda)^2$$

$$\delta_{\text{rms}} \text{ (EFFECTIVE rms ROUGHNESS)} = (\lambda/4\pi)(\text{TIS})^{1/2}$$

EXHIBIT 18 - Schematic Diagram of TIS Instrument

collecting mirror. This one-to-one object-image situation makes the hemispherical collector configuration very efficient for measuring small amounts of scattered light—considerably more than a roughened integrating sphere in which the detector sees only a small fraction of the light scattered by the sample. An additional detector can be used to monitor the stability of the laser by measuring the light reflected from the chopper blades.

The relation between the scattered light, specularly reflected light, and effective roughness δ_{rms} of the sample is shown in the relation below the Schematic in Exhibit 18. This is a variant of the same relation provided earlier in Section 4.1. Note that the effective rms roughness (assuming that the scattering is produced by microirregularities and not by dust particles) is proportional to the square root of the TIS at a constant wavelength. The actual measurements procedure, including system calibration, used to obtain TIS will be detailed later.

The design of the TIS flight system will closely follow the schematic design just described with a few exceptions (Exhibit 19). The basis and justification for the following design were developed during the TIS breadboard experiments, described in Section 6.2.4. First, there will be no incident beam detector and no specularly reflected beam detector. The availability of

41
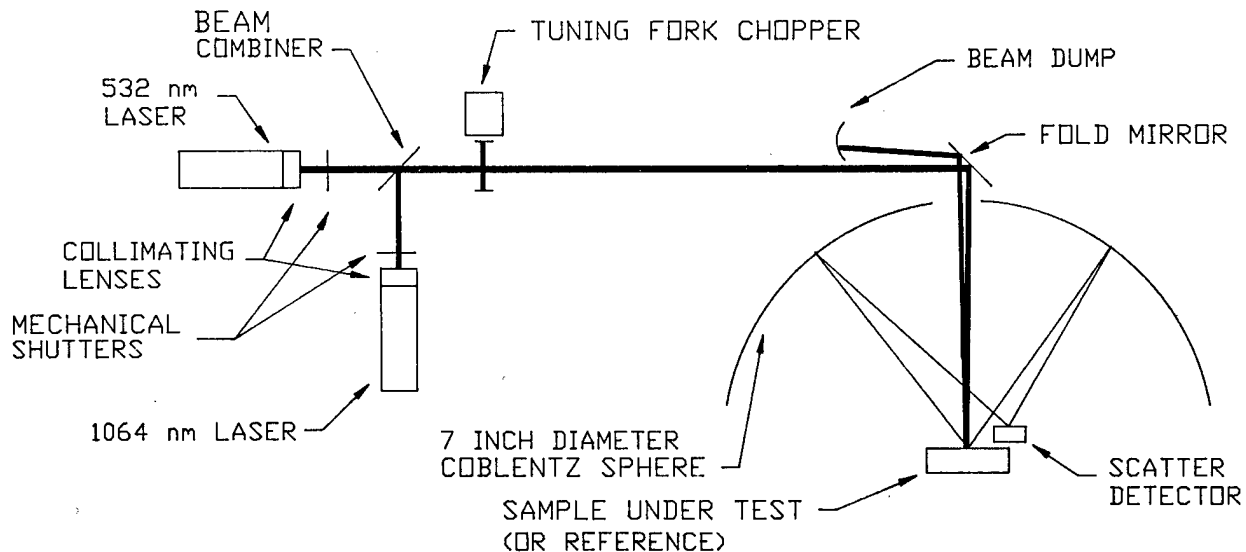
EXHIBIT 19 - TIS Optical Schematic

compact, rugged, high stability microlasers (diode-pumped, solid-state) from
Amoco Laser Company makes a real-time measurement of the incident power
unnecessary for short missions. An incident power detector can be added easily
at the beam combiner for long missions. The 532 and 1064 nm lasers are stable
to within $\pm$ 1% and $\pm$ 2% within eight hours, respectively (these data were
confirmed by the Breadboard studies). This amount of power fluctuation is
acceptable within the required instrument performance. These lasers also come
with attachable collimators which produce a Gaussian beam of $\leq$ 1 mm diameter out
to about 330 mm (13 inches). The total path length from laser to sample is
about 305 mm (12 inches); therefore, no other beam focusing optics will be
required. The power and spatial stability of the beam delivered to the sample
results in a very stable specularly reflected beam. And, since the levels of
scatter for which the instrument is designed to detect result in extremely small
changes in the specular beam, no in-flight measurements of this quantity will be
required. The incident power and the specular signal for each sample can be
measured prior to flight and remeasured afterwards. Additionally, both an
incident and specular detector would require precise alignment to their
respective beams and thus increase the complexity of design. This is not
necessary and not desirable. The scatter detector is less sensitive to
alignment. The result is a design with only one detector and one signal per
measurement.

The second modification to the traditional design is, as mentioned before, the use of two laser sources instead of one. A simple glass beam combiner will be used to transmit or reflect the appropriate beam power required without the need for attenuation filters. Finally, a fold mirror will be required due to the geometry of the OPM to direct the light beam into the Coblentz sphere. This will be an extremely high quality mirror and will add insignificant scatter to the system.

Now that the general design has been established with its necessary differences from a laboratory system explained, a more detailed description of the flight instrument is presented. The visible (532 nm) laser will be angled to enable it's beam to pass through the beam combiner and proceed directly to the fold mirror mounted at the top of the Coblentz sphere (see Exhibits 20 & 21). The IR laser will be mounted perpendicular to the visible laser to enable its beam to reflect off the beam combiner. The angle of the beam combiner will cause the reflected IR beam to overlap the visible beam so both beams strike the same spot on the sample. In this configuration, simple Fresnel reflection results in about 4% of the 50 mw IR beam (2 mw) being reflected off the beam combiner and 96% of the 2 mw visible beam being passed through the beam combiner to give almost equal power at the sample for both wavelengths. With both beams aligned this way, the system can simply switch between the two wavelengths using mechanical shutters mounted in the path of each beam.

A tuning fork chopper will be used to modulate the beams to eliminate background radiation and increase the signal-to-noise ratio. Since tuning fork choppers have proven to be reliable on previous flight experiments, they were chosen instead of a rotating one. The beam will then be folded through the entrance aperture at the top of the sphere toward the sample. The Coblentz sphere will be a 178 mm (7 inch) diameter aluminum hemispherical reflector with a 5° diameter hole drilled at the top and 5 mm to the side of the optical axis. The hole will be located off-center to enable the beam to enter the sphere at a slight angle to the sample normal (1^O) and strike the sample at a point 5 mm to one side of—and 4 mm outside—the center of curvature of the sphere. This gives the optimum horizontal separation of the beam on the sample and the detector, as well as vertical separation of the sample and detector. The specularly reflected beam will then exit the sphere slightly separated from the incoming beam so that it may be absorbed by a beam dump. Because of the large

43
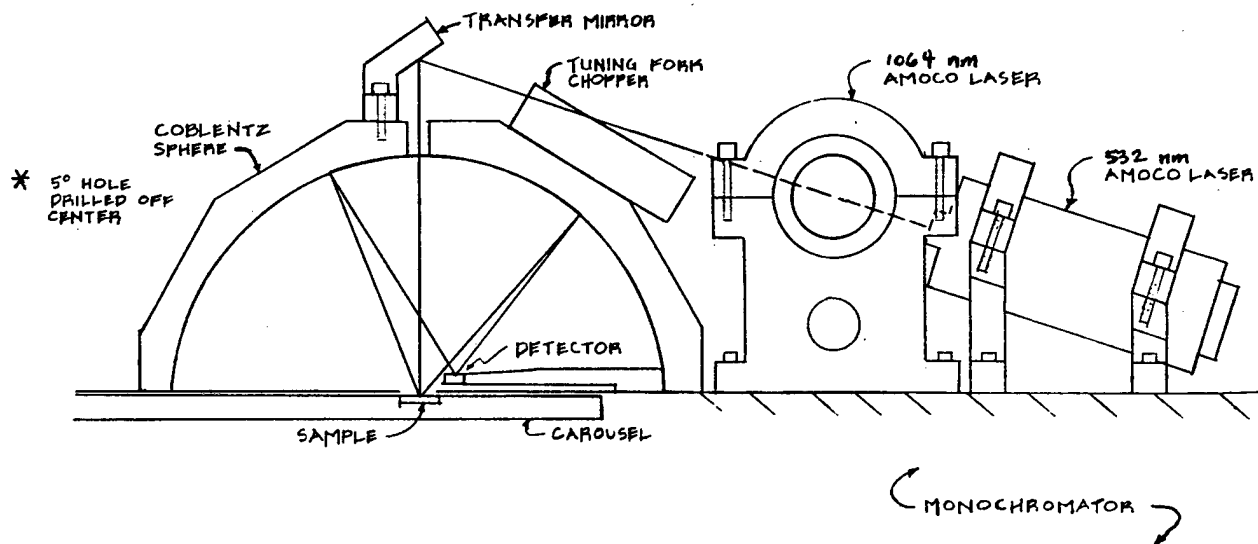
EXHIBIT 20 - OPM TIS Elevation
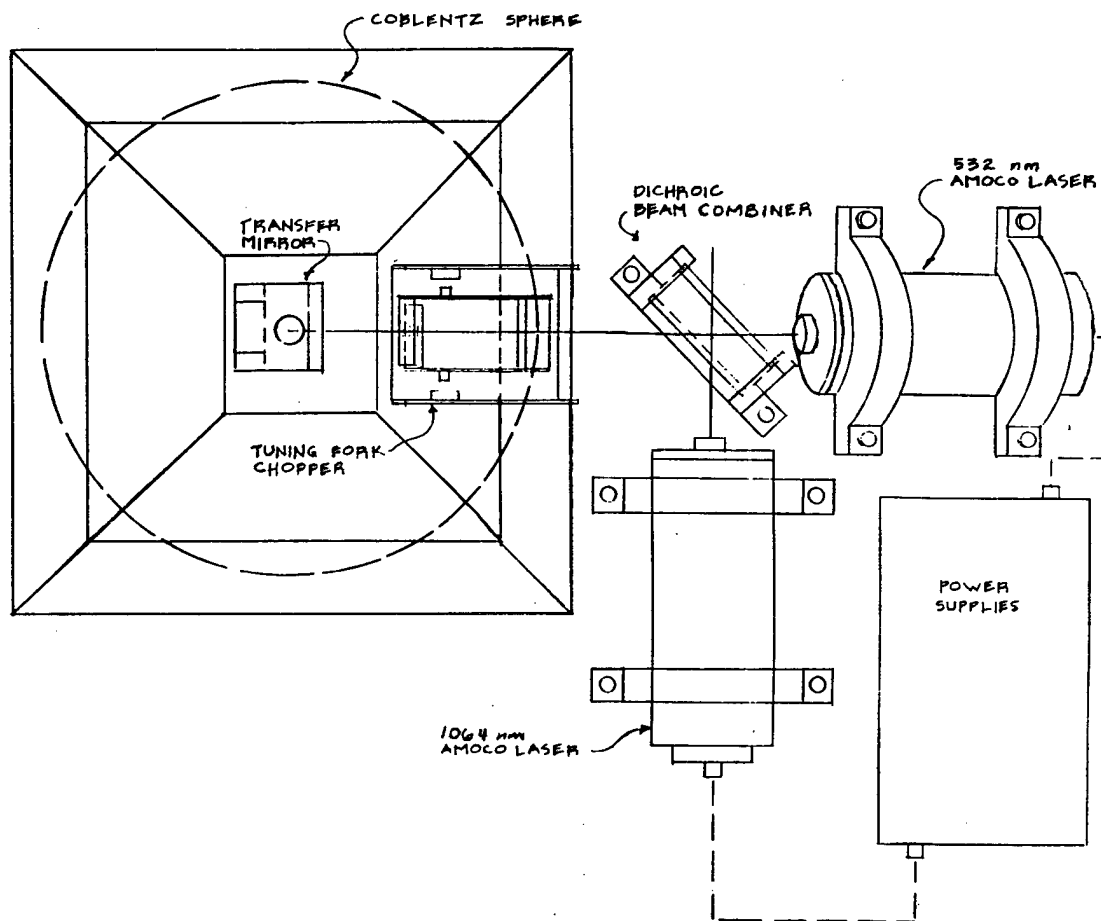
EXHIBIT 21 - OPM TIS Plan View

44

amount of spherical aberration and coma present at the outside edge of a hemispherical mirror, the flight sphere will be constructed to collect only out to 80° off-axis.

The scatter detector will be a Hamamatsu silicon photo-diode with a 3.7 by 3.7 mm active area in a 9 mm diameter canister. It will have linear response (to within 1%) over the several power decades that may be encountered. It will be mounted to a rigid arm that is mounted to the sphere. This way, alignment can be maintained—even through the launch environment. Its placement will be conjugate to the illuminated spot (i.e., 5 mm to the opposite side of—and 4 mm inside—the sphere's center of curvature). In this configuration, the image size is about 3.5 mm in diameter at best focus (4.055 mm inside center), and remains less than the detector size within ± 0.1 mm. To maintain the stated performance the detector will be held to within ± 0.25 mm for focus and ± 0.25 mm for lateral position. A simple op-amp/resistor preamplifier circuit will be located at the base of the detector arm assembly and will be optimized for the lock-in electronics. The noise contributed by the preamplifier is extremely low. In fact, the repeatability is limited primarily by laser power fluctuations. The final signal is processed by the DACS.

A certified Lambertian surface used to calibrate the system periodically will be among the samples on the carousel. Its placement will provide protection from the space environment at all times. This sample will be rotated in—and measured before—each round of sample measurements to re-calibrate the system. The reason and method for this calibration are discussed in Section 6.2.4. The carousel will be micro-stepped approximately 2 mm between measurements on each sample to better characterize the sample. For 25 mm (1 inch) diameter samples, this will allow 10 measurements per sample without getting too close to the edges. The time needed to take measurements of one spot on one sample with both wavelengths is approximately 2 seconds. If 4 seconds are allowed for carousel movement and settling between measurements, the total measurement time per sample is around 1 minute.

The TIS subsystem will be located just above the reflectometer subsystem (see Exhibit 11 on page 30) with the Coblentz sphere directly over the carousel next to the integrating sphere.

6.2.4 TIS Breadboard Studies

A breadboard TIS device was built and analyzed at the Center for Applied Optics, UAH to validate the concept of an in-space TIS measurement system. The basic OPM TIS instrument was assembled and the accuracy and repeatability determined. Next, a series of AO exposed samples were measured to verify that a TIS instrument is capable of measuring the effects of exposure damage on materials. Following this, a study of the use of a dual-wavelength system for discriminating between surface damage and contamination was performed. In addition, the effects on system performance caused by fold mirrors in the beam path (as used in the flight instrument) were analyzed. During these studies, other miscellaneous questions were answered, including: alignment tolerances, carousel positioning, baffling, laser warm-up time and stability, detector suitability, etc. With such thorough analysis, the viability of TIS for use on the OPM is well established.

6.2.4.1 Description of TIS Breadboard Instrument

A schematic diagram and photographs of the UAH breadboard are shown in Exhibits 22, 23, and 24). In this system, a laser beam passes through the
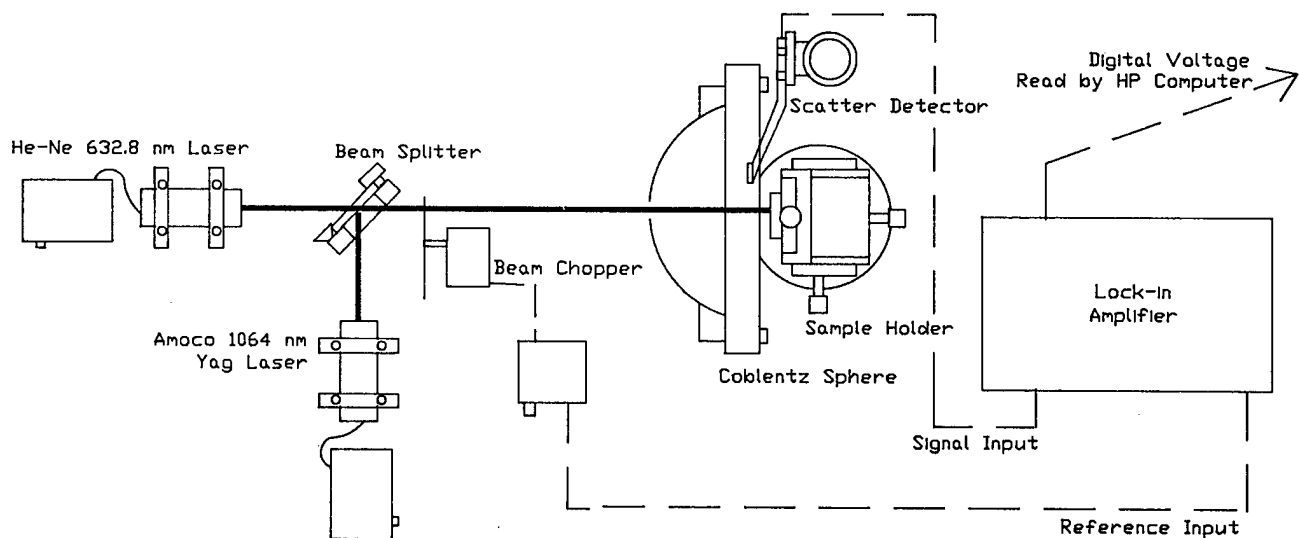
EXHIBIT 22 - TIS Breadboard Experimental Setup

entrance aperture of a Coblentz sphere slightly off axis and hits the sample at near normal incidence. The Gaussian beam diameter is 1 mm when it strikes the sample surface. It strikes the sample at a point 5 mm to one side and 4 mm

46
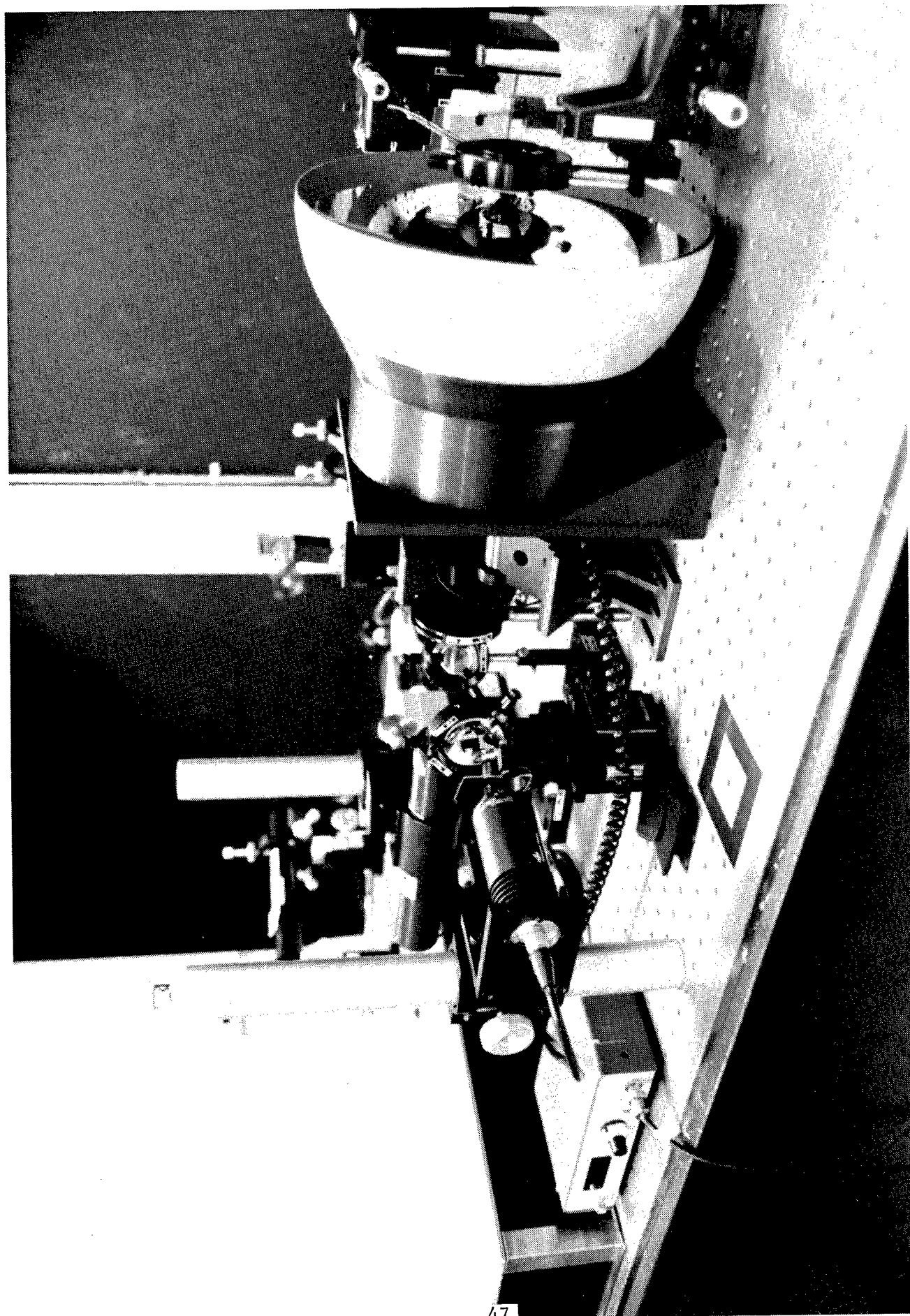
EXHIBIT 23 – Photograph of TIS Breadboard Experimental Setup
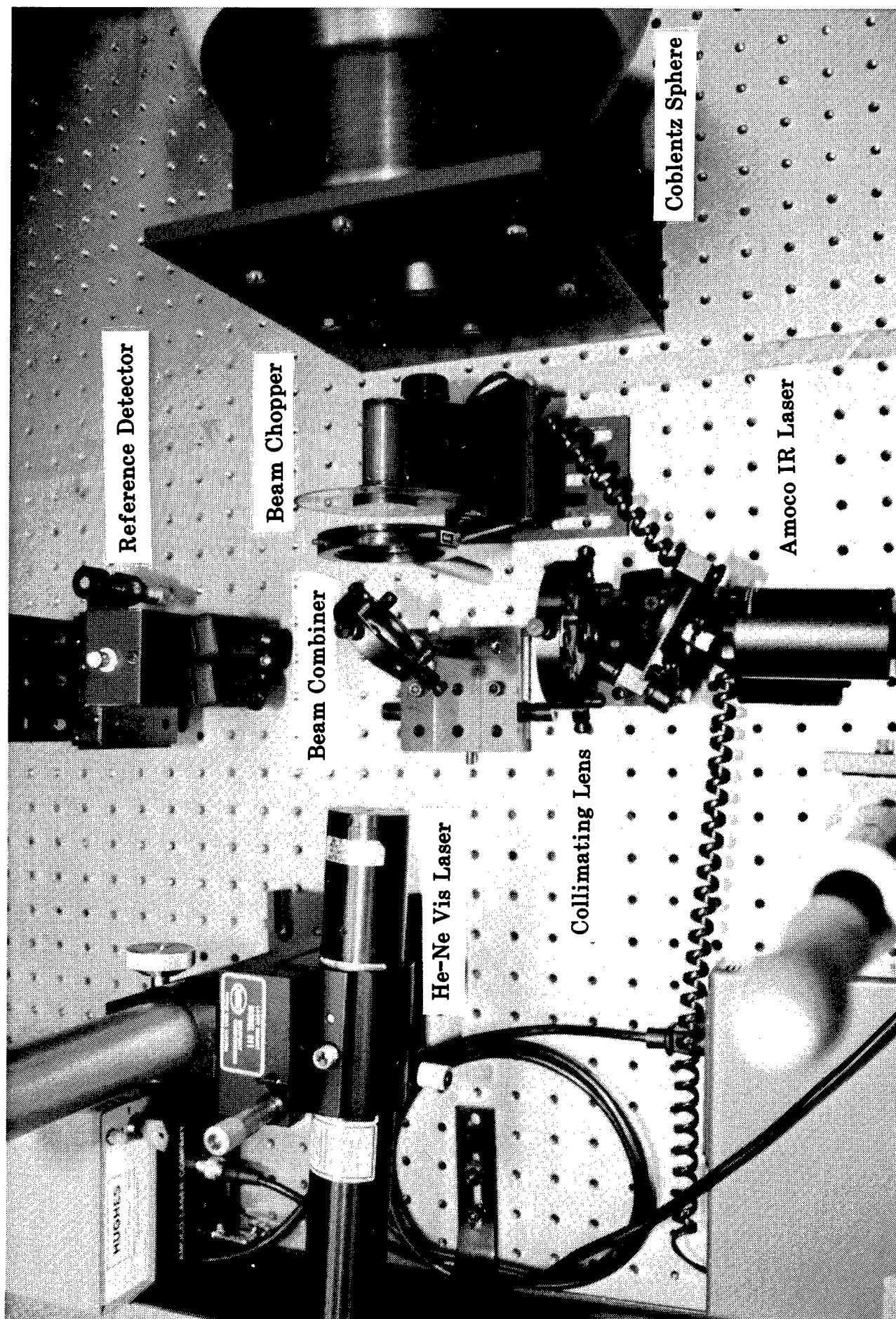
EXHIBIT 24 – Photograph of TIS Breadboard Experimental Setup

Coblentz Sphere

Reference Detector

Beam Chopper

Beam Combiner

Amoco IR Laser

He–Ne Vis Laser

Collimating Lens

outside the center of the sphere. The scattered light produced is imaged on the detector 5 mm to the opposite side and 4 mm inside the sphere, making it conjugate to the spot illuminated on the sample. The reflected specular beam exits through the entrance aperture separated from the incident beam by about 2^O. The Coblentz sphere is a 267 mm (10.5 inch) diameter rhodium coated electro-formed hemispherical mirror with a 5° hole (entrance aperture) at the vertex to allow the incident and specularly reflected beams to pass. The larger sphere was used instead of a 178 mm (7 inch) diameter sphere (as described in the flight design) because it was the only size that could be delivered in time to perform all of the desired studies. The results obtained, however, are still applicable to the flight design.

A ray trace, using the SYNOPSYS lens design software, determined there was a large increase in the spherical aberration and coma for collection angles between 80° and 90° from the specular direction. The image spot diameter, with sample and detector arranged as previously described, was calculated to be 3 mm if rays out to 80° were included. However, the image spot diameter increased to 9 mm if rays extending to 90° were included. Therefore the last 10° of the sphere was masked.

A Hamamatsu silicon photo-diode model S1336-44BK (same as for flight design) with a 3.7 by 3.7 mm sensitive area and a 9 mm diameter canister was used to measure the scattered light, specular beam, and incident beam. The responsivity of the detector is approximately the same (0.38 and 0.40 Amps/Watt) for both visible (632.8 nm) and infrared (1064 nm) wavelengths. The detector is unbiased and is linear to 1% over 9 power decades. The samples were placed in an adjustable holder attached to a three-way translation stage, which is mounted to a 360° rotation stage. The rotation stage was used to swing samples in and out of position. The translation stage was used to make the necessary adjustments on the sample once it was rotated into place and to translate the sample perpendicular to the beam for multiple measurements across the sample surface. A 5 mw 632.8 nm He-Ne and a 50 mw 1064 nm Amoco diode-pumped Yag laser (on loan for 1 month from Amoco Laser Co.) were used for the visible and infrared light sources. The two wavelengths were used to distinguish between rms surface roughness and particulate contamination. When both lasers were used, the He-Ne beam was aligned to pass through a beam splitter and enter the sphere directly. The Amoco beam was collimated by an 80 mm focal length lens and reflected off the beam splitter so the two beams overlapped and had comparable

power. The beams were chopped at 700 Hz with a Stanford SR540 beam chopper. The chopper blade had six 89 mm (3.5 inch) diameter blades, and rotated at 117 rpm to produce the 700 Hz signal. The signal was then pre-amplified and read by a Stanford SR510 lock-in amplifier. An oscilloscope was used to monitor the signal during alignment and focus the light on the detector. The pre-amp had two gain settings. The higher one was used during the alignment procedure with smooth samples to increase the signal to the oscilloscope, facilitating easier alignment. The lower setting was used when recording the sample measurements. An HP 300 series computer was used to read the data from the lock-in amplifier and calculate TIS for each spot measured on a sample and the mean and standard deviation. It also calculated rms for each spot and the resulting mean and standard deviation.

The stability of each laser was measured with the silicon detector over 2.5 hour periods by allowing the lasers to warm up the manufacturer's recommended time (approximately 30 minutes). The laser output was then measured every 10 minutes. The fluctuation of maximum to minimum output was around 1 percent for each laser, which is well within the performance of the system. Therefore, no laser intensity detector was required to ratio out fluctuations in laser intensity.

Since the breadboard instrument at UAH is new, its measurements were checked against an existing instrument at the Naval Weapons Center (NWC), China Lake, California.[19,28] A photograph of the China Lake instrument is shown in Exhibit 25. This instrument has a series of lasers operating in the visible and infrared. The red line at 647.1 nm from a krypton laser and the 1150 nm line from a He-Ne laser were used for the comparison measurements. Although these wavelengths are not identical to those of the UAH instrument, the differences are small and can be neglected when compared to other differences between the two instruments. The China Lake system has an 203 mm (8 inch) diameter Coblentz sphere with a central hole of 5.7° diameter. The maximum collection angle is about 80°. A pyroelectric detector is used at both wavelengths. The output is read using a Princeton Applied Research lock-in amplifier. A second detector and lock-in amplifier monitor the incident laser beam and compensate for variations in the intensity.
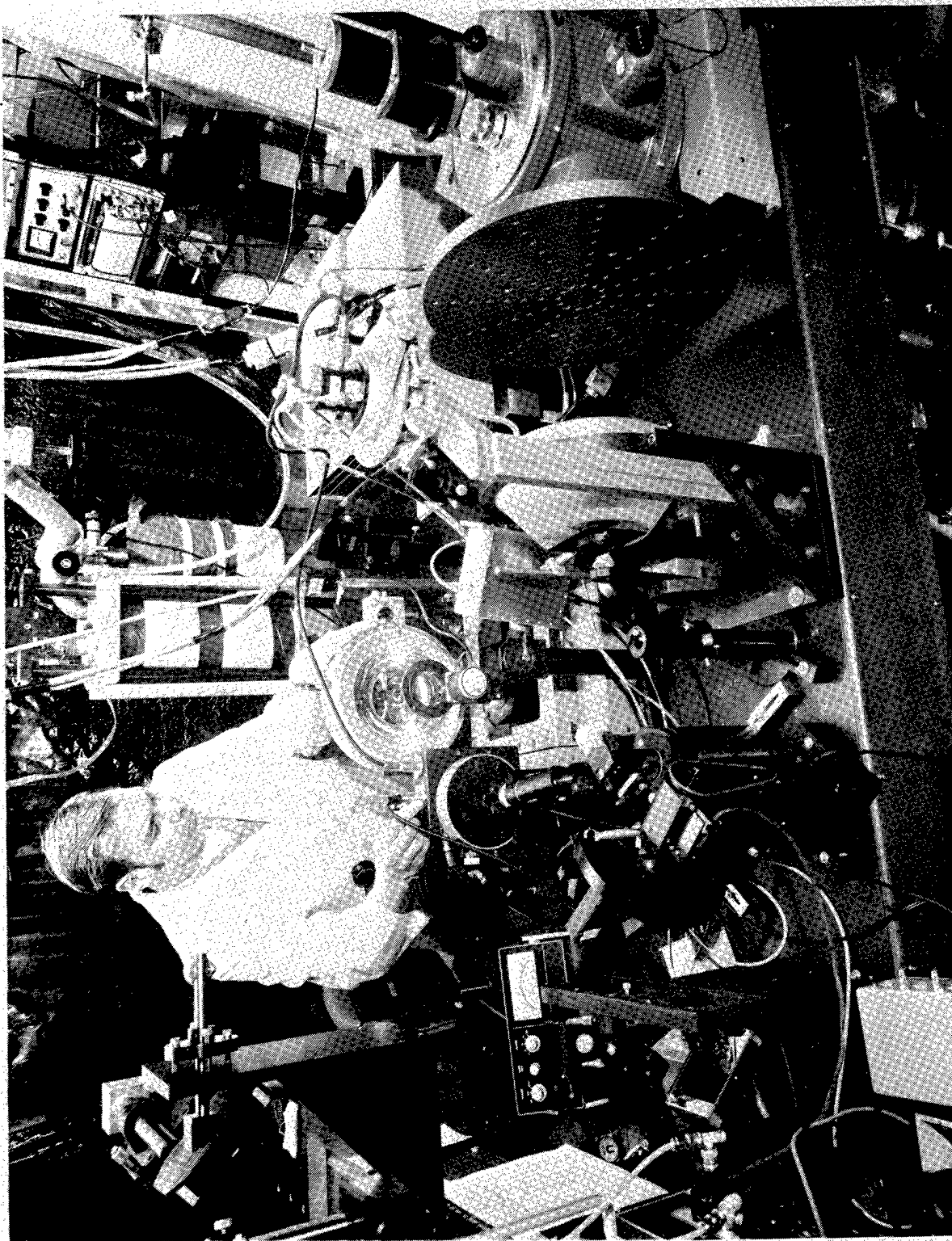
EXHIBIT 25 – Photograph of NWC Optical Evaluation Facility

6.2.4.2 TIS Measurement Procedure

The procedure used to measure TIS on all the samples at UAH followed the American Society of Testing and Materials (ASTM) procedure.[29] The ASTM method uses two assumptions: the detected scattered light is proportional to the true scattered light (i.e., light losses are constant), and the specular beam power is much greater than the scattered power. The constant of proportionality between the detected scatter and true scatter is obtained by measuring the scatter received at the detector from a Lambertian surface with calibrated reflectance. Since such a surface reflects evenly in all directions with no specularly reflected beam, the system losses are calculated easily as the received scatter divided by the incident power times the certified total hemispherical reflectance (see Eq. 2). Thus, the constant is essentially the efficiency of the hemisphere-detector system, which was found to be approximately 75% on the UAH system. The measurement procedure follows. First, the flux of the incident beam is measured by repositioning the silicon detector. The corresponding voltage, V_i, is recorded by the data system. The calibrated Lambertian surface is then placed in the sample holder and rotated into position. The calibration sample and the detector are adjusted until the scattered light is focused onto the detector and they are conjugate to one another (as previously described). The oscilloscope is used to optimize the detector signal to determine the position of the Lambertian surface that best focuses the scattered light onto the detector. Once these adjustments have been made, the reference scattered light is recorded as V_{rs}. Then the calibrated reference and test sample are exchanged. Without moving the detector, the pre-amp gain is increased, and the signal on the oscilloscope is monitored while the sample is translated in and out to find the position of best focus. Once the signal is optimized, the pre-amp is switched to its original gain setting, the sample is translated perpendicular to the optical axis to its first measurement position, and the first scatter reading is recorded as $(V_s)_1$. Then the sample is translated 2 mm perpendicular to the incident beam and a second measurement is recorded as $(V_s)_2$. This is repeated six-to-10 times, depending on the amount of measurable area available on the sample. On most samples, nine positions were recorded and the group of measurement positions were taken across a diameter of the sample. Once all the scattered light readings are taken, the detector is moved to the other side of the sphere, just outside the entrance aperture, to record the specularly reflected beam as $(V_{sp})_1$, $(V_{sp})_2$, etc. If the specular beam is somewhat diffuse, the oscilloscope is used again to

optimize the signal before recording. The specular measurements are taken in the same spots that the scattered measurements were taken. The values obtained from these measurements are fed into the equation

$$(TIS)_j = [(V_s)_j/(V_{sp})_j][LV_i/V_{rs}] \qquad j=1,2,3,\ldots\ldots \qquad (2)$$

where L is the calibrated reflectance of the Lambertian surface. TIS is calculated separately for each position measured, and then the mean and standard deviation are calculated. The major difference between the procedure used at UAH and the procedure used at NWC is how the specular beam was recorded. At NWC, the sample was rotated until the specular beam and the near angle scatter reflected off of the Coblentz sphere. The specular beam and the near angle scatter were then measured by the scatter detector.

6.2.4.3 Accuracy and Repeatability Study

The accuracy of the baseline instrument was determined through a combination of comparisons to Wyko TOPO-3D rms roughness measurements and NWC TIS measurements. The Wyko instrument uses phase shifting interferometry at 650 nm to measure the rms surface roughness of clean, high-reflecting optical samples. Several metal mirrors were measured on the TIS and Wyko instruments, ranging from a Newport aluminum-coated mirror (about 10 Å rms) to a diamond-turned aluminum flat (about 60 Å rms). The results were generally within ±10% between the two instruments. The agreement between TIS measurements made at UAH and NWC was not as good. This can be attributed to differences in sample condition and in measurement technique. For those samples that remained in good condition and for which the measurement techniques were not much of a factor, the agreement was very good (see discussion of lightly dusted mirrors in Section 6.2.4.5). From these studies, the accuracy of the UAH TIS instrument was determined to be within ±10%.

The measured repeatability of the UAH TIS instrument was better than 2%. TIS readings were taken at particular locations on a Lambertian surface and a high-quality Newport mirror. After the measurements were taken on the Lambertian surface, the system was shut down and allowed to cool completely. Without moving the Lambertian surface or the detector, the system was warmed up again and readings were taken on exactly the same positions. The same procedure was then used on the Newport mirror. The largest difference between any two

53

readings taken on the same position but on separate runs was 1.2%. Most of the differences were generally around 0.6%. The repeatability of the smooth surface (low scatter signal) was about the same as the Lambertian surface (high scatter signal). The difference between readings was due primarily to the power fluctuations of the laser.

6.2.4.4 TIS Measurements on Samples Exposed to AO

Two series of experiments were performed to determine the effect of atomic oxygen on optical and thermal control surfaces. In both cases, the samples were measured with the breadboard instrument at UAH and with the laboratory instrument at the NWC. In the first series of measurements, the breadboard instrument at UAH was just coming "up to speed." Therefore, the results obtained on the NWC instrument will be described, followed by comments on the measurements made at UAH.

In the first experiment, samples of platinum, gold, and magnesium fluoride overcoated aluminum mirrors, kapton and teflon materials were exposed to AO. The oxygen exposure was done at the Materials and Processes Laboratory, NASA MSFC. The samples were exposed for about eight hours in a Radio Frequency (RF) excited oxygen facility and placed down stream of the plasma to eliminate RF heating and heavy ion bombardment. The flux produced by the facility is approximately 1.5×10^{16} atoms/cm^2/sec at 0.2 Torr. The exposure environment is largely neutral, thermal energy, atomic oxygen with some molecular oxygen and other gases. The total fluence was 1.2×10^{17} atoms/cm^2. Half of each sample was covered to protect it from the AO exposure. The results of the measurements are shown in Exhibits 26 and 27. These exhibits show changes in the TIS at two wavelengths caused by exposure of the samples to AO. The measurement wavelengths are the 647.1 nm red line of a krypton laser and the 1150 nm line of a He-Ne laser. There are three data points at each wavelength: the first point is for the sample in the as-received condition before exposure to atomic oxygen. The second and third points are for the covered and uncovered halves of the sample after exposure to AO. Exhibit 26 shows the results of TIS measurements on platinum, gold, and aluminum mirrors, respectively. Most data points are averages of 19 measurements on the sample surface. As shown in the Exhibit, there was no change in the surface of the platinum and overcoated aluminum mirrors upon exposure to atomic oxygen. The gold sample was abraded in the area exposed to atomic oxygen, so the large measured increase of scatter did not relate to the oxygen exposure. Hence the solid data points were not plotted.

54

PLATINUM FILM		GOLD FILM		MGF$_2$ ON ALUMINUM	
VIS	IR	VIS	IR	VIS	IR

TOTAL INTEGRATED SCATTERING
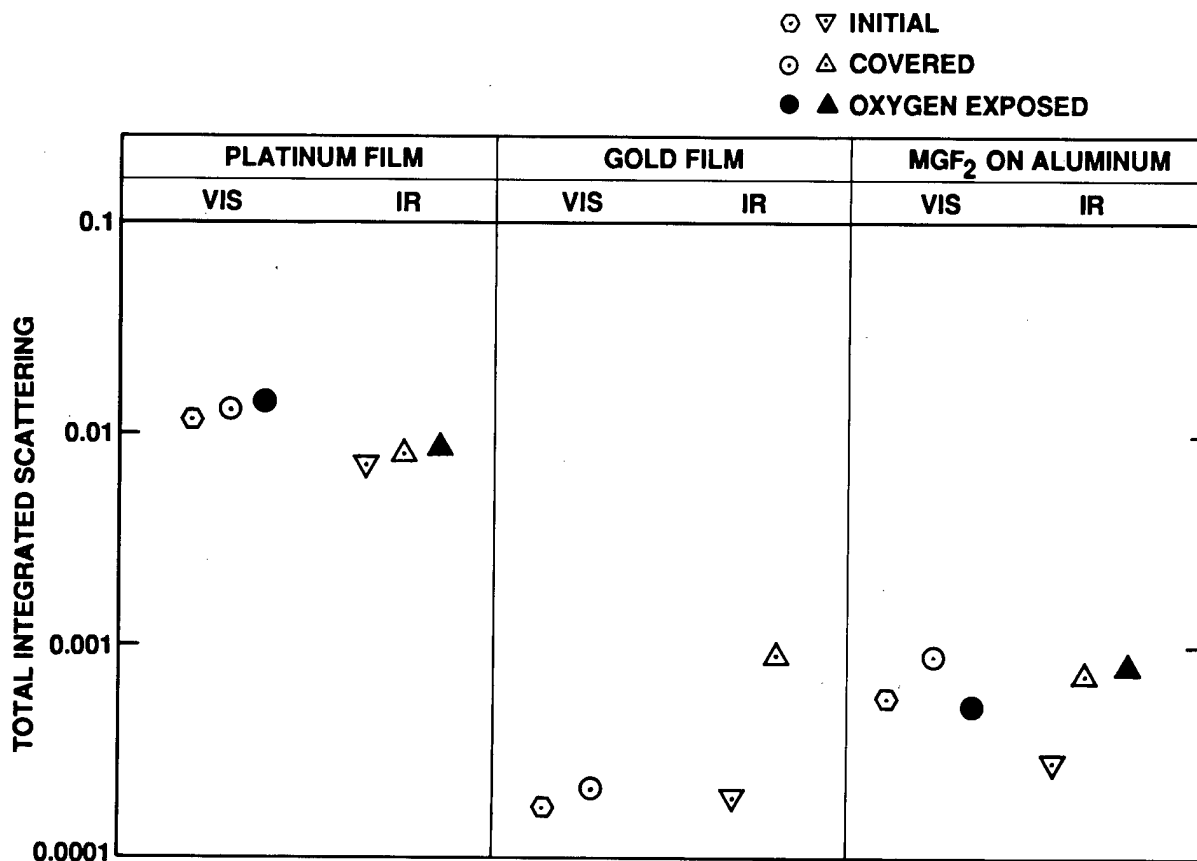
EXHIBIT 26 - AO Exposure Experiment (Mirrors)

Upon observing this sample carefully under the Nomarski microscope, the gold surface appeared to have a slight haze everywhere except where it had been exposed to AO. The AO appeared to remove the contamination that produced the haze. The haze was apparently slight enough that it did not affect the measured TIS at the visible wavelength.

Exhibit 27 shows similar TIS measurements on three organic films—two thicknesses of Kapton and one thickness of Teflon. Since these materials are transparent, they were coated on the back sides with aluminum to enhance the reflectance. Kapton has a yellowish color in transmission, so the aluminized samples appeared gold colored (1 mil thick sample) and copper colored (5 mil thick sample), respectively. The aluminized Teflon appeared aluminum colored. The Teflon remained relatively unaffected by atomic oxygen, but distinct changes occurred in the two Kapton samples. Although it was originally intended that

55
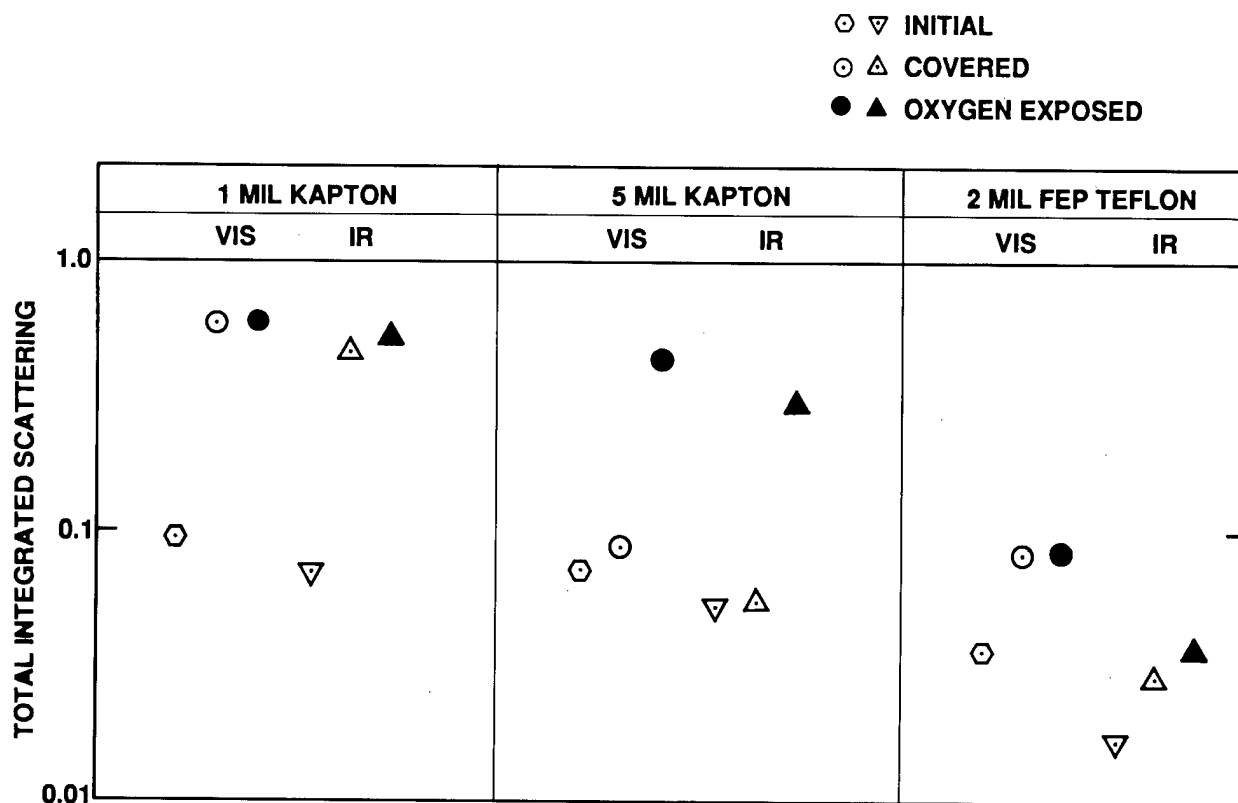
EXHIBIT 27 - AO Exposure Experiment (Films)

the 1 mil thick Kapton sample would be only half exposed to AO (as the others were), it was determined later that the entire surface had been inadvertently exposed. Thus, both points labeled "covered" for the 1 mil Kapton sample in Exhibit 27 are actually "oxygen exposed." Observing the sample under the Nomarski microscope, a light-colored ring could be seen around the edge of the sample where the surface had been protected from the oxygen irradiation. The entire central area had darkened considerably , and scratches had become more pronounced. The scattering level increased by about six times in both the visible and the infrared. The 5 mil thick Kapton sample clearly showed the effect of the atomic oxygen over the irradiated half of the sample. The scattering on the exposed part of this sample increased by about five times in the visible and infrared spectral regions. The sample surface darkened and roughened, as shown in the Nomarski micrograph in Exhibit 28.

OXYGEN EXPOSED   COVERED

|←——————————— 0.5 mm ———————————→|
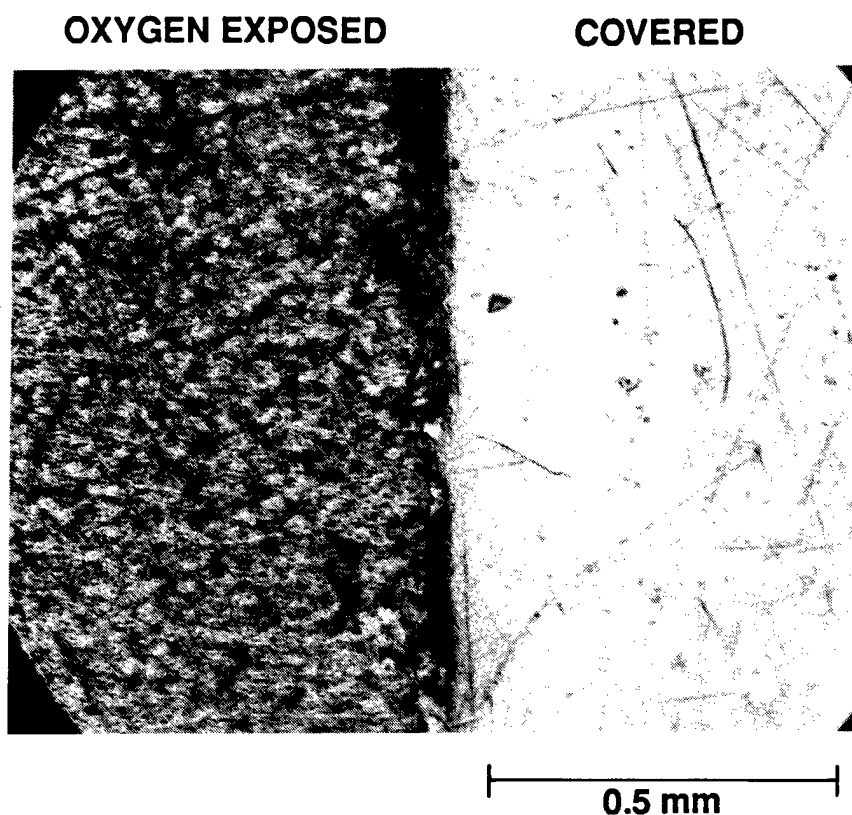
EXHIBIT 28 - Nomarski Micrograph of 5 mil Kapton

At UAH, TIS values were an average of seven-to-10 measurements across the sample surface. Although consistently higher in magnitude than NWC measurements, the UAH TIS instrument measurements on these samples were in excellent agreement considering the differences between exposed and unexposed regions. The increased TIS values of the samples were possibly caused by extensive handling during the trip between NWC and UAH, and they may have collected additional contamination (the IR laser was not available during these measurements to verify this). It may have also been caused by differences in the instruments and measuring techniques. In addition to the TIS measurements, observations were made under a Nomarski microscope. Under this microscope, both sides of the 5 mil Kapton sample showed several scratches and imperfections, but the exposed side also showed a dense orange peel texture. To the naked eye, it looked hazy or cloudy. The 1 mil Kapton had the same hazy appearance to the

57

naked eye, but under the microscope the scratches seemed more predominant. The Teflon did not show a perceivable difference in surface quality under the microscope, although the TIS measurement did increase on the exposed side. The platinum mirror had extremely dense thin random hairline cracks that were not visible to the naked eye. But under the microscope, the density of the cracks seemed to be slightly greater on the exposed side than on the unexposed side.

The second series of AO exposure experiments was performed on a new set of Kapton samples. Six 5 mil Kapton samples were exposed to AO in the same facility at NASA/MSFC for different exposure times. Two were exposed for 1 hour, two for 4 hours, two for 8 hours, and one was left unexposed to be used as a control. The data obtained at UAH are compared with the measurements taken at NWC in Exhibit 29. The measurements on the UAH TIS system were taken exactly as described previously. The difference in procedure between NWC and UAH was the method used in measuring the specular beam. At NWC, the sample was tilted so the specular beam and the near-angle scatter did not exit back through the

Sample	Oxygen Exposure	TIS - VIS		TIS - IR		TISvis/TISir	
		UAH	NWC	UAH	NWC	UAH	NWC
CTL	control	0.287	0.105	--	0.092	--	1.14
K1	1 hr.	0.260	0.115	--	0.102	--	1.13
K2	1 hr.	0.269	0.131	--	0.109	--	1.20
K3	4 hrs.	0.276	0.108	--	0.099	--	1.09
K4	4 hrs.	0.262	0.108	--	0.095	--	1.15
K5	8 hrs.	0.323	0.130	--	0.097	--	1.33
K6	8 hrs.	0.313	0.108	--	0.091	--	1.18

EXHIBIT 29 - TIS Comparison of AO Exposure

entrance aperture like they did at UAH (consistent with the ASTM procedure). They were also imaged by the sphere onto the detector. Since there was significant near-angle scatter that could not be collected by the UAH detector due to its size, the specular beam intensity recorded by the NWC procedure was larger. This number increased the denominator of the TIS equation and therefore contributed to the smaller TIS values obtained by NWC. These TIS values were approximately a factor of 2 smaller than those obtained at UAH. There was no visible damage to the naked eye on any of the samples, but under the Nomarski

microscope it was observed at NWC that the scratches were somewhat enlarged on sample number K5. This sample showed the largest TIS value on the UAH system. These slight differences are visible in the Nomarski micrographs shown in Exhibit 30. These results suggest the early onset of atomic oxygen damage. The oxygen fluence used in the first series of experiments was higher than in the second series of experiments, and none of the samples in the second set darkened like the Kapton samples in the earlier experiment. The importance of this study is not so much the absolute magnitudes of the scattered light levels, but the ability of the instrument to measure changes in the scattering intensity due to AO exposure.

6.2.4.5 Dust Contamination Study

This study was conducted to verify the wavelength dependence of the TIS measurements on dust particle contaminated samples (as discussed in Section 4.1). Four high-quality 25 mm (1 inch) diameter aluminized samples were dusted to four different degrees of coverage at MSFC--from very light coverage to heavy coverage. Appendix A describes the preparation and characterization of the dusted samples. Nomarski micrographs of three of the four samples with light to heavy coverage are shown in Exhibit 31 with a micrograph of the control sample. The particle density and percent obscuration, measured at MSFC, and the TIS values obtained for each sample, are listed in Exhibit 32.

The particle density measurements were confirmed at UAH by counting the number of particles in a well-defined aperture under the Nomarski microscope, and then computing the density. The TIS measurements were made at UAH, and the system was recalibrated each time between measurements at the two wavelengths. The measurements made with the UAH instrument are shown in Exhibit 33. The TIS measurements are shown for the visible (circles) and infrared (squares), as they include the ratios between them (triangles with the scale at the top right). Also shown are the particle area densities for each sample (solid diamonds with the scale at the bottom right).

There is clearly a correlation between both the visible and infrared scattering and the particle density. An even better correlation was obtained with the TIS measurements when the percent coverage was used, which considers the different sizes of the particles. The ratio of visible to infrared scattering changes from 2.27 for the control surface B4 to 0.787 for surface B8 with the maximum particle density. As the particle density increases, the
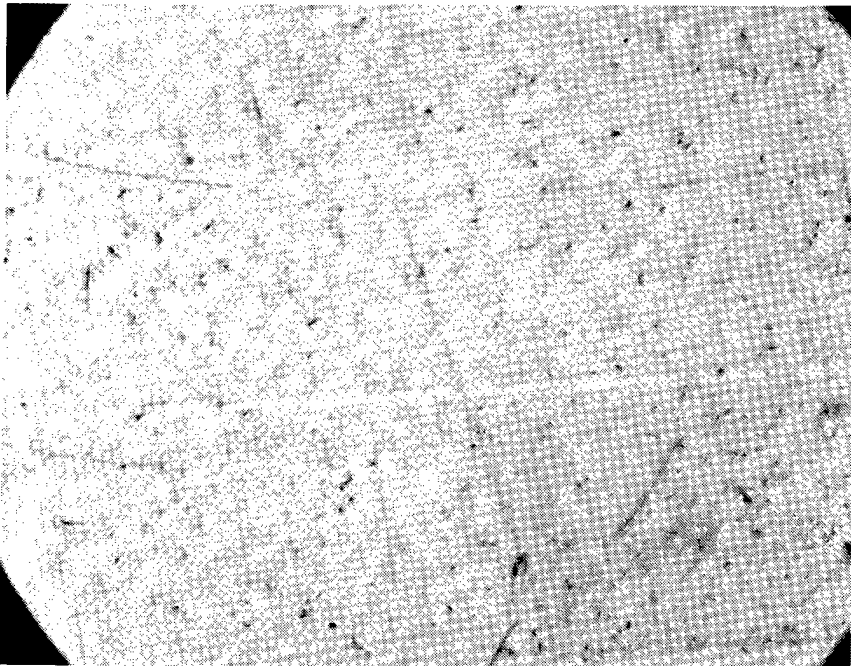
8 HR OXYGEN EXPOSED
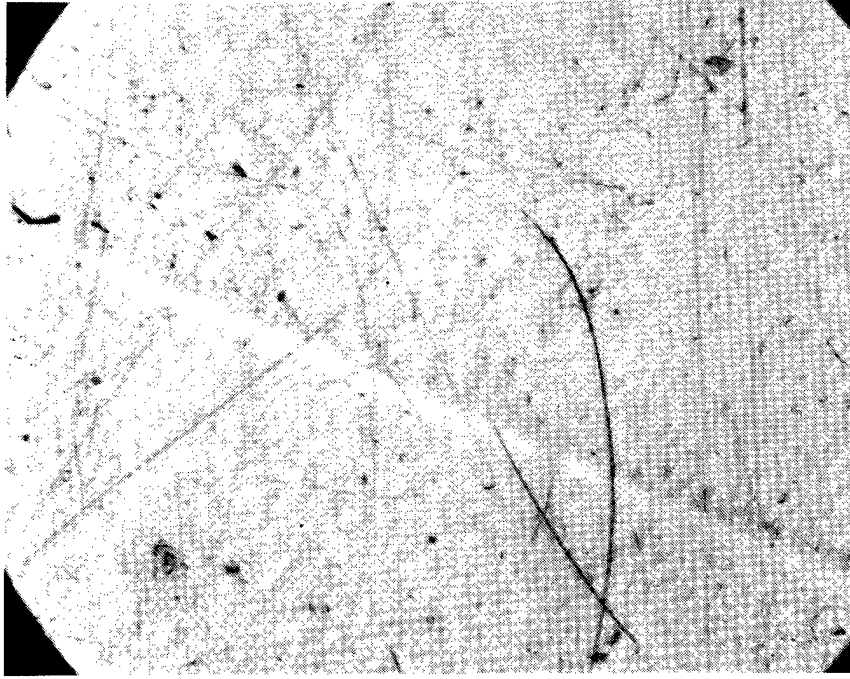
CONTROL

0.5 mm

EXHIBIT 30 – Nomarski Micrograph of 5 Mil Kapton

60
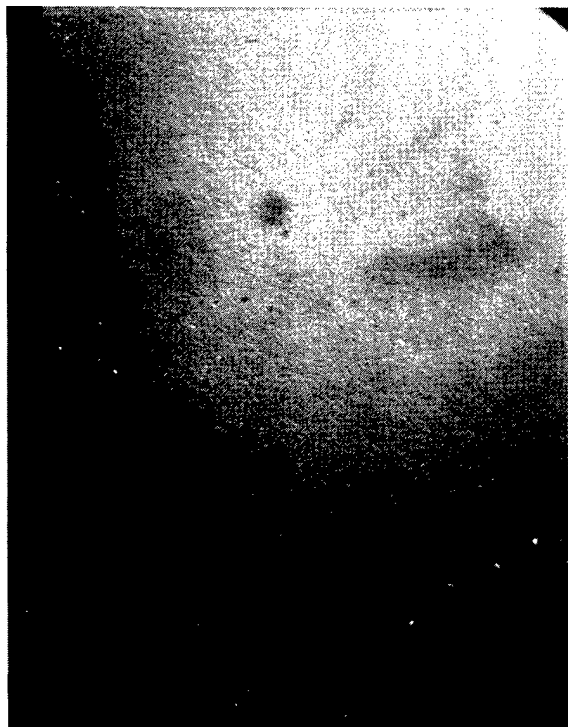
B6 LIGHT DUST

B8 HEAVY DUST

0.5 mm

B4 CONTROL

B7 MODERATE DUST
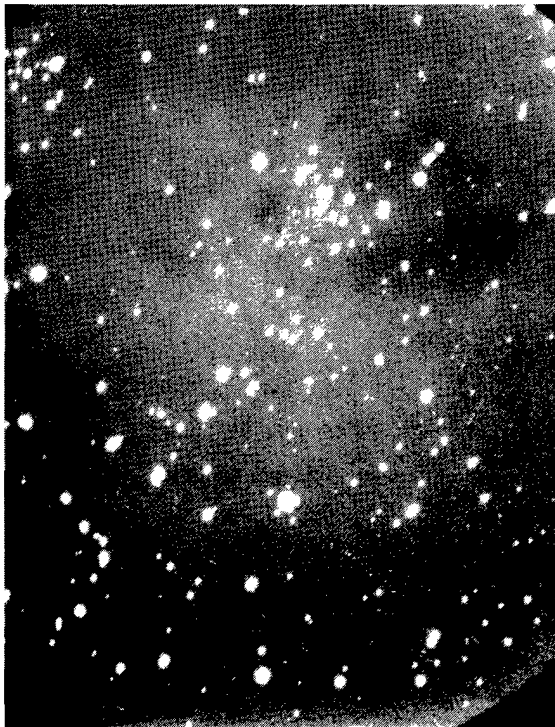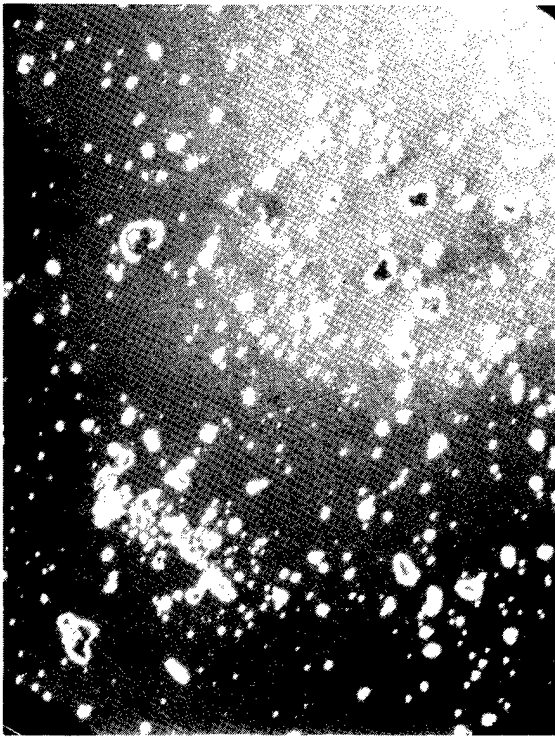
EXHIBIT 31 – Nomarski Micrograph of Dusted Mirrors

61

Sample #	% obs.	Particles per mm^2	TIS-VIS UAH	TIS-VIS NWC	TIS-IR UAH	TIS-IR NWC	TISred/TISir UAH	NWC
B4 (control)	.006	.397	.000893	.000998	.000393	.000809	2.27	1.23
B5	.038	.957	.00131	.00158	.000711	.00137	1.84	1.15
B6	.534	14.0	.00644	.00674	.00696	.00749	.925	.900
B7	.628	24.2	.0106	.00932	.0124	.0101	.855	.923
B8	1.805	61.5	.0404	.0291	.0513	.0359	.787	.809

29-4061-1089

EXHIBIT 32 - TIS Measurements of Dusted Samples

infrared scattering, which is more sensitive to particles, increases faster than the visible scattering. The visible TIS data measured at NWC were in excellent agreement with the UAH results (see Exhibit 32). However, the infrared NWC TIS measurements did not agree as well--probably because of differences in the instruments and the way the measurements were taken. The important point is that the TIS breadboard instrument has sufficient sensitivity to detect changes in particle coverage from a fraction of a particle/mm^2 to about 60 particles/mm^2 (and probably more), representing a 45-fold increase in scattering.

6.2.4.6 Fold Mirror Study

The fold mirror study was conducted to determine the effect of using two fold mirrors to fold the beam into the sphere, as may be necessary on the flight system. The highest quality Newport mirrors were used as the fold mirrors. First, TIS was measured on a number of samples of varying rms roughness without the fold mirrors in place. Then two fold mirrors were used to fold the beam into the sphere (see Exhibit 34), and the same samples were measured again to check for any substantial difference in TIS. The TIS values obtained with--and without--fold mirrors are compared in Exhibit 35. The TIS measurements could not be made in exactly the same spots on the sample each time; therefore, the standard deviation of TIS for each sample is included as a measure of deviation in roughness over the surface. Since the differences in TIS values can be attributed mostly to the deviations in TIS over each of the samples, and since some samples showed a slight increase and others a slight decrease in TIS, it is

62
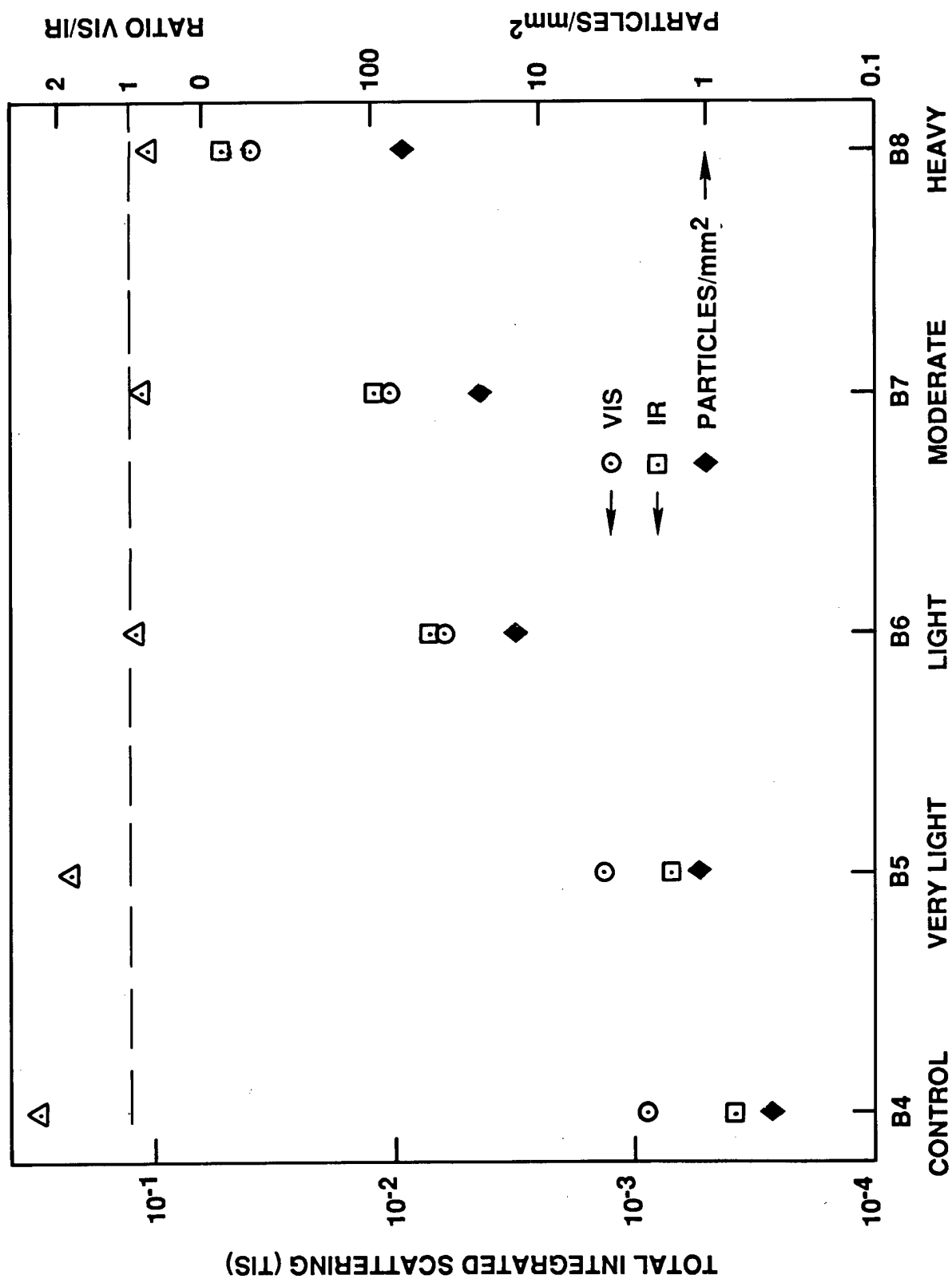
EXHIBIT 33 — TIS Measurements on Dust–Covered Samples

He-Ne 632.8 nm Laser   Beam Splitter   Fold Mirror   Scatter Detector   Digital Voltage Read by HP Computer

Amoco 1064 nm Yag Laser   Beam Chopper   Sample Holder   Coblentz Sphere   Lock-In Amplifier   Signal Input   Reference Input
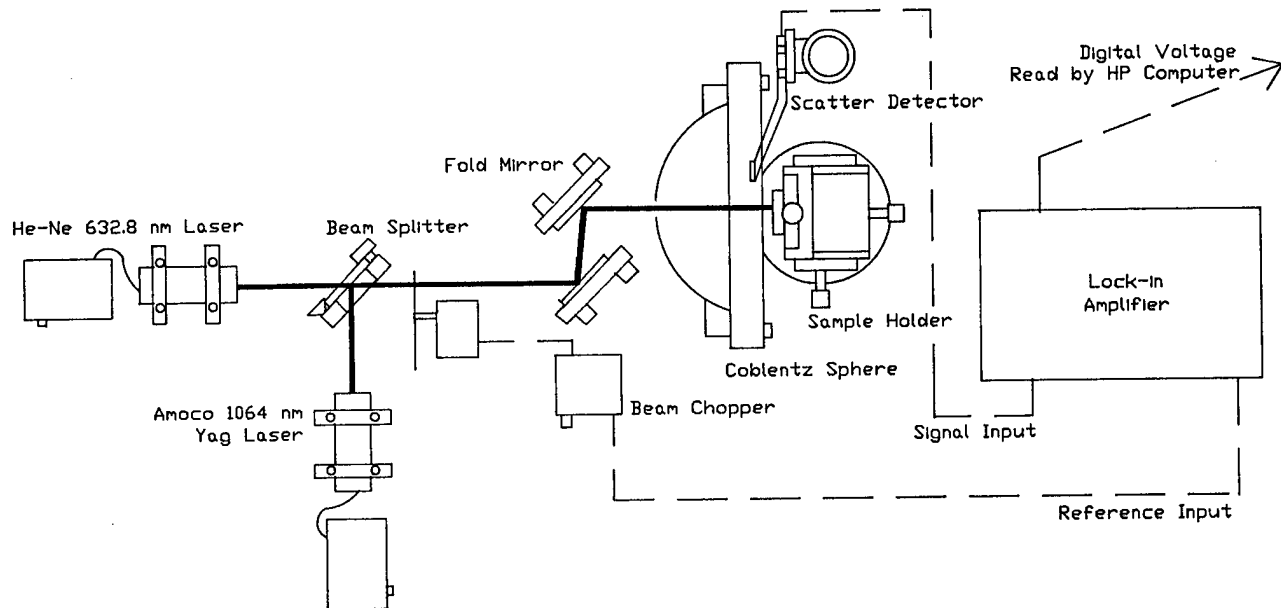
EXHIBIT 34 – TIS Breadboard Fold Mirror Setup

Sample	Wavelength	Without Fold Mirrors		With Fold Mirrors		% Difference
		TIS	% Std. Dev.	TIS	% Std. Dev.	
1	632.8 nm	.000129	16%	.000111	31%	-13%
	1064 nm	.0000751	24%	.0000984	35%	31%
2	632.8 nm	.00131	9%	.00146	14%	11%
	1064 nm	.000791	13%	.000829	19%	16%
3	632.8 nm	.00644	32%	.00690	16%	7.1%
	1064 nm	.00696	33%	.00628	24%	-9.7%
4	632.8 nm	.0597	15%	.0765	2.5%	28%
	1064 nm	.0309	17%	.0574	5.0%	85%
5	632.8 nm	.350	11%	.409	4.0%	16%
	1064 nm	.349	21%	.223	12%	-36%
6	632.8 nm	.0293	26%	.0344	24%	17%
	1064 nm	.00731	11%	.0100	35%	37%

Samples: 1.) High quality Newport AL mirror, 2.) B5 Dusted AL mirror,
3.) B6 Dusted AL mirror, 4.) 5 mil Unexposed Kapton, 5.) 5 mil
Exposed Kapton, 6.) Diamond Turned

EXHIBIT 35 – TIS Fold Mirror Study Measurements

64

concluded that the fold mirrors have no net effect on the performance of the system.

6.2.5 Summary

An instrument designed to measure the total integrated scattering of samples in space has been incorporated into the OPM instrument package. A breadboard version of this instrument has been built and various types of tests and measurements have been made. The instrument has demonstrated an excellent sensitivity for detecting the types of changes in samples that can be expected during flight. The dual-wavelength capability should make it possible to determine the causes of changes measured by the other instruments in the OPM package. Experiments performed in the laboratory have shown that the infrared TIS increases more rapidly than the visible TIS when samples become dusted. If AO, for example, increases the overall roughness of the samples, this should be distinguishable from particulate contamination by showing that the TIS at both wavelengths increases in the same proportion. Furthermore, with the technology currently available (micro-lasers, enhanced silicon detectors, etc.), the instrument can fit easily into the OPM package area and still perform within the desired specifications. Such a tool should prove to be invaluable in studying the optical properties of space-borne materials that will be vital to the success of future missions, such as Space Station Freedom and a manned mission to Mars.

6.3 Vacuum Ultraviolet Spectrometer

The OPM VUV Spectrometer measures the specular reflectance and transmittance of test samples at selected wavelengths in the vacuum ultraviolet from Lyman α (121.6 nm) through 250 nm. The range from 200 to 250 nm permits check-out and test of the VUV System in air while overlapping the wavelength range covered by the integrating sphere reflectometer.

The design chosen for the VUV spectrometer (shown in Exhibit 36) is a
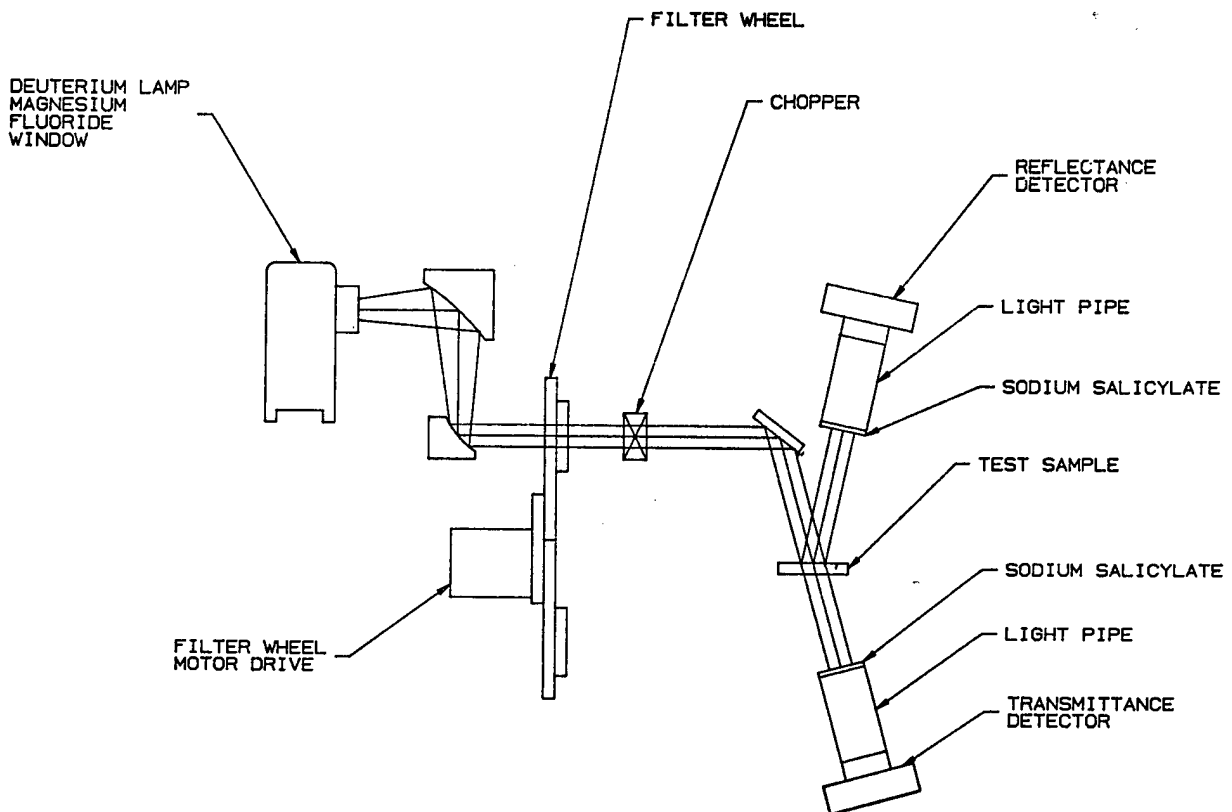
EXHIBIT 36 - VUV Spectrometer Optical Schematic

simple, straightforward design using primarily off-the-shelf optical components. The system consists of a deuterium lamp, filter wheel monochromator, UV enhanced photodiode detectors and associated optics. A standard deuterium lamp with a magnesium fluoride window, developed by Acton Research, is used. Two element-collecting and collimating optics create a 6.3 mm (1/4 inch) diameter collimated beam and direct it though the filter wheel monochromator.

66

The monochromator uses standard narrow bandpass UV filters to select the UV wavelength desired. The major deuterium lines at 121.6 nm and 160.6 nm and selected wavelengths from the continuum that are longer than 170 nm are selected by the individual filters on the filter wheel. The filter wheel is rotated to select the desired filter by a stepper motor controlled by the DACS. The monochromatic beam is chopped using a tuning fork chopper and directed onto the sample at a 15° angle of incidence. Reflectance from—and transmission through—the sample are detected by two UV detector modules. Each module (shown in Exhibit 37) consists of an EG&G HUV4000B UV enhanced silicon detector with a

1. UV light is incident on the flourescent coating
2. The flouresence at 420 nm is emitted evenly with a cosine distribution
3. The light pipe mixes the light rays creating the effect of a spatially uniform detector
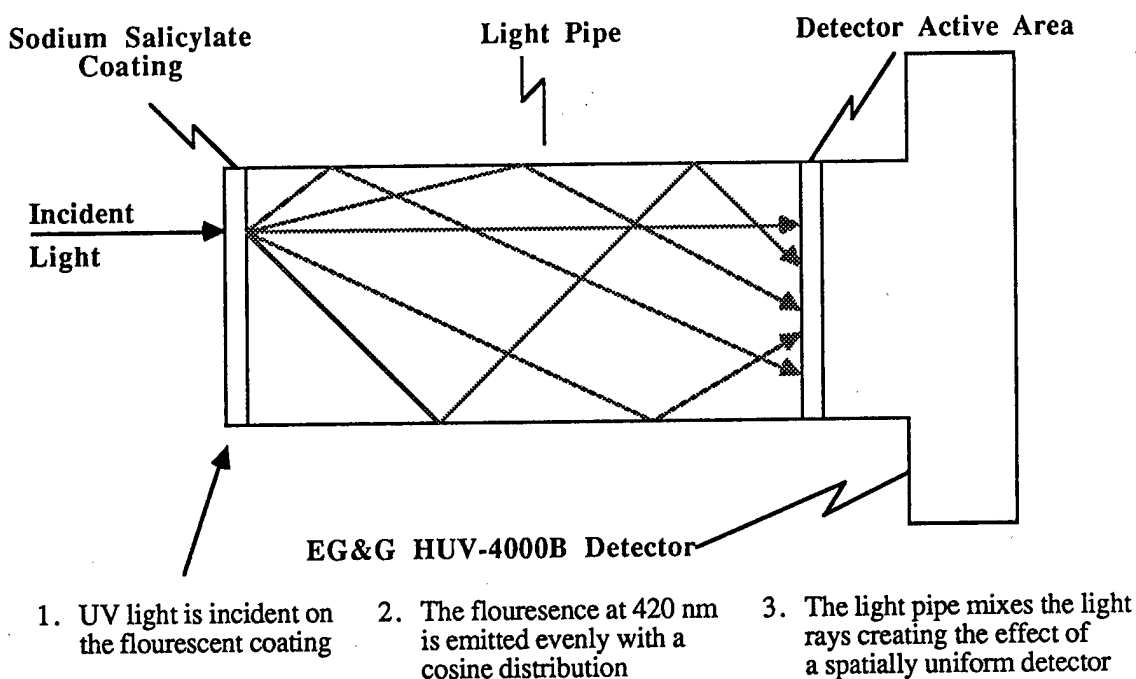
EXHIBIT 37 - UV Detector Module

25 mm (one inch) long light pipe and a sodium salicylate phosphor coating. The transmitted or reflected UV light beam produces fluorescence in the sodium salicylate. The short light pipe acts as a diffuser to correct for non-uniformities in the sodium salicylate coating and detector.

An important calibration feature of the OPM VUV Spectrometer design is the ability to reverse the two detector modules (see Exhibit 38). To reverse the detectors, the detector assembly is retracted, rotated 180°, and translated back into position. This capability—combined with an empty sample position (a hole) on the carousel—provides for calibration of both detectors.

67

TRANSLATION

180 ROTATION
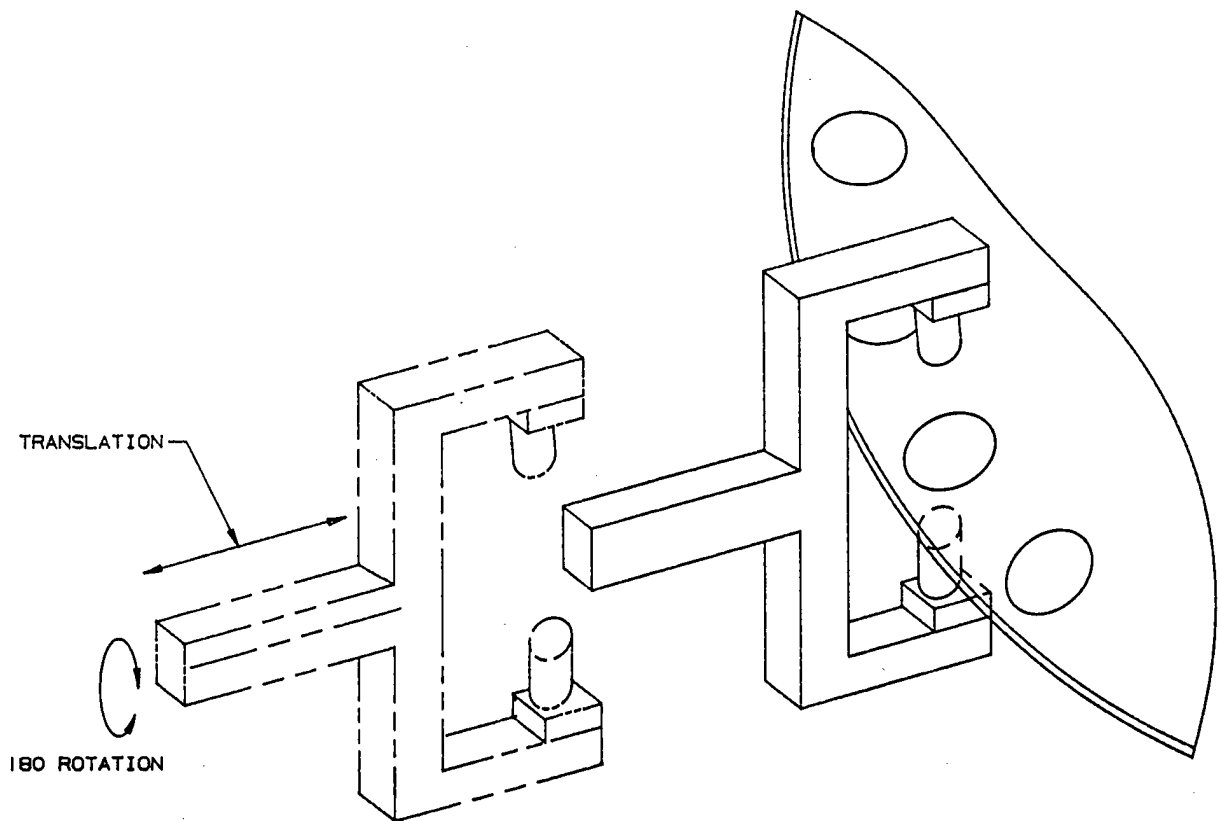
EXHIBIT 38 - VUV Spectrometer Detector Calibration

The outputs of the detectors are read with a phase-sensitive detection analog processor similar to the one used in the Reflectometer and described in Section 6.1.4. This will reduce the effects of stray light, drift and offset. Detector noise then becomes the dominant noise source.

The EG&G detector, with its internal preamplifier, is well characterized for noise.

$$V_n = V_d \sqrt{f}$$

where: V_n = noise voltage at the amplifier output
          V_d = detector noise = 50 $V/(Hz)^{1/2}$
           f = chopping frequency = 160 Hz

So the expected noise at the preamp output is:

$$V_n = 0.632 \text{ mV}$$

68

The expected signal is the product of the lamp intensity, throughput of the optical system, and the detector responsivity. Using worst case values, the throughput of the optical system is:

$$t = t_w \, t_f \, t_o \, a_f \, t_s$$

where:

t_w =   transmission of the magnesium fluoride window = 50%

t_f =   transmission of the UV filter = 10%

t_o =   transmission of transfer optics = 50%

a_f =   quantum efficiency of sodium salicylate = 60%

t_s =   transmission of test sample = 10%

then:

$$t = 1.5 \times 10^{-3}$$

The lamp irradiance with a 25 nm bandpass UV filter is 2.5×10^{-6} watts/cm^2. The detector responsivity from the detector datasheet is 1×10^8 volts/watt at the output of the preamplifier. Therefore, the worst case signal is conservatively 375 mV. With a system noise level of 0.632 mV, this provides a signal-to-noise ratio greater than 500, easily providing the needed 1% measurement repeatability.

6.4 Calorimeter

Calorimeters provide a simple method to determine the solar absorptance (alpha) and total emittance (epsilon) of test samples. The calorimetric technique measures the inputs to the heat balance equation and calculates solar absorptance and total emittance for the test sample. In-space measurements required are the temperature of the test sample and the external heat inputs as measured by the irradiance monitors. The design of the calorimeters isolates the test sample thermally from the OPM to minimize errors caused by radiative and conductive losses. The OPM calorimetric design is the same as that used on the TCSE. This design was developed originally by the GSFC and flown on the ATS-1, ATS-2, and OAO-C satellites.[12]

The calorimetric measurement procedure used on the TCSE and planned for the OPM is an improvement over past experiments for determining total emittance. Previous experiments determined total emittance when the calorimeter viewed deep space only (i.e., no view of the sun or earth). This orientation was difficult to insure, and the time spent in this orientation was, at times, too short to provide accurate measurements. The TCSE and OPM procedure, however, rotates the samples inside the instrument, eliminating any view of the sun or earth.

6.4.1 Calorimeter Description

The calorimeter consists of three major parts: the sample disk, the inner cup, and the outer cup. Exhibit 39 illustrates the construction of the calorimeter.

The concept for the three-part calorimeter is for the inner cup to act as a thermal guard for the sample disk. This design features virtually zero conduction back through the sample holder, low measurable radiative heat transfer to the carousel, and no radiative heat transfer to the sides. The inner cup, or "guard," has the same area and coating as the sample disk to maintain the inner cup temperature close to the temperature of the sample. The thermal capacitance of the inner cup is also as close as possible to the that of the sample disk to ensure the guard is effective—even during transient sample temperatures. Kapton films, formed into cylinders, are used to fasten the sample disk to the inner cup and to fasten the inner cup to the outer cup (as illustrated in Exhibit 39). Crimped double-faced aluminized Mylar sheets are placed inside each cylinder to reduce the radiative heat losses. Vent holes are put in the cylinders and bases of the inner and outer cups, enabling the
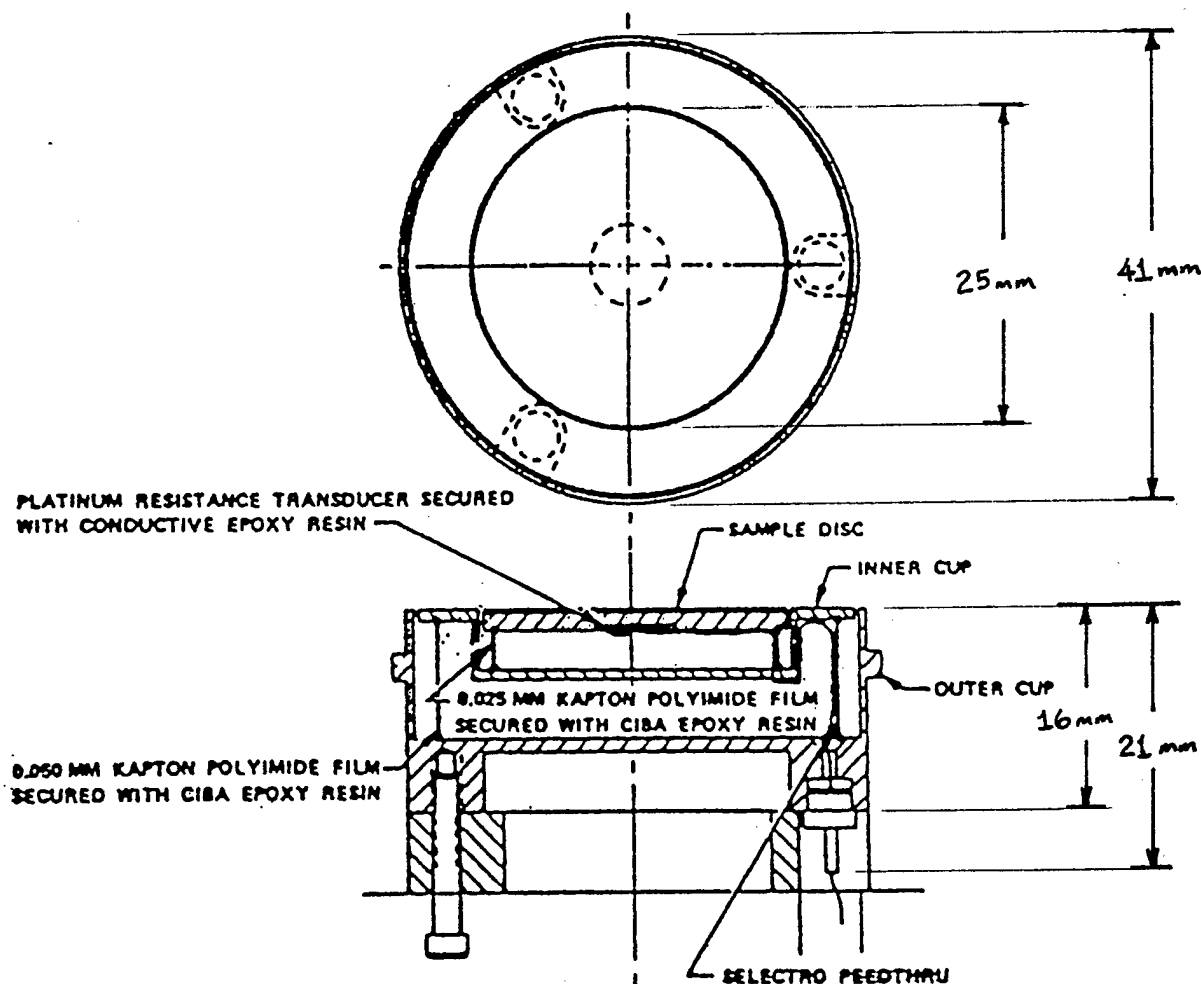
EXHIBIT 39 - Calorimeter Sample Holder

interior of these cups to vent to the vacuum environment. A solar absorber
material is applied to the inner sides of both the inner cup and the outer cup
to minimize errors caused by light leaks through the gaps between the sample,
inner cup, and outer cup. A Platinum Resistance Thermometer (PRT) is attached
to the underside of each sample disk with thermally conducting silver epoxy to
assure good thermal contact with the sample substrate. The DACS monitors the
PRT to measure the temperature of the sample disk.

The calorimeter is clamped onto the carousel by the carousel mounting
cover. The top of calorimeter is flush with the top of the carousel.

Since the materials to be studied using the calorimeters are the same as the materials for the reflectometer measurements; the calorimeter sample holders are used for the reflectance measurement samples only.

6.4.2 Measurement Analysis

The solar absorptance and total emittance of the calorimetric samples are calculated from the energy balance equation for the calorimeter. The energy balance equation for an exposed sample is given as:

Exposed Sample

Energy Balance Equation
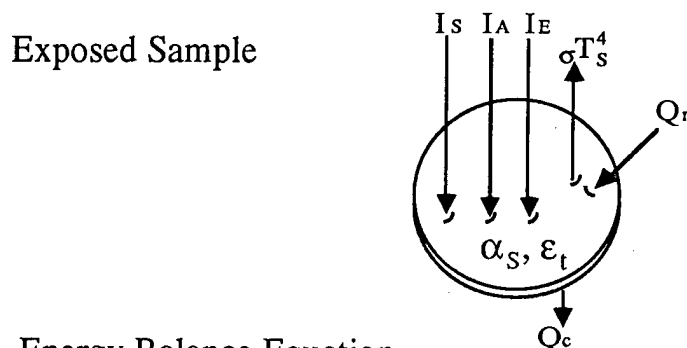
$$A\alpha_S I_S + A\alpha_S I_A + A\varepsilon_t I_E + Qr = A\varepsilon_t\sigma T_S^4 + Qc + [M_S C_S + M_C C_C + M_t C_t]\frac{dT}{dt}$$

where:

I_S = Solar Radiation	A = Area
I_A = Earth Albedo	M = Mass
I_E = Earth Emitted	C = Specific Heat
α_S = Solar Absorptance	
ε_t = Thermal Emittance	Subscripts
Qr = Radiation (gain)	S = Substrate
Qc = Conduction (loss)	C = Coating
T_S = Sample Temperature	t = Temperature Sensor

The solar absorptance will be calculated in terms of total emittance. When the samples are rotated inside the OPM and face the emittance plate, the emittance is calculated directly from temperature data. Once the value for total emittance is known, the solar absorptance can be determined. Specifics of the measurement process follow.

Solar Absorptance/Total Emittance:

The general energy balance equation can be solved for solar absorptance in terms of total emittance. This equation can be simplified in practice when the

72

temperature of the test sample stabilizes. With $dT/dt = 0$ and solving for α_s, the energy balance equation reduces to:

$$\alpha_s = \left[\frac{\varepsilon_t}{I_S + I_A}\right]\left[\sigma T_S^4 + \frac{Q_c - Q_r}{\varepsilon_t A} - I_E\right]$$

This condition occurs on most orbital cycles. To ensure the data for this condition are recorded, the OPM will measure the temperature of the sample and the external heat input (measured by the irradiance monitors) once every minute for one complete orbital cycle. The terms in this equation are either measured or calibrated values and allow the solar absorptance to be calculated in terms of total emittance.

The error sources for determination of α_s/ε_t were analyzed previously for the TCSE mission.[30] From this analysis, the mean error in the alpha/epsilon ratio is 4.8 percent.

Total Emittance:

The energy balance equation can be further simplified by rotating the test samples inside the carousel and exposing them to a massive thermal emittance plate. In this scenario, the insolation and the radiative energy gain from external sources are zero. The energy balance reduces to the classical form where the sample and emittance plate become, in effect, parallel plates. The energy balance becomes

$$\varepsilon' = \frac{Y \frac{dT}{dt} + Qc}{A\sigma (T_P^4 - T_S^4)}$$

where:

$$Y = [M_S C_S + M_C C_C + M_t C_t]$$

$$\varepsilon' = \frac{1}{\frac{1}{\varepsilon_t} + \frac{1}{\varepsilon_P} - 1}$$

ε_P = Plate Emittance

T_P = Plate Temperature

73

Therefore, by measuring the rate of change of temperature of the calorimetric sample while it is viewing the emissivity plate, the total emittance can be calculated. Once total emittance is known, the solar absorptance can be determined from the calculated α_s / ε_t value.

The terms of the energy balance equation that determine the epsilon value are measured or calibrated values. The error sources were also analyzed on the TCSE program[30] similarly to the alpha/epsilon values. From this analysis, the mean error for calculating total emittance is 2.7 percent.

6.5 Atomic Oxygen Monitor

The effects of AO are one of the primary concerns for materials operating in the Low Earth Orbit (LEO) space environment. To characterize the effect of AO exposure on materials, the total exposure or fluence and the time history of the exposure must be determined. To provide this required flexibility, the OPM AO monitor design must be sensitive enough to measure low AO flux levels where sensitive materials begin to exhibit changes. It must also provide a wide dynamic range for long duration OPM missions.

At the lower LEO altitudes (about 300 km) where the Shuttle normally operates, the fluence rate is 10^{18} to 10^{19} atoms/cm^2/sec[31,32] depending on the solar activity. The total fluence on typical shuttle missions has ranged from 6.5×10^{19} to 3.5×10^{20}.

Mission	Fluence
STS-3	2.16×10^{20} atoms/cm^2
STS-4	0.65×10^{20} atoms/cm^2
STS-5	1.00×10^{20} atoms/cm^2
STS-8	3.50×10^{20} atoms/cm^2
STS-41G	3.00×10^{20} atoms/cm^2

At the higher altitudes (up to 500 km) where the Space Station will operate, the fluence is significantly lower in the 10^{16} to 10^{18} atoms/cm^2/sec range, for a total fluence per year of 10^{23} to 10^{25} atoms/cm^2. [31,32]

Given the wide range of potential AO fluence rates and the AO sensitivity of different materials, the OPM AO monitor should be sensitive to less than 10^{18} atoms/cm and provide a wide dynamic range.

The OPM AO monitor consists of multiple carbon film sensors which are exposed sequentially to provide the needed sensitivity and wide dynamic range. The AO sensor uses a carbon film as the active element for detecting atomic oxygen. The carbon sensor is exposed to the AO environment and is eroded away by the reaction of carbon with atomic oxygen. The resistivity of the carbon element is measured by the OPM system to determine the erosion rate of the element. Combining this rate with the AO Reaction Efficiency (RE) for carbon, the total fluence of the exposure is determined. Carbon is chosen as the sensor

material because it has zero order reaction kinetics with atomic oxygen with the resultant products leaving the surface.[33]   It is also electrically conductive for ease of measurement.

The RE for carbon has been measured[20,32-34] at 1.2 x 10^{-24} cm^3/atom, and to lie in the range of 0.9 to 1.7 x 10^{-24} cm^3/atom depending on the temperature and form of the carbon. Other flight and ground experiments are planned, such as the Evaluation of Oxygen Interactions with Materials (EOIM) III[20] Experiment which will provide additional data to characterize carbon's RE better.

The AO sensor is shown in Exhibit 40. It uses two carbon film elements on

AO Monitor Element
Top View

Exposed Carbon Sensor
Cross Section

Protected Carbon Sensor
Cross Section

Gold Contact

Ceramic Substrate

Gold Contact

SiO$_2$ Protective Layer

SiO$_2$ Protective Layer

Exposed Carbon Sensor

Carbon Film

Protected Carbon Sensor

18-3108-0289

Gold Contacts
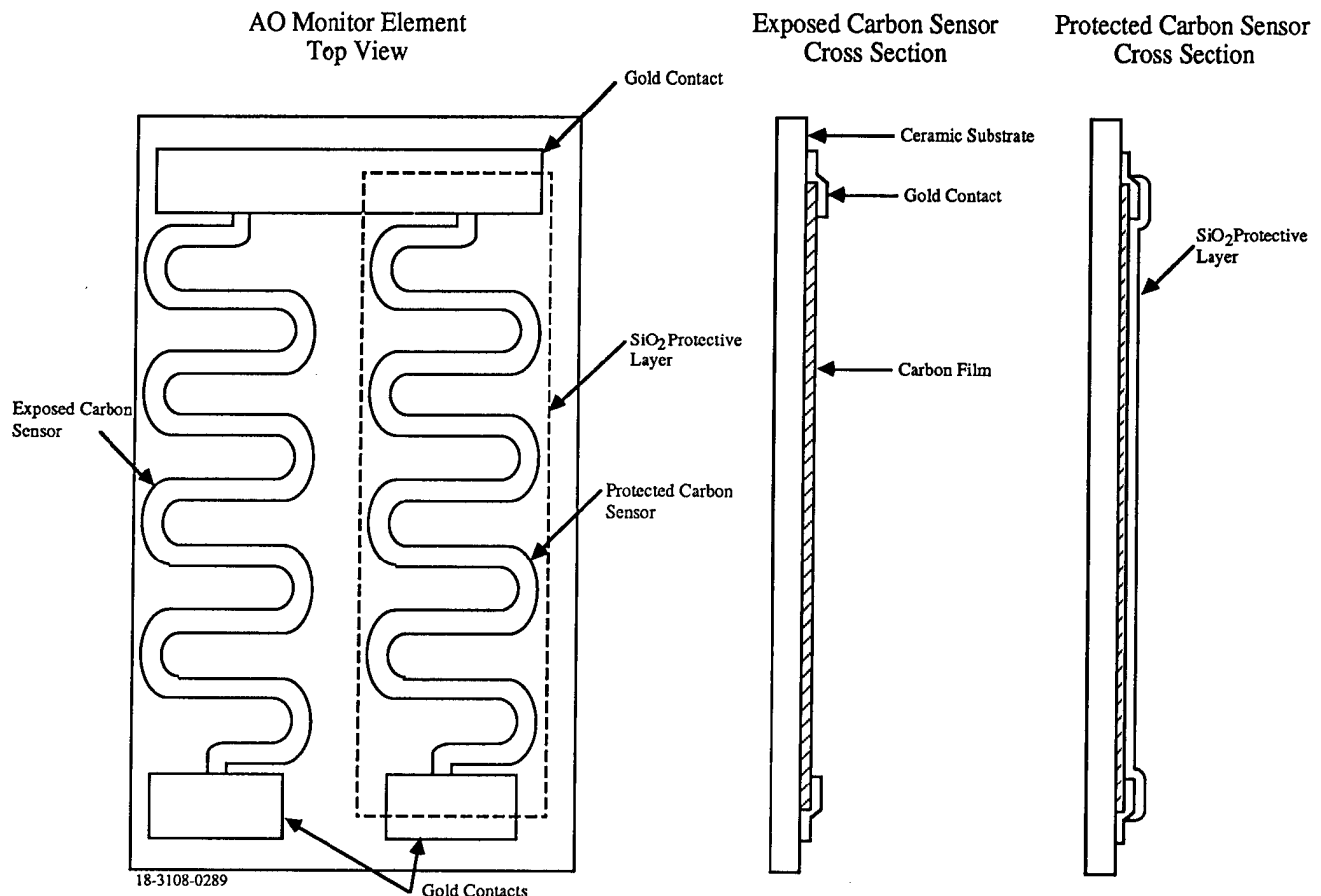
EXHIBIT 40 - AO Sensor Element

a thermally conductive ceramic substrate. One of the elements is overcoated with a protective coating of SiO$_2$ to prevent it from eroding and to account for temperature effects in the resistivity measurements of the sensor. The

76

resistance of each element and the temperature of the substrate are recorded by the OPM data system.

The thickness and dimensions of the carbon film can be selected for each mission to accommodate the expected total fluence. For example, a high fluence Shuttle mission with a fluence of 3.5×10^{20} atoms/cm^2, and an AO erosion rate of 10^{-24} cm^{-3}/atom of carbon, provides an expected loss of 3500 nm of carbon. Using five 1000 nm thick sensors in the AO monitor, the full fluence can be accommodated even with the failure of one sensor.

The carbon film is deposited on the ceramic substrate in serpentine pattern to provide a trace width of 2 mm and a length of 80 mm. At a resistivity of 6×10^{-5} Ω-m for amorphous carbon[35], this initial 1000 nm thick film has a resistance of:

$$R = \frac{\rho}{t} \times \ell$$

where:

ρ = resistivity = 6×10^{-5} Ω-m

t = film thickness = 1000nm

ℓ = film length in squares = 40 squares

and:

$$R = 2.4 \text{ k}\Omega$$

By using a relatively wide trace of 2 mm, the resistance of the carbon film element should remain linear to well below 10 nm in thickness. A more narrow trace could be used, but it would be more susceptible to uneven etching or microdebris impacts. The resistance of the element at 10 nm thickness (end of life) is 240kΩ.

During the OPM Development Phase, the carbon deposition process will be studied. The resistivity and uniformity of the carbon sensor will be dependent on the deposition method used.

The AO monitor assembly, as shown in Exhibit 41, consists of five sensors and a motor-driven mount to position each sensor under the exposure port. During ground processing and launch, all sensors are protected by the AO cover plate. During the OPM initialization, the first sensor is moved to the exposure position. When the resistance of an element rises above a preset value (due to

carbon erosion), the next sensor is moved into position. This preset high resistance value could be caused by the film thickness reaching the minimum value (10 nm) or could be caused by a sensor failure.

The OPM DACS will perform the measurement of the resistance of the sensors (as depicted in Exhibit 42). The analog measurement will be made with 14 bit accuracy providing better than .01% full scale accuracy. This results in better than 1% accuracy at the sensor's end of life.

Multiple AO
Sensor Substrate

28-3853-0989

Sensor Blank
Exposed During
Launch & Reentry

Top View

25.4 cm (10")

5.08 cm
(2")

Exposed AO Sensor

AO Monitor Cover

AO Exposure Port

Side View

Sensor Blank

AO Sensor

AO Sensor Positioning
Geneva Drive
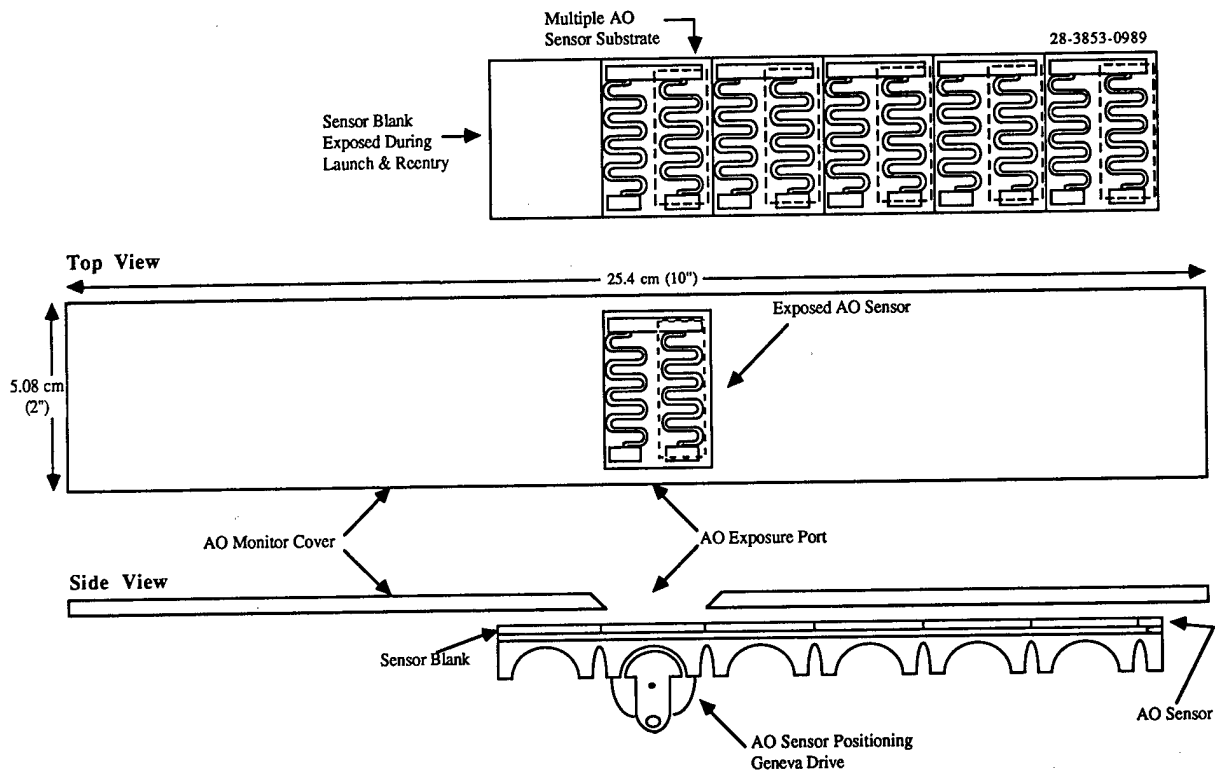
EXHIBIT 41 - AO Sensor Assembly

CMOS
ANALOG
SWITCH

CMOS
ANALOG
SWITCH

SYSTEM
A-D CONVERTER
SUBSYSTEM

CURRENT
SOURCE

AO SENSOR

22-3330-0489
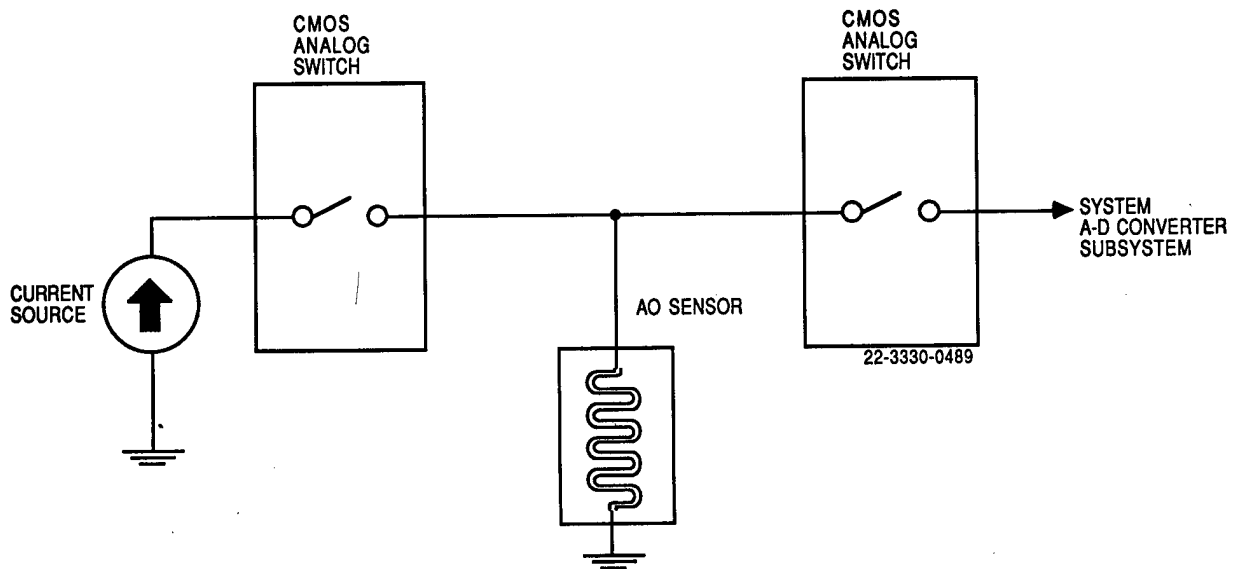
EXHIBIT 42 - AO Sensor Measurement System

79

6.6 Molecular Contamination Monitor

The OPM Experiment will use Temperature-controlled Quartz Crystal Microbalance (TQCM) sensors to monitor the molecular contamination environment to which the flight test samples are exposed. The TQCM sensor is a standard off-the-shelf flight qualified item and is available commercially through QCM Research or Faraday Laboratories. Many TQCM's have been flown with success in measuring contamination.

TQCM sensors have become the standard for measuring molecular deposition (contamination) in the space environment. These sensors feature measurement of partial monolayers of contamination, a wide range of operating temperatures typical of the space environment, and "self-cleaning" by burning off (at high temperature) volatile contaminants deposited on the sensor.

6.6.1 Design Description

The TQCM flight instrument consists of two sensors and the Flight Electronics Unit (FEU). Each TQCM sensor consists of a matched pair of quartz crystals—a sensor crystal and a reference crystal. Each crystal has a natural oscillation frequency of 15 MHz at standard temperature (normally 20 to 25 degrees C). The natural frequency of the sensing crystal is offset from the reference crystal by the beat frequency—typically several KHz. The sensing crystal is also plated with a material that approximates an optical surface. As mass deposition occurs on the sensing crystal, its frequency changes in proportion to mass accumulation. The FEU monitors the shift in the beat frequency and outputs a voltage proportional to the mass accumulation.

A thermoelectric device located in the sensor under the crystals controls the sensor temperature between -199 to +100 degrees C (nominally). The OPM uses two TQCM sensors—one maintained at the carousel temperature and the second controlled to a cold temperature of approximately -30 degrees C. The cold sensor measures the amount of contamination that will condense at the lowest expected mission temperature; the warmer sensor measures the mass accumulated near the temperature of the flight test samples.

The sensors will be mounted in the top plane of the OPM enclosure (refer to the OPM assembly drawing, Exhibit 11, page 30). The FEU will be positioned under the sensors inside the OPM enclosure. Exhibit 43 illustrates typical TQCM sensor and electronics parameters.

80

SENSOR

3"

120 g
(.25lb)

1 1/4"

2"

Temp Range: -199°C to +100°C

Flight Electronics Unit

1 1/2"

8"

• 4kg (8.75 lb)
• Serial Interface
• Z80 on-board processor
• Resolution ±1 Hz
• Total Error <1 Hz
• Control Up to 4 TQCM's

12 1/2"
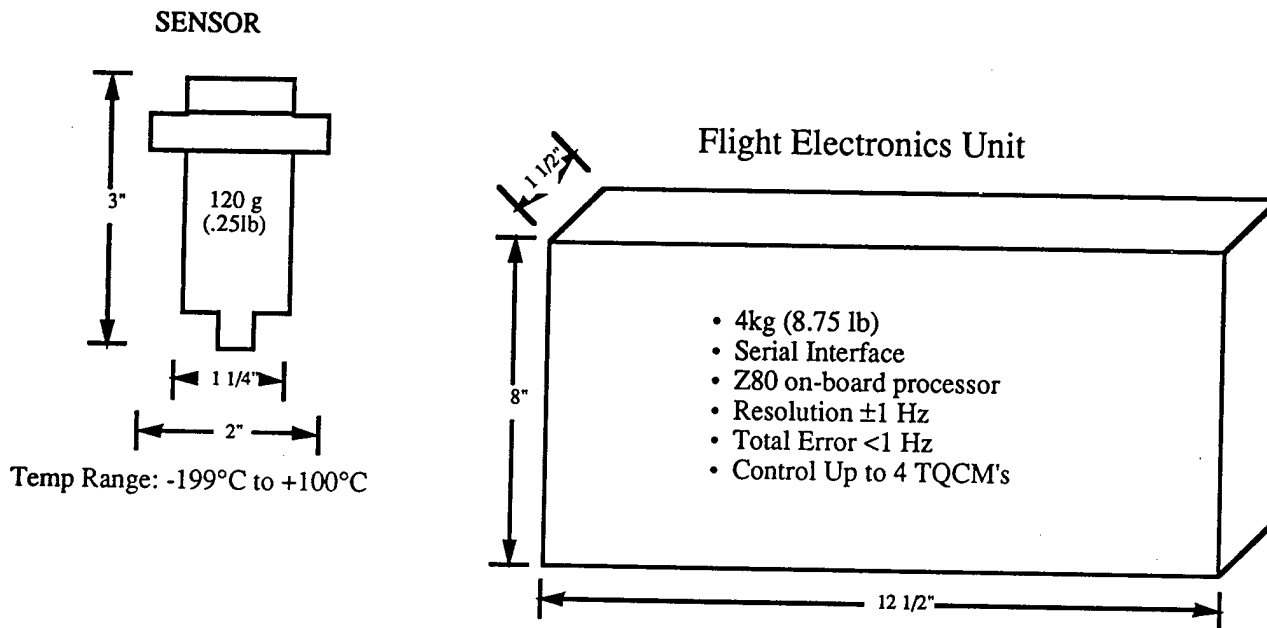
TQCM Sensor Repeatability - 2 Hz

EXHIBIT 43 - TQCM Electronics

The FEU provides power to the sensors and contains a serial data port that interfaces to the OPM DACS. An on-board processor provides temperature control of the sensors and processes the analog information from the sensors. The unit resolution is one Hz and adds less than one Hz error in its computations. The FEU interface to the OPM DACS will transfer data on the sensor temperature, beat frequency, and permit control of the thermoelectric device.

The flight-qualified FEU can accommodate up to four TQCM sensors. Only two sensors are baselined for use in the initial mission. Two other sensors may be added easily for other mission-specific requirements. For example, they may be used as AO monitors or for measuring contamination at other temperatures.

For measuring AO, the TQCM sensor crystal is coated with a material, such as Kapton or Osmium, that is known to erode at a prescribed rate in the presence of AO. Up to 5000 A of the material can be accommodated by the crystal. The FEU monitors the change in the sensor's beat frequency over time to measure mass loss and derive the AO fluence rate. The performance of a TQCM sensor as an AO monitor has been demonstrated on STS-8.[33]

81

6.6.2 Performance Analysis

The performance of the TQCM sensor is affected by temperature variations, irradiance effects, long-term drift, and beat frequency repeatability. TQCM accuracy is difficult to assess. For this analysis, IECM data from the Spacelab 1 mission[36] was used to establish a range of contamination level that should be similar for a short-term OPM mission. In comparison, a full-scale error is assessed based on the mass sensor full-scale deposition. Long-term missions (one year or longer) potentially have a lower full-scale error than short-term (seven- to ten-day) missions, if the mass deposition is permitted to accumulate to maximum levels. The long-term accuracy is better than one percent. Short-term accuracy is on the order of five-to-20 percent for low mass deposition. The parameters affecting the accuracy of the sensors follow.

For the short-term 10-day IECM mission flown on Spacelab 1[36], the mass deposition ranged from one to 40 $\mu g/cm^2$. During this mission, the sensor oriented in the +Z direction (out of the Shuttle bay) accumulated approximately 1.3 $\mu g/cm^2$ of contamination. If a 15 MHz sensor was flown having a sensitivity of 1.6 $ng/cm^2/Hz$, the shift in sensor frequency would have been approximately 810 Hz. The sensor mounted in the +X direction (looking forward in the shuttle bay) accumulated approximately 40 $\mu g/cm^2$. In this case, the shift in the sensor frequency would have been 25,000 Hz. The accuracy in measuring the true mass deposition is investigated to determine how the sensors might perform on the OPM mission.

For a "cold" TQCM sensor (-30°):

Measurement Error Source	Uncertainty Values (Hz) for Various Mission Durations	
	Short (7 day)	Long-term (1 yr)
Drift	3	155
Beat Frequency Repeatability	2	2
Temperature Stability	4	4
Irradiance Effects	150	150
Root-Sum-Square (RSS) Error	150 Hz	215 Hz

82

For the TQCM sensor maintained near carousel temperature:

Measurement Error Source	Uncertainty Values (Hz) for Various Mission Durations	
	Short (7 day)	Long-term (1 yr)
Drift	3	155
Beat Frequency Repeatability	2	2
Temperature Stability	40	40
Irradiance Effects	30	30
RSS Error	50 Hz	165 Hz

The full-scale mass range is approximately 100 $\mu g/cm^2$. The maximum sensor frequency shift, calculated by dividing the mass sensor range by the crystal sensitivity, would be about 62,500 Hz. Therefore, a sensor should not become saturated for the short-term mission. Using the uncertainty values from the data discussed previously, the anticipated range of errors are:

Sensor	Error (Percent)		
	Short-term mission		Long-term mission
	$.3 \mu g/cm^2$	$40 \mu g/cm^2$	
Cold Sensor	150/810=18.5	150/25000=0.6	215/62500=0.3
Carousel Sensor	50/810= 6.2	50/25000=0.2	165/62500=0.3

If the sensors become saturated, recognized by a predetermined shift in the sensor frequency, the sensor will be "cleaned" by raising the sensor temperature to approximately +80 degrees C and burning off the volatile contamination.

Partial monolayers of mass deposition can be measured effectively by the TQCM sensor. Exhibit 44 illustrates the TQCM sensitivity for one monolayer of water deposited on the TQCM sensor. The shift in the sensor frequency caused by one monolayer is 15 Hz. In comparison, the measurement resolution of the FEU is ±1 Hz.

Using Water as an example - A CM^2 area contains ~1×10^{15} molecules
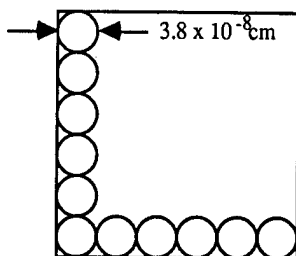
Diameter of Water Molecule = 3.8×10^{-8} cm

Gram Molecular Wt of H_2O = 18

Avogadro's Number = 6×10^{23} molecules/gram mole

The Number of $\dfrac{g}{\text{Molecule}} = \dfrac{18}{6 \times 10^{23}} = 3 \times 10^{-23} \dfrac{g}{\text{Molecule}}$

Then

The Number of $\dfrac{g}{CM^2} = (3 \times 10^{-23}) \times (1 \times 10^{15}) = 3 \times 10^{-8} \dfrac{g}{CM^2}$ or $\dfrac{g}{\text{*EML}}$

For 15 MHz CRYSTAL with Sensitivity ~ 1.6 to 2.0×10^{-9} $\dfrac{g}{CM^2 \, Hz}$ at 25° C

Δf Due to Mass Deposition = $\dfrac{3.0 \times 10^{-8} \, g/CM}{1.6 \times 10^{-9} \, g/CM^2 \, Hz} \simeq 15$ Hz

TQCM Resolution is ± 1 Hz

Equivalent Molecular Layer

∴ Partial Monolayers Can be Measured

EXHIBIT 44 - TQCM Sensitivity

6.7 Irradiance Monitors

The OPM irradiance monitor will measure the external incident energies for calorimetric determination of solar absorptance and total emittance of the flight test samples. It will also monitor the exposure of the flight samples to the direct solar environment.

Two radiometers will be used for irradiance measurements—one for the combined direct solar incidence and earth albedo, and the second for earth-emitted energy (infrared). The design is a simple one using standard detectors and optics similar to those used on the TCSE. Commercially available units (e.g., those manufactured by Eppley Laboratories) would also be suitable for the OPM.

6.7.1 Design Description

The radiometer for this experiment will consist of a thermopile detector (a multiple-junction thermocouple) painted flat black covered with suitable optics that selectively pass the external energy flux. Multiple junctions increase the sensitivity of the detector to the incident energy flux and give a greater voltage output. The optics, similar in design to those used in the TCSE, will be a concave/convex focusing lens to tailor the field-of-view of the radiometer to the flight test samples. The lens material is selected to tailor the spectral response of the radiometer. For the spectral region of 0.2 to 3 micrometers, a quartz lens is used. A germanium lens will be used for the infrared spectrum— between 2 and 20 micrometers. The unit will be recessed into the carousel to permit the top of the lens to be flush with the carousel top.

Data from the two radiometers will be recorded simultaneously with the calorimetric temperature measurements to enable calculation of solar absorptance and total emittance. The irradiance values for the solar incidence will be summed to determine the total solar exposure for the flight test samples.

6.7.2 Performance Requirements

Standard off-the-shelf calibrated "Meteorological" radiometers can give instrument accuracy better than one percent. By definition, the "instrument" meaning combines the thermopile (detector) and the optics (lens). This accuracy is degraded by temperature dependence, stability (drift), linearity, and other factors. However, for short-duration missions, measurement inaccuracies can be reduced by pre- and post-flight calibration. For long-duration missions, self-

85

calibrating units enhance performance by reducing measurement errors. When the irradiance "system" is defined to include the radiometer plus the OPM and spacecraft, a "system" accuracy of five percent is likely. The "system" accuracy depends on how well the angle of incidence and orientation to the energy sources are known. These data will be determined from the spacecraft attitude data. The radiometer "system" accuracy at near normal angles of incidence will not be significantly degraded because of errors in attitude data. However, due to the near cosine response of the radiometer, the "system" accuracy approaches five percent for low angles of incidence.

The spectral range of the three energy sources--direct solar, earth albedo and earth emitted IR--overlap, and, therefore, cannot simply be separately measured by the radiometers. The radiometer, with the quartz lens, will see mainly the direct solar and earth albedo. The radiometer with the germanium optics will see mainly the earth emitted IR. By knowing the spacecraft and OPM attitude with respect to the earth and sun, these three radiant components can be calculated.

6.8 Data Acquisition and Control System (DACS)

The OPM DACS will control all aspects of experiment operation, process and collect the analog and digital data, format and transfer data to the spacecraft data interface, and condition and distribute power to all OPM systems. Exhibit 45 summarizes the control functions that the DACS must perform. Exhibit 46 summarizes the measurements to be made.

Subsystem		Function
Reflectance	-	wavelength positioning
	-	slit positioning
	-	detector selection
	-	lamp selection
	-	analog integrator control
TIS	-	laser selection
	-	detector selection
VUV	-	filter wheel positioning
	-	detector reversal
	-	detector selection
TQCM	-	temperature control
AO Monitor	-	sensor positioning
	-	sensor selection
Sample Carousel	-	sample positioning
Power	-	subsystem power distribution

EXHIBIT 45 - OPM Control Functions

Analog Measurement	Number	Digital Measurement	Number
Reflectance - Reference	1	TQCM	2
Reflectance - Sample	1		
TIS - Scatter	1		
TIS - Laser	1		
VUV - Reflectance	1		
VUV - Transmission	1		
Radiometer	2		
AO Monitor Sensor	5		
AO Monitor Reference	1		
Pt Temp Sensor	30		
Pt Temp Reference	2		
Thermistor Temp Sensor	28		
Thermistor Temp Reference	2		
Voltage Monitor	15		
Voltage Reference	1		
Number of Analog Measurements	92		

EXHIBIT 46 - OPM Measurement List

The heart of the DACS (see Exhibit 47) is the microprocessor-based data system controller. It will use a stored program in system Programmable Read Only Memory (PROM) to issue the required control sequences and collect the measurement data. A real time mission clock is read by the data system controller to know when to perform scheduled functions and to time tag experimental data.

The DACS consists of six subsystems (see Exhibit 47):

- o Analog
- o Reflectometer
- o TIS
- o VUV
- o Sensor monitoring
- o Power.

These will be described with the Ground Support Equipment (GSE) and spacecraft interfaces and the DACS software in the following sections.

6.8.1 Analog Subsystem

The analog subsystem consists of the system analog multiplexer, which will select the appropriate analog signal for measurement as controlled by the data system controller. The system Analog-to-Digital (A-D) converter converts the analog signal to digital data for collection by the controller. A 15 bit A-D converter will provide a 14 bit measurement accuracy (better than 0.01%).

6.8.2 Reflectometer Subsystem

The reflectometer subsystem performs all the reflectometer control functions under direction of the system controller and processes the analog data from the two integrating sphere detectors. To perform a measurement, either the tungsten or deuterium lamp is selected and allowed to stabilize. The desired wavelength and slit position is selected by operating the appropriate stepper motor. The detector is selected and its output processed by the phase-sensitive detector system (as described in Section 6.1.4). The sample and reference signals, as indicated by the position of the beam director reference mirror, are measured by the system A-D converter system. Exhibit 48 illustrates the reflectometer measurement and control subsystem.
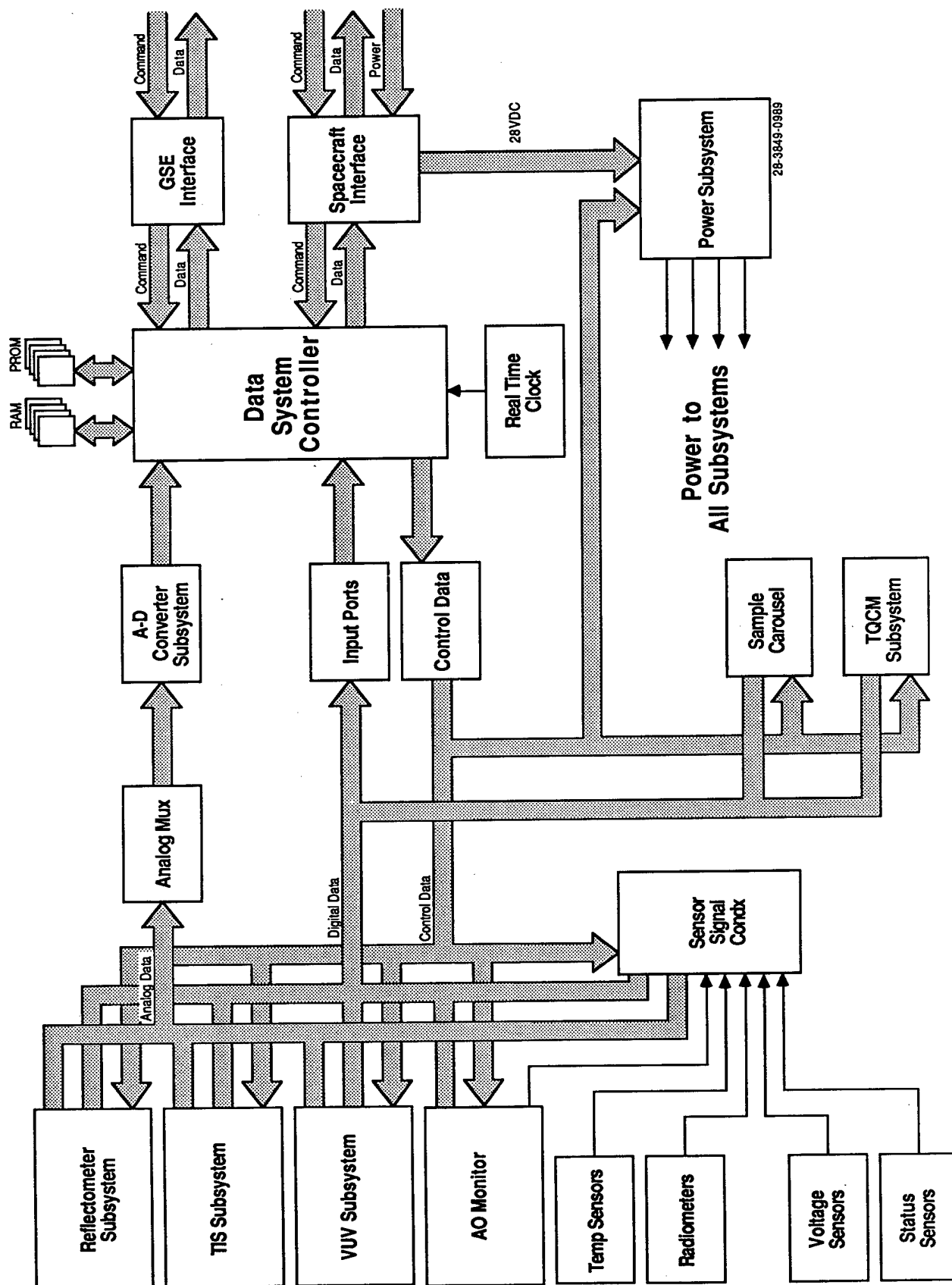
EXHIBIT 47 — OPM Data Acquisition and Control System

89
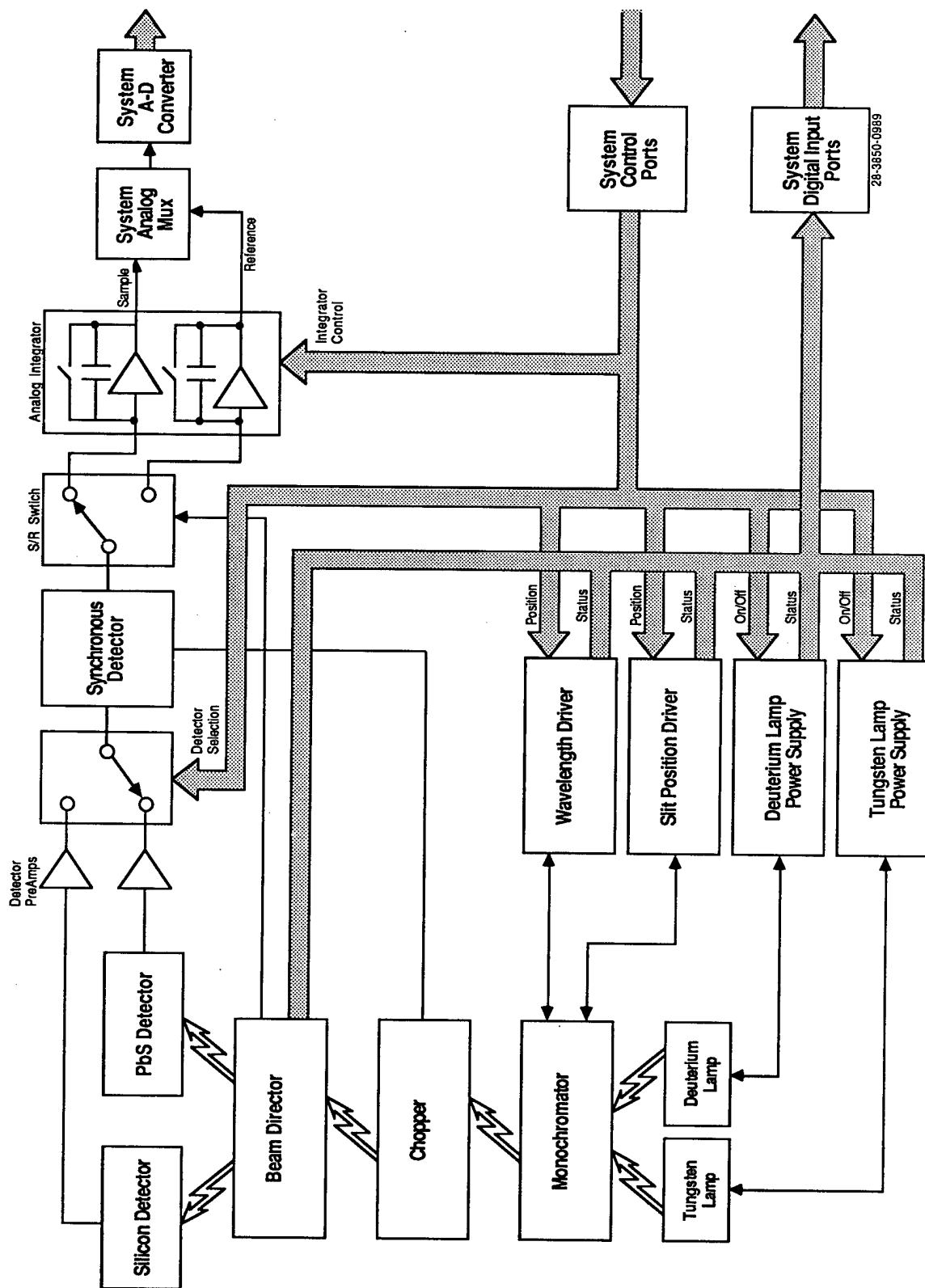
EXHIBIT 48 – Integrating Sphere Reflectometer Subsystem

28-3850-0989

90

6.8.3 TIS and VUV Subsystems

The TIS and VUV subsystems, as shown in Exhibits 49 and 50, respectively, operate similarly to the reflectometer subsystem. The lasers are turned on (TIS instrument), the proper filter (VUV subsystem) and detectors are selected, and measurements are made. All three optical instruments use a chopped optical system and synchronous electronic detection to provide an improved signal-to-noise performance. The VUV control subsystem has an additional function—to reverse the positions of the reflectance and transmission detectors for calibration.

6.8.4 Sensor Monitoring Subsystem

The sensor monitoring subsystem, as shown in Exhibit 51, controls the AO monitor and selects and conditions the radiometer data, AO sensor data, temperature data and system voltage monitors. This subsystem selects, conditions and multiplexes 86 of the 92 analog signals in the OPM. The AO monitor stepper motor is pulsed to move each AO sensor into exposure position under control of the system controller. Complementary Metal-Oxide Semiconductor (CMOS) analog multiplexers are used to select the sensor and apply the appropriate signal conditioning. Each analog multiplexer will have a reference channel to provide calibration data. Fifteen voltages will be monitored throughout the OPM to determine system status. A voltage reference is also provided to calibrate the A-D converter.

The TQCM FEU, also controlled by the DACS, contains a serial digital data port. The DACS will control the TQCM sensor temperatures and monitor the shift in crystal beat frequency to determine contaminant accumulation.

6.8.5 Power Subsystem

The OPM power subsystem converts the 28 volt Direct Current (DC) spacecraft power to the various voltages required to power the OPM systems, including electronics, lasers, lamps, and stepper motors. High efficiency–switching DC to DC converters will be used to provide these different voltages. This power is distributed to the appropriate systems under control of the data system controller.

91
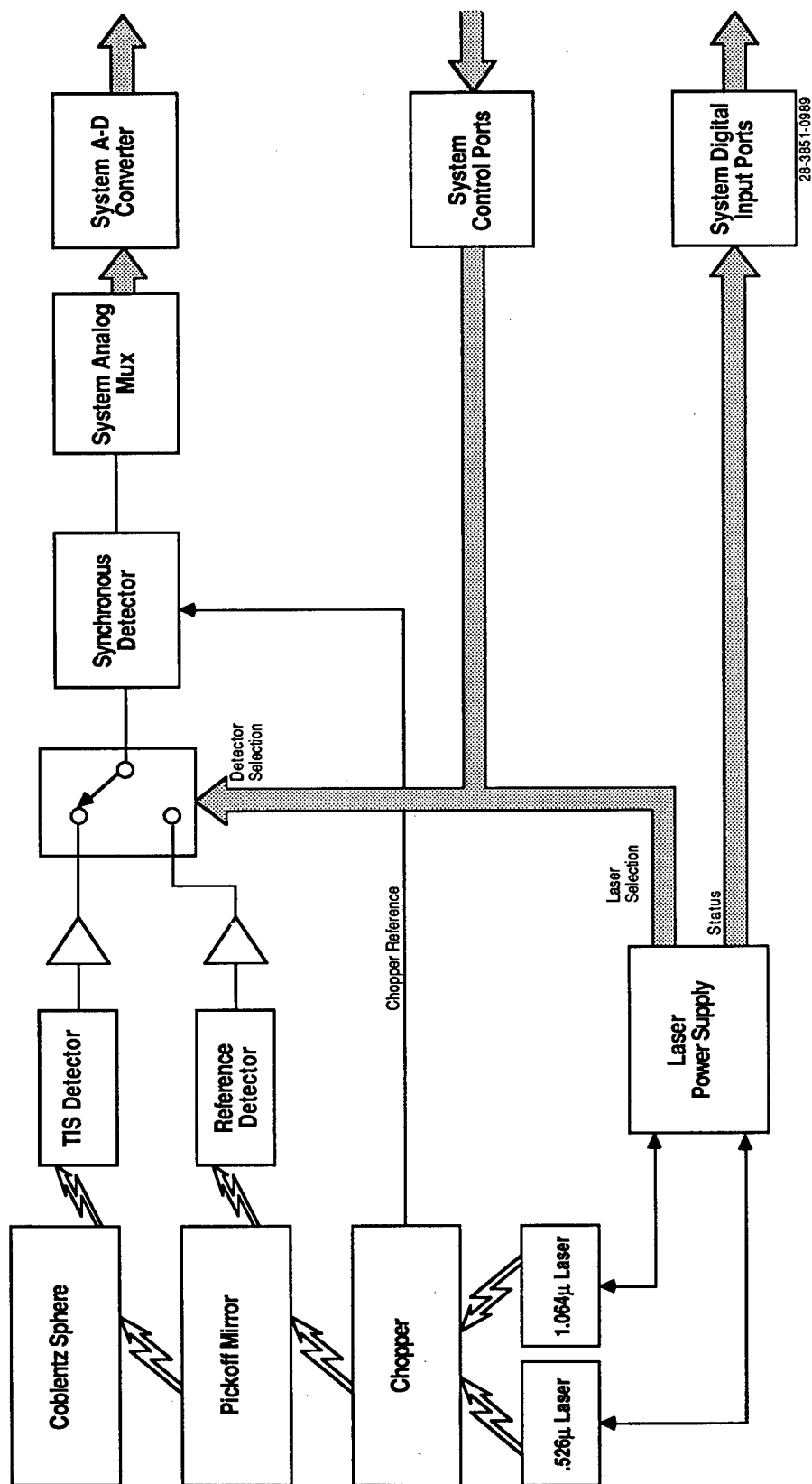
EXHIBIT 49 – TIS Spectrometer Subsystem

28-3851-0989

92

EXHIBIT 50 - VUV Spectrometer Subsystem

22-3324-0489

93
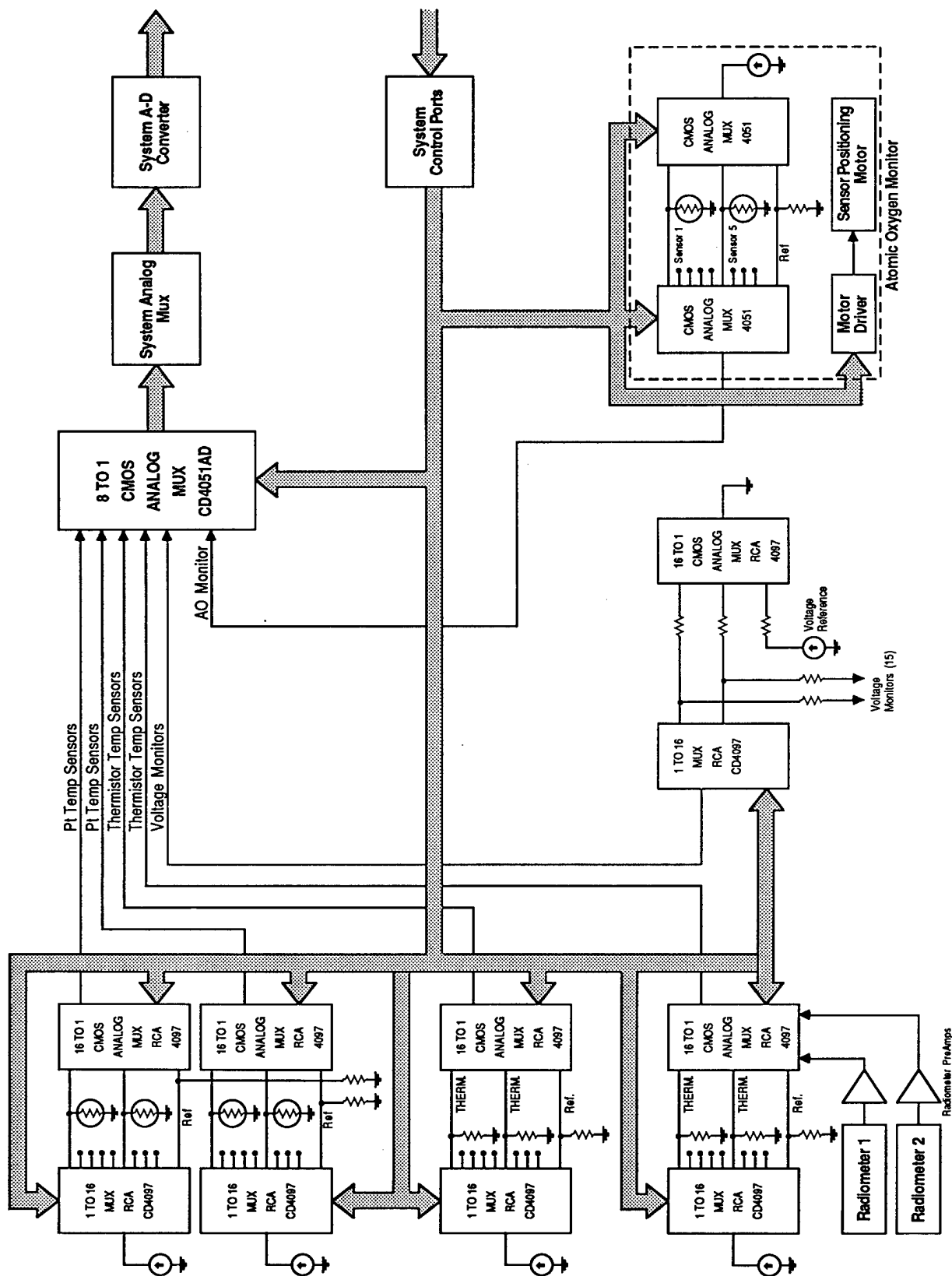
EXHIBIT 51 – Sensor Monitoring Subsystem

94

6.8.6 GSE and Spacecraft Interface

There are two external interfaces to the DACS--the GSE interface and the spacecraft interface. When the GSE is connected, the GSE assumes control of the operation of the DACS. When the GSE is disconnected, control is through the spacecraft interface. The GSE interface provides a high-speed serial command and bi-directional data transfer capability. The spacecraft interface also provides a serial command and data transfer capability compatible with the payload carrier. The DACS will collect the experimental data and assemble them into appropriately-sized buffers for transfer to the spacecraft data system. The data will then be sent to the ground through the spacecraft telemetry system. The quantity of data collected by the OPM for a seven-day mission is:

Reflectometer Data Set	15,076 bytes
TIS Data Set	15,600 bytes
VUV Data Set	1,884 bytes
Calorimeter Data Set	15,360 bytes
TQCM Data (1 minute intervals)	23,040 bytes/day
House Keeping	11,520 bytes/day
Total Data for 7 Day Mission	**577,360 bytes**

The spacecraft interface also provides the 28 volt DC spacecraft power to operate the OPM.

6.8.7 Software

The OPM DACS software will be developed in modular form as a task-driven system. A subroutine or task for each control and measurement function will be developed and tested separately. Flight software and test software will be a sequential task scheduling system. The design will provide the required flexibility to reprogram the OPM easily for different missions. This also provides the inherent capability to command special real-time operations of the OPM from the ground through the spacecraft command interface. The GSE will serve as the flight or test software development system. The developed or modified software can be downloaded into transient Random Access Memory (RAM) for testing or programmed into PROM for qualification testing and for the OPM mission.

6.9 OPM Power/Weight

The power and weight budgets for the OPM experiment have been developed to determine the suitability of flying the OPM on the standard payload carriers. The power requirements and the weight of the OPM are modest and can be accommodated on many different carriers.

6.9.1 Power Budget

A preliminary power budget has been prepared that assesses the power and energy requirements of the OPM experiment. Each subsystem was evaluated individually for instantaneous and operating power requirements, and then integrated to determine accumulated energy requirements.

The measurement timeline, (Exhibit 52) illustrates the power requirements
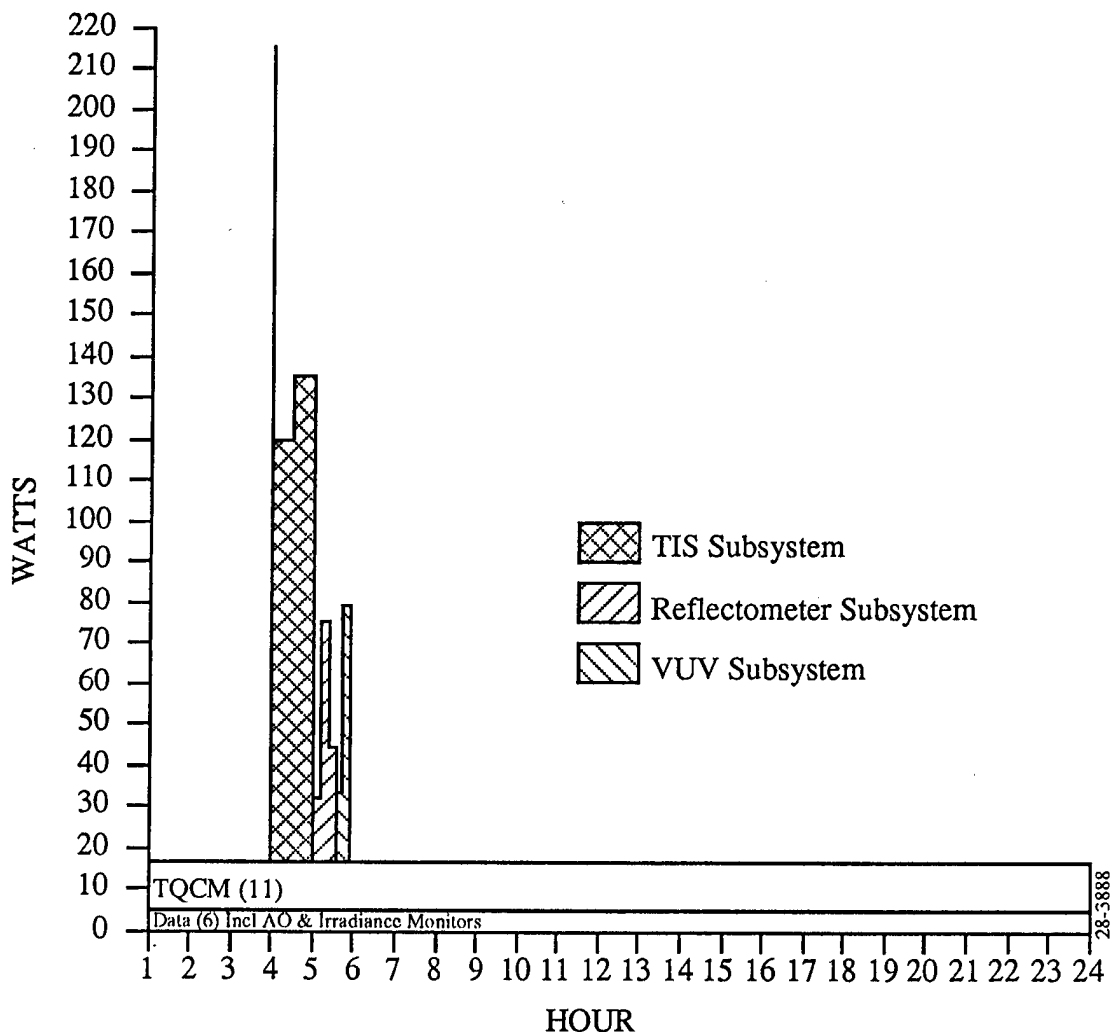
EXHIBIT 52 - Measurement Timeline

for a typical 24-hour day for the initial OPM mission. This timeline includes power requirements for the monitor and measurement subsystems. The monitor subsystems include the DACS, AO, irradiance, and the TQCM subsystems and they operate continuously throughout the mission. The measurement subsystems include the VUV, TIS, and reflectometer subsystems. They are operated once per day. The three optical measurement subsystems are operated sequentially so that only one is operating at a time. The time for the measurement subsystems to operate is estimated at 1 1/2 hours per measurement cycle.

The basis for developing the measurement timeline and preliminary power budget are:

- 7-day mission
- daily reflectometer measurement, duration of less than 20 minutes
- daily TIS measurement, duration of less than one hour
- daily VUV measurement, duration of less than 15 minutes
- continuous measurement of the AO, Irradiance, TQCM, and DACS subsystems

The preliminary power budget is shown in Exhibit 53. The continuous power

Item	Power (Watts)		Duty Cycle	Energy (w-hr)
	Turn-On	Peak Operating		
TIS Subsystem	200	120	daily	101
Reflectometer Subsystem		60	daily	9
Data System		6	100%	150
TQCM System (2 sensors)		11	100%	265
AO System		<.1	100%	2
VUV System		60	daily	9
Irradiance System		<.1	100%	2
				538

Continuous Power	<20 watts
Peak Operating Power	137 watts
Instantaneous Peak Power	200 watts
Total Energy Requirements	538 watt-hr
Average Power Requirement	22.4 watts

EXHIBIT 53 - Daily Power Budget

97

requirements are quite low, averaging less than 20 Watts. The peak operating power is estimated to be 137 Watts and is comprised of the TIS instrument and the monitoring subsystems. There will be very short periods--around 5 seconds--when the peak power will rise to approximately 200 Watts. This power peak occurs when the TIS lasers are turned on. The daily total energy requirements of the OPM experiment are also shown in Exhibit 53. A nominal seven-day mission would require less than 4 kWh. The main energy consumers are the TQCM system and the DACS.

The modest power requirements of the OPM can be accommodated by most available payload carriers. By comparison, the lowest power offered by any Shuttle payload carrier for a single payload is 500 Watts. The 140 Watt requirement is even less than the lowest projected power payload for the Space Station--the SARR Generic payload.

6.9.2 Weight Budget

A preliminary weight budget has been developed that addresses the requirements of each subsystem and the OPM enclosure. Exhibit 54 contains the weight by subsystem. The total projected weight is approximately 77 kg (170 pounds). This weight is accommodated easily by every payload carrier considered.

Item	lbs
TIS Subsystem	24
Carousel (including motor drive)	50
Reflectometer Subsystem	26
Data and Control System	10
TQCM Subsystem (2 Sensors)	9
AO Subsystem	2
VUV Subsystem	5
Irradiance Subsystem (2 Radiometers)	4
OPM Enclosure	40
Total (Estimated) Weight	170 lb
	(77 kg)

EXHIBIT 54 - Weight Budget

98

6.10 Thermal Design

The OPM is required to operate with a range of payload carriers for different mission duration and orbital parameters. The OPM thermal design must be flexible enough to accommodate these differences and maintain the internal components within their rated temperatures. The OPM thermal design will be passive, but will be adjustable for the different mission conditions. This will be accomplished by providing the capability to adjust the conductive and radiative coupling of the OPM to the payload carrier structure and the thermal environment of space.

The L-shaped baseplate is the major structural and thermal element in the OPM design. All other systems are mounted to the baseplate or thermally sinked to it. Mounting brackets will be used to fasten the baseplate to the payload carrier. Different configurations of these mounting brackets will provide either a thermally conductive path between the carrier and the OPM or a thermally insulating path.

The top and side panels of the OPM enclosure will be mounted to the baseplate in a similar manner allowing these panels to serve as thermal radiators if needed. The thermal coatings on these panels can also be changed to provide an additional measure of adjustment.

A thermal model of the OPM will be developed during the flight hardware development phase to evaluate the adjustable thermal configuration of the OPM system for different missions. When an OPM mission is approved, this model will be used to determine the optimum configuration for that mission.

6.11 Spacecraft Interface

The spacecraft interface is the interface between the OPM and the payload carrier. Through this interface, the spacecraft (or payload carrier) provides the mechanical mounting of the OPM, a thermal sink, power, and a data interface.

6.11.1 Mechanical

The OPM is mounted onto the payload carrier with the OPM sample carousel exposed to the space environment with a field-of-view of 150° in all directions. The payload carrier must support the OPM's weight of approximately 77 kg (170 pounds) at the dynamic loads throughout the mission. The OPM can be mounted from the bottom or from one side (see the OPM assembly drawing in Exhibit 11, page 30). For a side mount, the carrier mount must be able to support the 77 kg experiment with a CG at 38 cm (15 inches) from the side.

6.11.2 Thermal

The payload carrier provides a thermal sink to the OPM through the mounting structure. This conductive thermal sink combined with the thermal radiative properties of the OPM top and side panels provide the passive thermal control of all the OPM components.

6.11.3 Power

Twenty-eight volt DC power is supplied by the payload carrier to the OPM. The average power requirement is less than 25 watts, with an instantaneous peak power of 200 watts. The total energy requirement for a seven-day mission is 3.8 kilowatt-hours.

6.11.4 Data

The payload carrier and the spacecraft provide the capability to collect the OPM experiment data and transmit the data to the ground for analysis. This data interface also provides a command capability to control the OPM from the ground for special measurements and diagnostic tests. The data interface is a bi-directional serial digital link. The OPM data interface will provide a programmable transmission rate to match the capability of the different payload carriers. The OPM will generate about 577 kilobytes of data over a seven-day mission.

6.12 Ground Support Equipment

The GSE for the OPM will serve multiple functions, including development test support, qualification test support, mission programming, integration support, and data analysis. The GSE connects to the OPM through two interfaces--the GSE control port and the spacecraft interface (as discussed in Section 6.8.6). When the GSE is attached to the OPM, it will operate in three modes:
   o Full control mode
   o Flight simulation mode
   o Interface test mode.

In the full control mode, the GSE will control all aspects of OPM operation. It will be able to control individual operations such as stepper motor control, select a detector or take a single analog or digital measurement. The full control mode will be able to initiate full measurement sequences for individual instruments or for all instruments. It will also be able to upload test sequences to the DACS for development or qualification test support.

In the flight simulation mode, all aspects of the spacecraft interface, including power, control, and data collection are simulated. This mode will be used to test the OPM hardware, without the GSE connected, through its main control port which simulates normal flight operation.

The interface test mode will be used to verify the spacecraft interface during payload integration. In this mode, the OPM will be operated with the spacecraft interface and the GSE connected through the GSE control port.

The GSE will provide two off-line functions of software development and data acquisition/analysis. Both test and operational software will be developed on the GSE. The GSE will be used to program the system PROM's for each mission. Data collected during testing and the flight mission will be decoded and processed to provide tabular and graphical reports.

The GSE is shown in Exhibit 55 and consists of a computer with appropriate standard peripherals, a PROM board programmer module, GSE interface, and simulated spacecraft interfaces for power, control and data.

High Speed
Serial Interface

GSE
Control
Port

GSE Computer

Standard I/O

Custom I/O

Keyboard

Graphics
Display

Disk Drives

Tape Drive

Printer

Plotter

OPM
Spacecraft
Interface

Spacecraft
Command
Simulator

Spacecraft
Data
Simulator

28V Power
Supply

PROM Board
Programmer
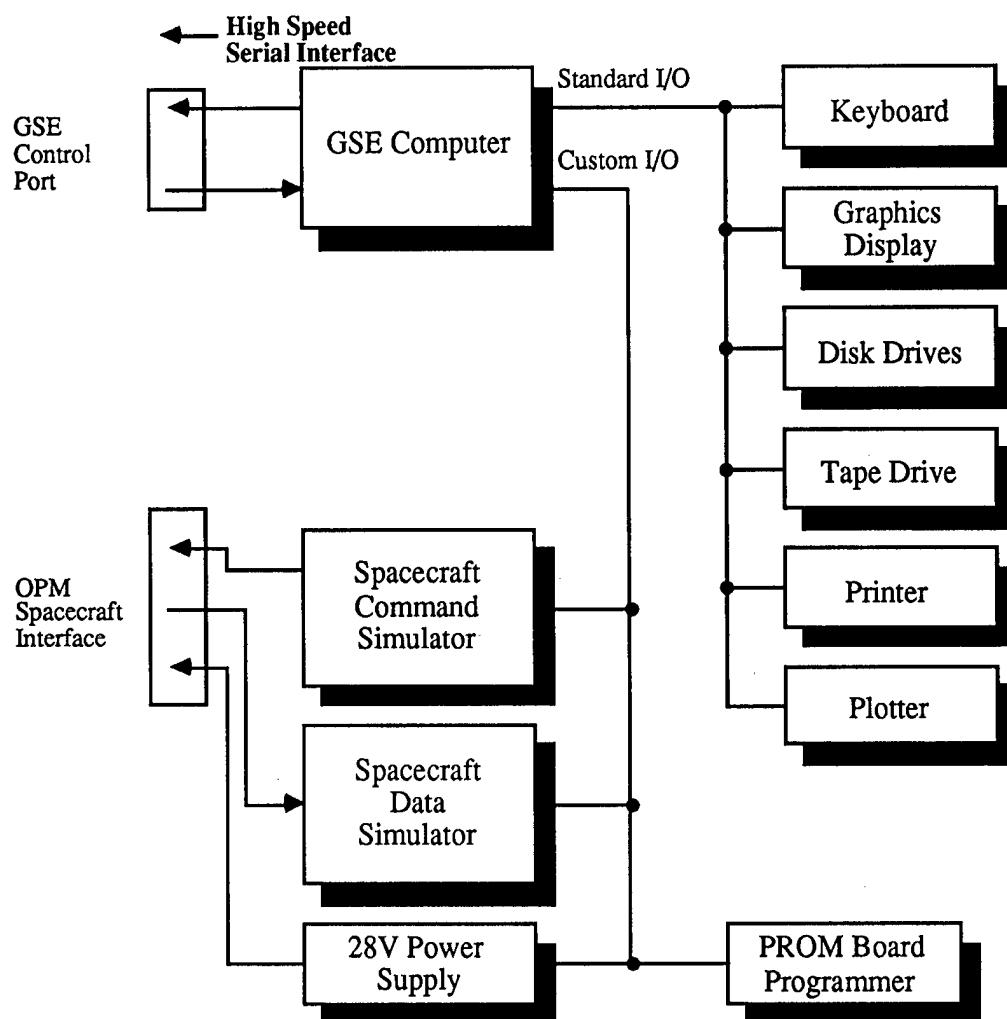
EXHIBIT 55 - OPM Ground Support Equipment

102

6.13 Design Guidelines

These design guidelines are issued for use by the OPM system designers as a guide for the design, fabrication and testing the OPM flight hardware. These design guidelines are applicable to the OPM Experiment and the individual components within the OPM. The guidelines will be updated as required during the Developmental Phase effort.

6.13.1 Documentation

Documentation requirements shall be minimized where possible for lower costs. Functional, performance, and quality tests are required and shall be documented. All test procedures shall be approved prior to testing. Test data shall be included with the shipment of each instrument. Drawings shall be constructed using a PC-based Computer Aided Design (CAD) package:

6.13.1.1 Applicable Documents

The following documents are included for reference to the extent specified. If there is a conflict between this document and any other document referenced, the contents of this document shall apply.

6.13.1.1.1 NASA Documents

- HHG-730-1503-04; Hitchhiker Shuttle Payload of Opportunity Carrier, Customer Accommodations and Requirements Specification, GSFC, July 1988.

- NHB 1700.7,RevA; NASA Handbook "Safety Policy and Requirements for Payloads Using the Space Transportation System (STS)", latest date of issue

- JSC-SN-C-0005A   Specification, Contamination Control Requirements for the Space Shuttle Program

- JSC-R-0022A   General Specification Vacuum Stability Requirements of Polymeric Material for Spacecraft Application

- JSC-08962   Compilation of VCM Data of Nonmetallic Materials

- MSFC-HDBK-527   Materials Selection List for Space Hardware Systems

- (MSFC) 40M38277   Specification, connectors, electrical, circular, miniature high-density, environment resisting

- (MSFC) 40M39569   Specification, connectors, electrical, miniature circular environment resisting

- MSFC-STD-506   Standard, material and process control

- (MSFC) 50M02442   ATM material control for contamination due to outgassing

6.13.1.1.2 Military Documents

- MIL STD 810C   Environmental Test Methods
- MIL Spec MIL-B-5078B   Bonding, Electrical, etc.

6.13.1.1.3 Other Documents

- (JSC) SL-E-0002   Specification, electromagnetic interference characteristics requirements for equipment for the Space Shuttle program

6.13.2 Electrical Requirements

Twenty-eight volt DC power is provided by the payload carrier. The OPM power system will convert this power to that required by each measurement subsystem.

6.13.2.1 Supply Voltage

Unregulated supply voltage variations caused by mission environmental conditions shall not affect the function or accuracy of the experiment adversely.

6.13.2.2 Electrical Connectors

External interface connectors shall be the standard Special Payload Opportunity Carrier (SPOC) electrical interface connectors for the Hitchhiker program.

6.13.2.3 Electromagnetic Interference (EMI)

EMI compatibility of the OPM experiment hardware shall be assured by compliance with the Johnson Space Center (JSC) specification SL-E-0002.

6.13.2.4 Electronics Design

To reduce system power requirements, every effort should be made to utilize low power devices such as CMOS, Metal-Oxide Semiconductor Field Effect Transistor (MOSFET), or other low power devices or techniques where possible. However, digital interfaces should be Transistor-Transistor Logic (TTL)/Diode-Transistor Logic (DTL) logic compatible. Analog and discrete control and data signals should be standard 0 - 5 volts.

6.13.2.5 Spacecraft Interface Data Signals

All analog data signals for the spacecraft interface should be conditioned for a 0 to 5 volt level. For discrete output signals the following logic levels apply: $-.5 < "0" < +.5$, and $4.0 < "1" < 6.0$. Rise and fall times of the discrete signals shall be $1 < t < 20$ microseconds. Additional information is contained in Table 2.9 of the HHG-730-1503-04 document.

6.13.2.6 Command and Control

Control signals shall be discrete 5 volt signals with amplitudes and rise and fall times as defined under paragraph 6.13.2.5.

6.13.2.7 Noise

The following types of noise will be investigated and mitigated as required, using appropriate specifications:

- o Ripple and Transient
- o Conducted
- o Radiated.

6.13.2.8 Electronic, Electrical, and Electromagnetic Parts Selection

If the design requires the use of a part that is not on the preferred parts list, a military version of the part should be used if available. Commercial parts may be used where preferred parts or military parts are unavailable, or the use of preferred parts would significantly impact the hardware delivery schedule.

6.13.3 Material Selection and Process Control

The selection of materials and processes to be used in fabricating the flight hardware will utilize MSFC-STD-506 as a design guideline for all pertinent specifications and requirements. MSFC specification 50M02442 should be used as a guideline for selection of materials to control contamination caused by outgassing. The list of materials, parts and processes to be used in the fabrication of the flight hardware will be submitted for approval at the Critical Design Review (CDR).

6.13.4 Quality and Safety Provisions

Quality assurance requirements will be specified depending on the individual component category, such as off-the-shelf hardware, design and development, or procured to a manufacturer's part number. Each major component

will be reviewed and quality provisions specified by a quality representative. Workmanship will range from good commercial practice to NASA specifications, depending on individual components.

NASA Headquarters's document, NHB 1700.7, Revision A, shall be used as a guideline in performing safety and hazards analyses and developing proper safety compliance data to prepare the Safety Data Package (SDP). A list of hazards is included in this NASA document.

6.13.5 Hardware Life Requirement

Experiment hardware will be designed for a minimum mission lifetime To Be Determined (TBD), in addition to pre-launch use such as ground testing, checkout, and storage. The Experiment, any spares, and associated GSE shall have a minimum storage life of TBD years under warehouse storage conditions inside the shipping container. All parts and materials which are sensitive to age shall be identified and reviewed as an item in the CDR. Where deterioration may be a factor, the maintenance procedure shall indicate a replacement cycle and/or the required retesting.

6.13.6 Flight Hardware

The flight hardware shall be designed as a reusable, multifunction flight instrument capable of performing in-space optical studies.

6.13.6.1 Quantity of delivered flight hardware

One flight qualified (protoflight) model of the OPM experiment will be delivered with associated GSE, data package, and shipping container. The end item shall be packaged, marked and shipped in accordance with TBD specification.

6.13.6.2 Data Package

An Acceptance Data Package (ADP) shall be shipped with each contract end item consisting of the following:
- o Shipping document
- o Complete set of as-built reproducible design drawings
- o As-run Acceptance Test Procedure and data
- o List of installed nonflight and temporarily installed hardware
- o Log book (initiated with the assembly of the flight unit)
- o Calibration instructions and data
- o Limited life-time and age sensitive data
- o End item specification
- o Installation assembly instructions

A Certificate of Qualification (COQ) shall be prepared and submitted with the Qualification Test Report.

6.13.6.3 Shipping Containers

Shipping containers shall be constructed to transport the OPM experiment and the GSE.

6.13.7 Ground Support Equipment (GSE)

The GSE will be designed using standard commercial practice and off-the-shelf parts where practical.

6.13.8 Environmental Design Requirements

The OPM experiment will be subjected to many--and varied--environmental conditions. Consequently, tests to simulate expected conditions must be conducted to verify the OPM's capability to withstand the extreme environmental conditions expected during a space mission. A written test procedure outlining the types of tests shall be approved by the OPM Chief Engineer before tests are conducted. The types of tests envisioned include functional, performance, and qualification tests. The functional test will verify an instrument's capability to measure the desired parameter as stated by the manufacturer. The performance test will verify each measurement subsystem's capability to measure the desired parameter as intended in the OPM experiment. The qualification tests will verify the OPM instrument's capability to measure and survive the mission of environmental conditions. A list of these test conditions includes, but is not limited to:

- o Acceleration
- o Vibration
- o Shock
- o Acoustic
- o Thermal Vacuum
- o Temperature

6.13.8.1 Ground Handling Environments

The ground handling environments consist of the naturally occurring exposures to pressure and atmosphere, temperature, humidity, and material contamination, plus the dynamically induced conditions of acceleration, vibration, and shock. These conditions will be in effect from the time the OPM experiment leaves the final assembly point until integrated into the Shuttle at

the Kennedy Space Center (KSC) and through post-flight processing. The planned procedures and flow during First Article Test (FAT) and OPM integration are intended to minimize exposures to uncontrolled conditions.

o Pressure - Atmosphere

- Pressure:

  Surface Nominal   12.36 to 15.23 psia

  Air Shipment - 35000 feet   3.28 psia minimum

- Atmosphere:

  Normal Atmospheric Constituents

o Temperature

- Uncontrolled areas (loading docks, aircraft cargo areas, etc.)

  Surface   - 23 to + 150 degrees F

  35000 feet   - 65 degrees F minimum

- KSC areas   TBD

- Orbiter Processing Facility   TBD

o Humidity

- Uncontrolled areas: For design purposes, 0 to 100 percent relative humidity at the temperature extremes defined for uncontrolled areas.

- KSC   TBD

o Contamination Considerations

- Atmospheric Cleanliness

  —Uncontrolled areas   None

  —KSC   TBD

- Other contaminating conditions present in uncontrolled areas:

  —Salt Spray   TBD

  —Sand/Dust   TBD

- Conditions resulting in contamination by reaction with materials within the experiment

    —Fungus   TBD

    —Ozone   TBD

- Acceleration

The acceleration of gravity at 1 g, 9.18 m/sec^2 (32.14 ft/sec^2), may be considered a constant applied at all times during ground testing; however, ground handling will superimpose short term (greater than 0.1 sec) steady state accelerations of up to 2 g vertical loads, with a cone angle of 20° from the vertical.

o Vibration (Transportation)

The exposure is defined as equal to a minimum of four (4) sinusoidal sweeps at 1/2 octave per minute as follows:

- 2 to 5 Hz: 1.0 inch double amplitude displacement
- 5 to 26 Hz: 1.3 g 0 to peak
- 26 to 50 Hz: 0.036 inch double amplitude displacement
- 50 to 1000 Hz: 5 g 0 to peak

o Shock (Bench Handling)

The maximum conditions are defined as exposures to 20 g terminal peak saw-tooth pulses of 11 millisecond durations in both directions along each of the three mutually-perpendicular axes.

6.13.8.2 Flight Environments

The flight environments consist of the naturally occurring exposures to pressure and atmosphere, thermal vacuum, temperature, humidity, and material contamination, plus the dynamically-induced conditions of acceleration, vibration, and shock. These conditions will be in effect from the time the OPM experiment is launched through landing. A list of these flight conditions include, but is not limited to:

    o Pressure - Atmosphere
    o Thermal Vacuum
    o Temperature
    o Humidity
    o Material Contamination
    o Acceleration
    o Vibration
    o Shock

109

The effects of each environment on the OPM hardware will be verified through either analysis or test. The test environment will be defined during the OPM Development Phase.

7.0 OPM FLIGHT EXPERIMENT

In Section 6 the design and capabilities of the OPM flight system were described. In this section, the design of the initial OPM flight experiment that uses these capabilities to satisfy the OPM experimental objectives will be discussed. The baseline mission configuration and the payload carrier are also discussed.

To satisfy the overall objectives of the OPM, more than one OPM flight will be required. This is necessary to study the effects of the space environment in different orbits and for different mission durations. These potential OPM missions include:

o Short-Term Low Earth Orbit (Shuttle)
- High Atomic Oxygen (AO) fluence rate
- Particulate and molecular contamination
- Initial OPM hardware flight test

o Long-Term Low Earth Orbit
- Long term and high fluence AO exposure
- Long term exposure to:
— Solar UV
— Low level radiation
— Thermal vacuum
— Micrometeoroids and debris

o Long-Term Geosynchronous Orbit
- Long term exposure to:
— Moderate radiation
— Solar UV
— Thermal vacuum
— Micrometeoroids

o High Radiation Orbit
- Exposure to:
— High radiation levels
— Solar UV
— Thermal vacuum
— Micrometeoroids

7.1 Baseline Mission Objectives

The In-Space Technology Experiments Program offers the opportunity to develop the flight hardware and perform the first OPM Experiment. The mission opportunities for this first flight are limited to a Shuttle mission. A Shuttle mission dictates a short-term, low earth orbit mission. This mission will allow the OPM to measure the effects of materials exposed to this environment and to flight test the OPM hardware. For this short-duration mission, the exposure

111

environments of the most concern are AO and spacecraft contamination—both particulate and molecular. To maximize the effectiveness of this mission, the spacecraft attitude should provide a relatively high exposure of the OPM samples to the AO environment. This requires that the Shuttle bay have a high view factor of the orbital RAM direction for significant portions of the mission.

As discussed in Section 5, several Shuttle payload carriers can accommodate the OPM for this mission. Of these, Hitchhiker M (HHM) and Hitchhiker G (HHG) are the most probable choices. Either carrier provides an interface with adequate power and weight capacity and a suitable data link. The HHM would be the best carrier because of the simpler OPM mounting configuration on the HHM truss. HHG is the most likely payload carrier for this mission because it is smaller and lighter, and therefore, easier to manifest on the Shuttle.

The HHG large plate mount dimensions are 1270 mm x 1524 mm (50 x 60 inches). It is positioned vertically in the Shuttle bay on the starboard side in bay locations 2 or 3 (see Exhibit 4, page 24). The OPM is mounted to the HHG and extends into the bay as shown in Exhibit 56. The sample carousel points in the +Z direction out of the bay. The major concern in using the HHG carrier is the OPM Center of Gravity (CG). NASA has defined a restriction for a flight experiment's center of gravity flown on the HHG. According to the HHG Accommodation Guide, "In general, the flight unit's CG can be no farther than 10 inches from the mounting plate if the maximum weight of 250 pounds is being accommodated. However, if lower weight is being applied, the CG may be extended farther away from the mount." This is in general agreement with verbal communication with the NASA GSFC Hitchhiker office which stated the permissible CG is "14 to 16 inches for a 200 pound payload." Thus, the maximum allowable moment is approximately 3000 inch-pounds. For the OPM, the estimated experiment weight is 77 kg (170 pounds). At this weight, the maximum moment could be as much as 432 mm (17 inches) from the mounting plate. By judicious placement of the internal OPM components as close as possible to the HHG mount, the CG constraint can be met.
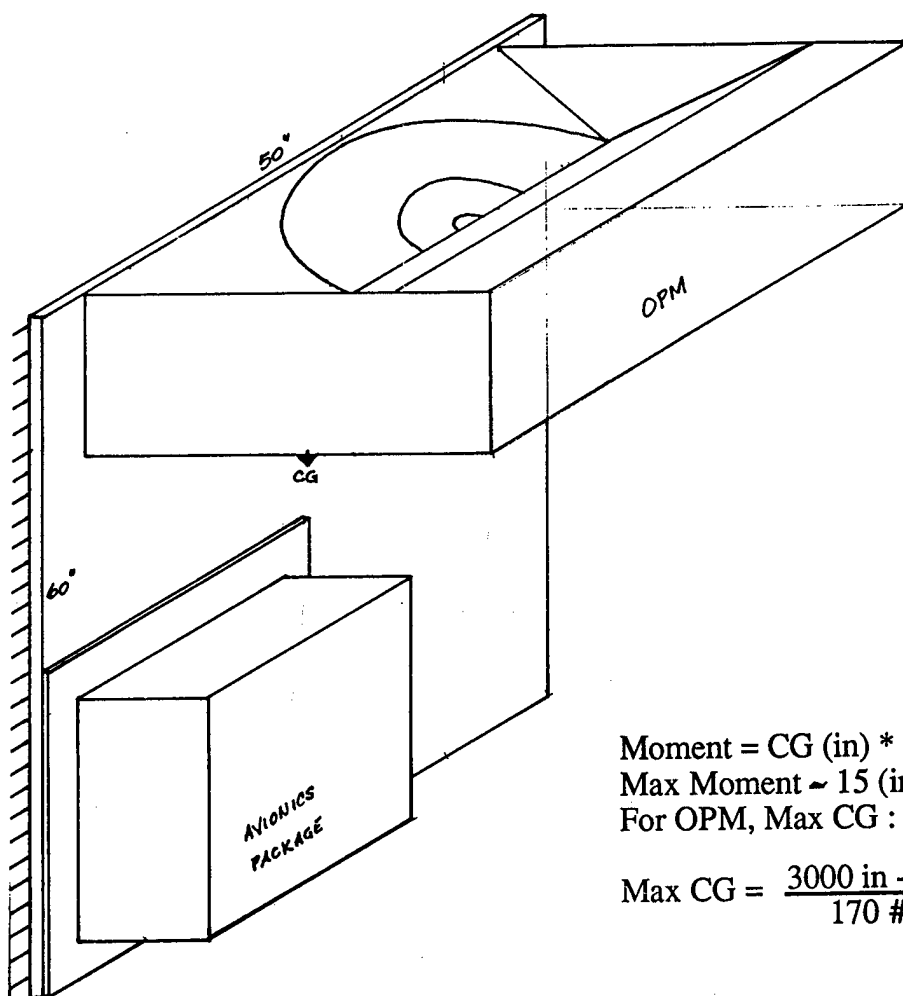
Moment = CG (in) * wt (#)
Max Moment ~ 15 (in) * 200 (#) = 3000 in -#
For OPM, Max CG :

$$Max\ CG = \frac{3000\ in\ \text{-}\#}{170\ \#} \sim 17.5\ in$$

EXHIBIT 56 - OPM HHG Large Plate Mount

7.2 Baseline Mission Timeline

The timeline for the initial OPM mission can be described in three phases - pre-launch and launch operations, orbital and deorbit operations, and post-flight operations.

7.2.1 Pre-launch and Launch Operations

After the integration of the OPM onto the Shuttle payload carrier, the sample carousel will be rotated to expose one set of test samples. These samples will passively monitor the pre-launch and launch environment. The OPM will not be operated during this phase.

7.2.2 Orbital Operations

After the Shuttle reaches orbit and the payload bay doors are opened, the OPM is turned on through the payload carrier command interface. At turn-on, the DACS will initialize all OPM systems and begin the first set of measurements. This set of measurements determines the condition of the flight samples after launch and before space exposure. The TQCM, irradiance and AO monitors are turned on and a set of measurements are made on the monitors and housekeeping sensors.

The TIS measurements will be made first and will require about one hour. Both TIS lasers are turned on and allowed to warm up for about 30 minutes. The sample carousel is rotated to position the first TIS sample under the Coblentz sphere and its TIS measured. This procedure is repeated until all TIS samples have been measured. The TIS instrument is turned off and the reflectometer is turned on. After a short time to warm up the lamp, the carousel is rotated to position the first reflectance sample under the integrating sphere. The reflectance of each sample is measured at 100 points between 250 and 2500 nm. This procedure is repeated until all 25 of the reflectance samples have been measured. This measurement will require about 20 minutes.

The reflectometer is turned off and the VUV spectrometer is turned on. Like the reflectometer measurements, each VUV sample is positioned at the VUV measurement position and the transmission and reflectance are measured at each of the six VUV wavelengths. The VUV measurements will take about 15 minutes.

After completion of the optical measurements, the carousel will be rotated to expose the samples to the space environment. The samples will remain exposed for the remainder of mission day one. Data from the environment monitors and the OPM housekeeping sensors will be recorded periodically throughout the exposure period.

The measurements made on day one are repeated each day of the seven-day mission. The final set of optical measurements will be made on the test samples before the payload bay doors are closed on the last mission day. At the completion of these measurements, the carousel is rotated to the IN position to protect the samples from the deorbit and post-flight operations. The OPM is then powered down.

7.2.3   Deorbit and Post-flight Operations

The OPM is not operated during Shuttle deorbit and post-flight operations. When the OPM is de-integrated from the payload carrier, it is returned to the OPM Experiment Team for data analysis.

8.0 DEVELOPMENT PHASE IMPLEMENTATION PLAN

The Development Phase for the OPM includes all activities required to develop the OPM flight hardware, conduct an OPM experiment on the Shuttle, and perform the post-flight data analysis. A preliminary schedule and cost estimate has been performed and is presented in this section.

Consistent with the guidelines for the In-Space Technology Experiments Program, the OPM Development Phase has been designed with a reasonable compromise between minimum risk and minimum cost. The OPM flight hardware will be built as a protoflight unit, similar to the way the TCSE was built for the LDEF. The protoflight concept requires that only one OPM system will be built, tested, and flown. Component spare parts will be limited to critical items. Full qualification testing will be done at the OPM system level with component and subsystem level environmental testing limited to special items.

Single Failure Points (SFP) will be allowed in the design, but system critical SFP's will be minimized through the use of redundant components where the cost impact is minimal. Other features of the design guidelines are presented in Section 6.13.

A significant portion of the effort is to prepare documentation and support reviews required for flying on the Shuttle. This effort by the OPM team could be minimized if the In-Space Technology Experiments Program performed this function for its experimenters.

8.1 Schedule

A top-level logic network was developed as part of the planning of the OPM Development Phase. This plan considered all aspects from hardware design through flight and data analysis. A summary schedule is shown in Exhibit 57. A start date of April 1, 1990, is projected for the beginning of the OPM Development Phase. This program can be broken into three sequential phases. Phase I begins with the authority to proceed with OPM development, and continues through delivery of the qualified flight hardware for payload integration. Phase II includes payload integration and mission support. Phase III is the post-flight data analysis.

116

Activity	CY 1988				CY 1989				CY 1990				CY 1991				CY 1992				CY 1993			
	1	2	3	4	1	2	3	4	1	2	3	4	1	2	3	4	1	2	3	4	1	2	3	4
Performance & Requirements Definition					▭																			
Preliminary Design						▭▭																		
Definition Phase Complete							▽																	
Proposal/Evaluation									▭															
Detailed Design									1 Apr ▭▭▭															
Critical Design Review									1 Feb ▽															
Procure, Fab & Assemble													▭▭ 15 Nov											
Integrate, Test & Check Out													1 Jun ▭											
Performance Testing																	15 Feb ▭							
Flight Qualification Tests																	▭ 15 May							
Payload Integration																				▭ 15 Nov				
First OPM Mission																				▽				
Data Analysis																				▭▭ 1 Jul				

EXHIBIT 57 – OPM Summary Schedule

8.1.1 Phase I

The initial phase is broken down into two areas—hardware development and the mission planning support activities. Within these two areas, major milestones define the schedule progress. The milestones for the hardware development include Systems Requirement Review (SRR), Preliminary Design Review (PDR), CDR, and the Acceptance/Readiness Review (A/RR). The milestones for the mission planning support activities include multiple Safety Reviews, Cargo Integration Review (CIR), Flight Operations Review (FOR), and the Payload Readiness Review (PRR). Phase I is expected to take 25 months to complete.

8.1.1.1 Hardware Development

The hardware development phase includes all activities to design, fabricate, and test the OPM hardware. The major milestones relate to the stage of hardware development (see Exhibit 58). At the beginning of hardware development, the mission definition, design guidelines, and system requirements are reviewed for completeness and adequacy to meet OPM objectives. The SRR is

	CY 1990				CY 1991				CY 1992				CY 1993			
	1	2	3	4	1	2	3	4	1	2	3	4	1	2	3	4
Requirements Review		▭														
Systems Requirements Review	SRR ▽															
Preliminary Design			▭													
Preliminary Design Review		PDR ▽														
Final Design				▭▭												
Critical Design Review					CDR ▽											
Fabrication					▭▭											
Assembly and Integration							▭▭									
Subsystem Testing							▭▭									
Performance Testing								▭								
Qualification Testing									▭							
Acceptance/Readiness Review									A/RR ▽							

EXHIBIT 58 - OPM Hardware Development Phase Schedule

held to ensure that all ground rules for the final design and development are complete and to signify that the preliminary design effort is ready to proceed.

The preliminary design effort begins with updating the definition phase information where necessary. The major details of the design are checked for completeness and to verify component and/or subsystem availability. The interface between all subsystems is verified. Make/buy trade studies are performed. Vendor selection is made for those parts to buy; the remaining parts are identified for manufacture. The specifications required for the final design are identified. Test plans are outlined that identify components for test, type of tests to be conducted, and variance limits. The software to operate the experiment is functionally defined and documented with flowcharts.

118

The payload accommodations are checked to assess the latest requirements and compatibility for the OPM experiment. The PDR is held to ensure that all aspects of the design are covered prior to beginning the final design.

The final design proceeds with the development of specifications, documentation, detailed test procedures, and detailed drawings. The specifications list will consist of NASA, commercial, and military documents. The documentation provides the audit trail of design changes, revisions, and configuration management. Detailed test procedures are necessary to define the types, conditions, and expected results of each test. The "nuts and bolts" of the detailed design are finalized and documented. The drawings, documentation, and specifications become the Technical Data Package (TDP) for procuring and fabricating the OPM experiment. During this phase, software is designed to the subroutine level. Data and control flow for each routine is developed. Long-lead items are procured. At the CDR, the detailed design is reviewed for completeness. Action items are resolved prior to completing the CDR.

After the CDR, hardware is procured or fabricated according to the TDP developed in the final design. Piece-part subsystem assembly begins and continues through the final assembly of the OPM experiment. Integration of the OPM instrument is scheduled to begin with the mating of the baseplate and carousel assembly. Functional tests of specific subsystems are required to verify acceptable operation prior to integration in the OPM instrument. The GSE is procured, fabricated, and assembled. Functional testing of the GSE is performed to verify proper simulation of the flight hardware and spacecraft interface. During this phase, the software code is developed, tested, and verified through the GSE. Once the OPM integration is complete, the instrument is tested for functional performance verification.

Qualification tests are performed when the functional testing has been completed. Qualification tests will include tests for shock, vibration, thermal vacuum and EMI.

After completion of all testing, the Acceptance Readiness Review (A/RR) is held. During this review, the instrument is "cleared" as passing all requirements, all documentation is acceptable and ready for shipment, the test reports are completed and verified, the software has been demonstrated and validated, and the instrument "as-built" drawings are certified as complete. A

satisfactory review signifies that the hardware development is complete and the OPM flight hardware is ready for shipment. The flight samples are installed on the carousel and the OPM shipped to KSC for payload integration.

8.1.1.2 Mission Planning Support Activities

The mission planning support activities (as shown in Exhibit 59) include all payload safety and integration-related items that must be accomplished to verify that the OPM experiment is flight-ready. The major milestones relate to the stage of development and maturity of the instrument.

The Request for Flight Assignment (NASA Form 1628) is submitted once the Development Phase effort begins. The Phase 0 Safety review occurs early in the program to ensure the basic requirements and processes are understood. A list of hazards will be ready at this time. The payload requirements are identified.

The Phase I safety review occurs before the CDR. Items required for this review include a list of hazard controls for the hazards list identified for the Phase 0 safety review, a preliminary flight materials list, the preliminary structural and thermal analyses of the OPM instrument, the preliminary Payload Integration Plan (PIP); and the preliminary Interface Control Document (ICD).

The Phase II safety review will be concurrent with the CDR. The items required for this review include a hazards list updated with safety verification methods, the final materials list, the safety critical structures analyses package, the final structural and thermal analyses of the OPM instrument and applicable test reports, the final PIP and ICD, and a draft of the flight procedures.

The Phase III safety review precedes the delivery of the OPM instrument to KSC where the payload integration process begins. The hazards analyses are complete and the following items submitted: as-built drawings, the critical structures final report, and all final test reports.

The Cargo Integration Review (CIR) is conducted after an assessment is made of the instrument's compatibility with other payloads and the Shuttle. NASA requires detailed design information regarding the the development of the payload. This information is contained in the PIP and ICD documents. The CIR must be completed prior to final preparation for the mission.

EXHIBIT 59 – OPM Mission Planning Support Activities

Activity	CY 1990				CY 1991				CY 1992				CY 1993			
	1	2	3	4	1	2	3	4	1	2	3	4	1	2	3	4
Request for FLT ASSGN (NASA 1628) - LSA		▭														
Customer Payload Requirements		▭														
Phase 0 Safety Review				▽												
Safety (Including Hazards)			▭	▭												
Payload Integration Plan (PIP)			▭	▭												
Interface Control Doc (ICD) Development			▭	▭												
Phase I Safety Review					▽											
Safety - Complete					▭	▭										
PIP Annexes					▭	▭										
ICD Development					▭	▭										
Phase II Safety Review								▽								
Flight Compatibility Assessment (NASA)							▭									
Cargo Integration Review (CIR)								▭								
Flight Operations									▭	▭						
Landing/Launch Support									▭	▭						
Flight Verification Analysis									▭	▭						
Flight Operations Review (FOR)												▭				
Payload Readiness Review (PRR)												▭				
Phase III Safety Review												▽				

Mission training begins with the interface of the OPM experiment investigators with the Shuttle flight crew and flight operations personnel. Periodic reviews occur during flight operations and culminate with the FOR. This review is held to support the final phase of the flight crew and flight operations personnel training. It is noted that the OPM instrument requires minimal—or no—crew activity to conduct the in-space experiment.

The Payload Readiness Review (PRR) assesses the readiness of the payload and Shuttle for the integration process. It is conducted at KSC prior to initiation of payload integration.

8.1.2 Phase II

The second phase, payload integration and mission support, continues the mission support activities up through the Flight Readiness Review (FRR) and continues through the mission to the return of the hardware to the OPM team. Phase II is expected to take six months to complete.

During the payload integration process, the OPM experiment is integrated with other experiments flying on the payload carrier. The GSE checks and verifies OPM operation and the spacecraft interface. The FRR is conducted within the month before mission launch. It verifies that all requirements have been met and certifies that all flight elements are ready to perform the mission.

During the space mission, the OPM Team will provide mission support to assist with any hardware problems, to revise mission science objectives if necessary, and to review mission status.

8.1.3 Phase III

The Phase III effort will include all aspects of post-flight data analysis. A quick-look report will be issued three months after the mission and a final report completed after seven months.

8.2 Cost

A preliminary cost estimate for the OPM experiment has been developed using a bottoms-up engineering estimate approach. A parametric estimate of the different subsystems and their integration was also done as a cross check.

The cost estimate summary is presented in Exhibit 60. The costs are broken out by fiscal year and by function. The hardware cost to deliver a qualified OPM is less than $2 million, which reflects the low cost approach to the development effort.

	FY90	FY91	FY92	FY93	TOTAL
OPM Hardware	425	1075	400	0	1,900
Integration and Mission Support	0	0	30	20	50
NASA Documentation and Review Support	50	100	100	0	250
Data Analysis	0	0	0	225	225
TOTALS	475	1175	530	245	2,425

EXHIBIT 60 – Preliminary Cost Estimate

9.0 SUMMARY

The stability of materials used in the space environment will continue to be a limiting technology for space missions. The OPM offers a comprehensive space research program to study the effects of the space environment—both natural and induced—on optical, thermal and space power materials. This research is important to all users of space—NASA, DOD, Industry, and Universities. The initial and subsequent OPM missions will provide a materials testbed for the optical and thermophysical community. This common in-space testing facility can become an important part of many materials and space hardware development programs.

The OPM definition phase developed a functional design that has the capability and flexibility to satisfy the OPM experimental objectives. The integrating sphere reflectometer and the VUV spectrometer provide state-of-the-art measurements comparable to laboratory instruments. The TIS instrument is a new, effective tool to study the effects of the space environment on optical and other materials. The testing of the TIS breadboard instrument verified that TIS has the sensitivity and range for this purpose. The OPM support systems provide the versatility to allow the OPM to fly on missions with different payload carriers, in different orbits, and for different mission durations.

The OPM design is cost effective because of the use of proven designs from the TCSE program and the use of available off-the-shelf components. The reflyable OPM hardware will also reduce the per flight costs.

The OPM development concept is a compromise between low cost and low risk. The protoflight hardware concept minimizes the development of non-flight components and flight spares. Qualification testing will be performed at the system level with minimal component and subassembly environmental testing. To increase reliability, redundant components will be used at critical system failure points and where the cost impact is low.

The OPM is a needed technology experiment and the OPM hardware design is feasible and cost effective. The OPM should be selected for development and flight as part of the In-Space Technology Experiment Program.

REFERENCES

1. Zerlaut, G.A., Gilligan, J.E., and Ashford, N.A.; "Investigation of Environmental Effects on Coatings for Thermal Control of Large Space Vehicles." IIT Research Institute Report U6002-97, 1971.

2. Wilkes, D.R.; "Effects of the Solar Wind on Thermal Control Coatings." MSFC Achievements Review, NASA TMX-53820, January 1969.

3. Frienchtenicht, J.F., Bevans, J.T., McNamara, R. T., and Miller, W.D.; "Study of Micrometeoroid Damage to Thermal Control Material." TRW Systems Final Report, NASA Contract NAS8-20120, October 1966.

4. Hughes, T.A., Allen, T.J., Linford, R.M.F., T.E.; "Investigation of Contamination Effects on Thermal Control Materials." AFML-TR-74-218.

5. Leger, Lubert J.; "Oxygen Atomic Reaction with Shuttle Materials at Orbital Altitudes". NASA TM-58246, 1982.

6. Peters, P.N., Linton, R.C., and Miller, E.R.; "Results of Apparent Atomic Oxygen Reactions on Ag, C, and Os Exposed During the Shuttle STS-4 Orbits." NASA/SSL No. 82-125, December 1982.

7. Maag, C.R., Millard, J.M., Jeffery, J.A., Scott, R.R.; "Space Station Thermal Control Surfaces." Aerojet Electro-Systems Final Report, Contract NAS8-32637, April 1979.

8. Neel, C.B.; "Measurement of Thermal-Radiation Characteristics of Temperature-Control Surfaces During Flight in Space." ISA Trans. (1964).

9. Pearson, B.D., Jr.; "Preliminary Results From the Ames Emissivity Experiment on OSO-II." AIAA Progress in Astronautics and Aeronautics, ed. G. B. Heller. New York: Academic Press, 1966, Vol. 18, pp. 459-472.

10. Lewis, D.W. and Thostesen, T.O.; "Mariner-Mars Absorptance Experiment," AIAA Progress in Astronautics and Aeronautics, ed. G. B. Heller. New York: Academic Press, 1966, Vol. 18, pp. 441-457.

11. Schafer, C.F. and Bannister, T.C.; "Pegasus Thermal Control Coatings Experiment." AIAA Paper 66-419, 1966.

12. Reichard, Penelope J. and Triolo, J.J.; "Pre-flight Testing of the ATS-1 Thermal Coating Experiment." Proc. of the AIAA Thermophysics Specialist Conference, AIAA Paper 67-333, April 17-20, 1967.

13. Miller, E.R. (Editor); "STS-2, 3, 4 Induced Environment Contamination Monitor (IECM)." Summary Report NASA TM-82524, February 1983.

14. Finkel, M.W.; "Portable Reflectometer." 4th Thermophysics Conference (San Francisco, CA), Paper 69-599, June 1969.

15. Wilkes, D.R. and Brown, M.J.; "An Active Thermal Control Surfaces Experiment (TCSE)." AIAA 14th Thermophysics Conference, Orlando, Florida, Paper No. 79-1073, June 1979.

16. Nomarski, G.; "Microinterféromètre différentiel à ondes polarizées," J. Phys. Radium 16, 9S-13S, 1955.

17. Normarski, G. and Weill, A. R.; "Application à la métallographie des Méthodes Interférentielles à deux ondes Polarizées." Rev. Metall. 52, 1955, pp. 121-134.

18. Bennett, J.M. and Mattsson, L.; "Introduction to Surface roughness and Scattering." Optical Society of America, Washington, DC, 1989.

19. Bennett, H.E.; "Scattering Characteristics of Optical Materials," Opt. Eng., Vol. 17, 1978, pp. 480-488.

20. Bareiss, L.E. and Payton, R.M.; "Shuttle/Spacelab Contamination Environment and Effects Handbook." NASA Contractor Report 3993, NAS8-35770, September 1986.

21. Wilkes, D.R.; "A Numerical Integration Scheme to Determine Hemispheric, Emittance, Solar Absorptance, and Earth Infared absorptance from Spectral Reflectance Data." NASA TMX-53918, September 1969.

22. Johnson, Francis S.; Satellite Environment Handbook. Stanford, CA: Stanford University Press, 1965.

23. Brown, M.J.; "Thermal Control Surfaces Experiment Preliminary Design Review." Aerojet Electro-Systems Report 5600, Contract NAS8-32537, September 1977.

24. Edwards, D.K. et al.; "Integrating Sphere for Imperfectly Diffuse Samples." J. Opt. Soc. Am., Vol. 51, 1961, pp. 1279-1288.

25. Miller & Sant; "Incomplete Integrating Sphere," J. Opt. Soc. Am., Vol. 48, 1938, pp. 828-831.

26. Eastman Publication JJ-32, July 1969.

27. Wilmshurst, T.H.; "Signal Recovery from Noise in Electronic Instrumentation." Adam Hilger Ltd, 1981.

28. Archibald, P.C. and Bennett, H.E. ; "Scattering from Infrared Missile Domes," Opt. Eng., Vol. 17, 1978, pp. 647-651.

29. "Standard Test Method for Measuring the Effective Surface Roughness of Optical Components by Total Integrated Scattering." ASTM Doc. F1048-87, August 1987.

30. Brown, M.J.; "Thermal Control Surfaces Experiment Critical Design Review." Aerojet Electro-Systems, Contract NAS8-32537, May 1978.

31. Minzner, R.A., ed.; "The 1976 Standard Atmosphere above 86 km Altitude." NASA SP-398, 1976.

32. Teichman, Louis A. and Stein, Bland A. ed; "Space Environmental Effects on Materials Workshop." NASA Conference (Hampton, VA) Publication 3035, 1988.

33. Triolo, J., McIntosh, R. Kruger, R. and Pugel, N.; "Goddard Space Flight Center Atomic Oxygen Monitor." Atomic Oxygen Working Group Meeting, (Washington, DC) January 23, 1984.

34. Leger, L.J.; "Oxygen Atom Reaction with Shuttle Materials at Orbital Altitudes Data and Experimental Status." AIAA 21st Aerospace Sciences Meeting (Reno), AIAA-83-0073, January 1983.

35. Kaye, G.W.C. and Laby, T.H.; "Tables of Physical and Chemical Constants." London: Lougman, 1973.

36. Miller, E.R., ed; "Induced Environment Contamination Monitor, Preliminary Results From The Spacelab 1 Flight." NASA TM-86461, MSFC, August 1984.

APPENDIX A

Preparation of Dust Contaminated Samples

PREPARATION OF DUST CONTAMINATED SAMPLES

Dust samples were prepared to test the capability of TIS measurements to detect the change in scatter due to increasing dust particle densities. This section describes the sample preparation, measurement technique, and data analysis conducted at MSFC prior to measurements at UAH and NWC. The samples were prepared and measured in a class 10K clean room located in the MSFC Materials and Processes Laboratory, building 4487. All standard operating procedures dictated for this type of installation were used.

Sample Preparation:

Five high-quality 25 mm (one inch) diameter aluminized mirrors were used in this test. Each sample was identified by marking it with a unique number. Additionally, each sample was marked to identify where the samples were to be handled to ensure the measurement area would be left intact.

Four samples (identified as B5 - B8) were dusted with "Arizona Road Dust." One (B4) was not dusted and served as the control sample. The density distribution of the dust is given in Exhibit A-1. A flexible bulb filled with the dust was used to dust the four samples. The samples were dusted to various particulate densities by squeezing the bulb and expelling the dust at various distances from them.

Sample Measurement:

A computer-controlled image analyzer was used to count the dust particles on the samples by scanning across their diameter over eight discrete areas. Each area was 2.55 mm (X direction) by 2.10 mm (Y direction). The area scanned for each discrete area was 5.36 square mm. The total scanned area per sample was 42.84 square mm. Exhibit A-2 depicts the scanned area for a typical sample. The image analyzer was initialized to count particle sizes between a range of 2 and 10,000 microns. Particles outside of this range were not counted. Based on the particle "upper limit" size from the dust distribution data, this range would account for more than 96 percent of all particle sizes.

129

Sample Analysis:

The image analyzer computer-based measurement system provided software to analyze the particle density distribution based on the number of particles counted in the measurement window and the particle area in square microns. The percent obscuration was calculated by dividing the particulate area coverage by the total sample area scanned. The particle distribution frequency vs. particulate (object) area for each sample are presented in Exhibits A-3 through A-7. The percent obscuration is given for each sample. Also listed in the tables accompanying each graph are the number of particles observed, the minimum and maximum particle areas, and the total (summed) particulate area for each sample.

COARSE AIR CLEANER TEST DUST DATA SHEET
BATCH NO. 2281

CUMULATIVE DATA % SMALLER THAN CHANNEL UPPER LIMIT

CHANNEL UPPER LIMIT (MICROMETERS)	% SMALLER THAN CHANNEL UPPER LIMIT	% DIFFERENCE BETWEEN CHANNEL & NEXT SMALLER CHANNEL
176	100 .0	5 .5
125	94 .4	10 .4
88—	84 .0 oK	16 .2
62	67 .7	12 .1
44—	55 .6 oK	8 .5
31	47 .0	9 .3
22—	37 .6 oK	7 .7
16	29 .9	6 .0
11—	23 .9 oK	6 .4
7 .8	17 .5	2 .6
5 .5—	14 .8 oK	5 .3
3 .9	9 .5	5 .7
2 .8	3 .8	3 .8

L & N MICROTRAC COARSE DUST SPECIFICATION

MICROMETERS	% SMALLER THAN
5.5	13 ±3
11	24 ±3
22	37 ±3
44	56 ±3
88	84 ±3
176	100

ROLLER COARSE TEST DUST SPECIFICATION (FOR REFERENCE ONLY)

MICROMETERS	%
0-5	12 ±2
5-10	12 ±3
10-20	14 ±3
20-40	23 ±3
40-80	30 ±3
80-200	9 ±3

THIS PARTICAL SIZE DISTRIBUTION IS BY L & N MICROTRAC ANALYZER. PARTICAL SIZE ANALYSIS SHOWN ABOVE AND NOT USED IN THE SPECIFICATION IS PROVIDED AS REFERENCE INFORMATION ONLY.

5-80
25041113

Total Surface Area Counted

$$42,840,000 \, \mu m^2$$

Box 2.55 mm → X direction
2.10 mm → y direction

5.355 mm²

8 boxes / sample

EXHIBIT A-1

Contamination on 5 mirrored surfaces was measured at NASA MSFC building 4487. ~~Two~~ One sample was not contaminated and served as the CONTROL sample.

Sample ID	Control ID	Status Prior to Contamination	Contamination Amount	Remarks
B4	JMcB4	Cleaned w/Compr Freon "Air Duster"	N/A	Control Sample
B5	JMCB5	"	Very Light	
B6	JMcB6	"	Light	
B7	JMCB7	"	Moderate	
B8	JMcB8	"	Heavy	

Notes :

1. Contamination measured by an Image Analyzer

2. Dusting of samples with "Arizona Road Dust" - Coarse grit (Data sheet attached)

3. Particle size measured was a range of $2 < x < 10,000 \mu M$
   i.e. Particles larger or smaller "not seen"

4. Total Surface Area measured = $42,840,000 \mu M^2$, as illustrated below

Sample   Y

Measured Area (8 sections 2.55 mm → X dir.)
                            2.10 mm → y dir)

X
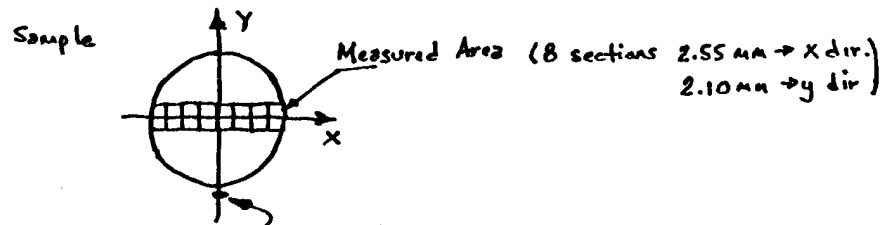
5. Black dot on edge of sample represents orientation for handling, at 6 and 12 O'clock positions to keep measurement area intact. All future handling should be similarly done.

6. Sample ID written on the back of each sample.

Sample B4

Test Date 6/19/89
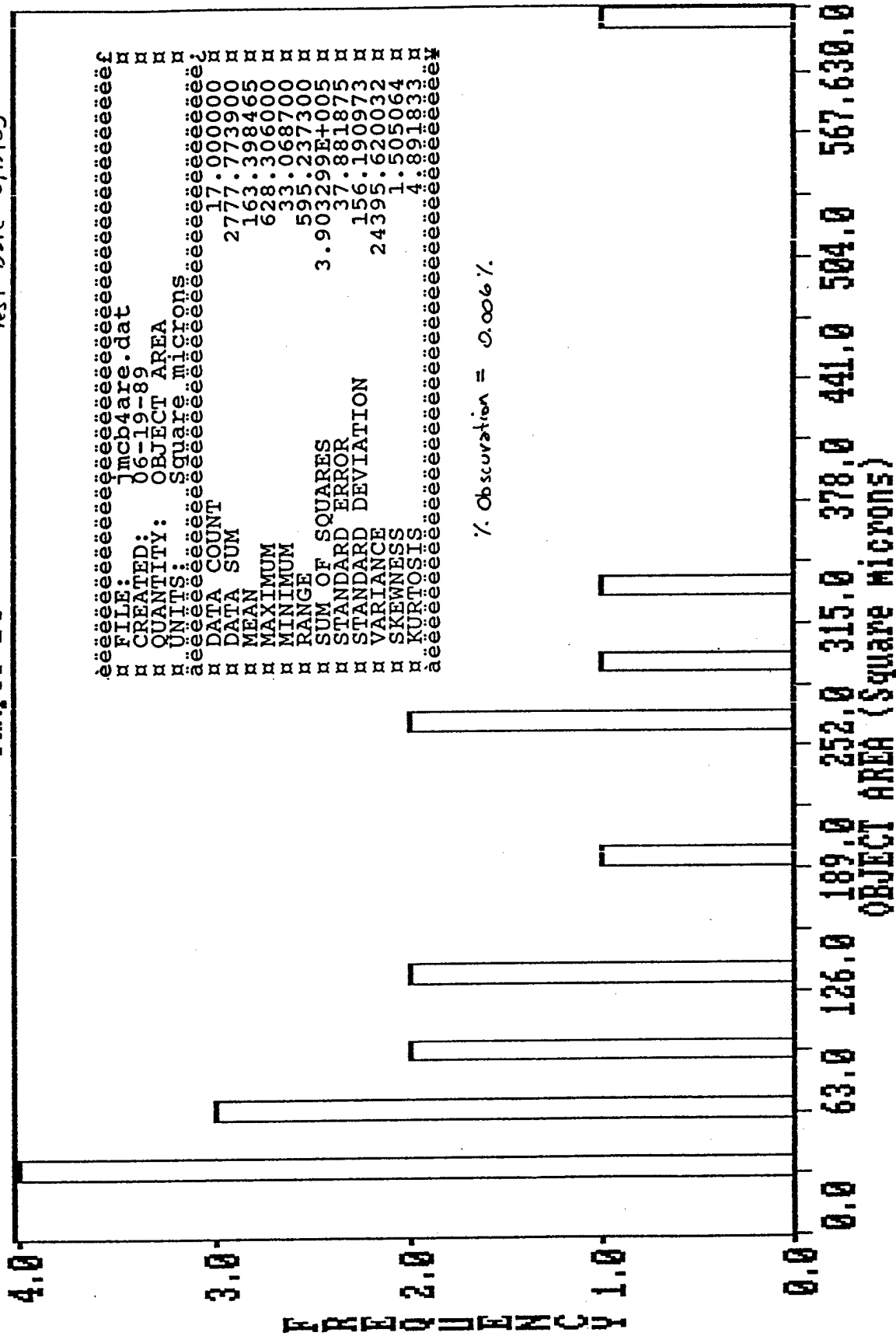
```
ëeeeeeeeeeeeeeeeeeeeeeeeeeeeeeeeeeeeeeeë3
¤ FILE:      jmcb4are.dat            ¤¤ ¤
¤ CREATED:   06-19-89                ¤¤ ¤
¤ QUANTITY:  OBJECT AREA             ¤¤ ¤
¤ UNITS:     Square microns          ¤¤ ¿
äeeeeeeeeeeeeeeeeeeeeeeeeeeeeeeeeeeeeeeë
¤ DATA COUNT              17.000000  ¤¤ ¤
¤ DATA SUM              2777.773900  ¤¤ ¤
¤ MEAN                   163.398465  ¤¤ ¤
¤ MAXIMUM                628.306000  ¤¤ ¤
¤ MINIMUM                 33.068700  ¤¤ ¤
¤ RANGE                  595.237300  ¤¤ ¤
¤ SUM OF SQUARES    3.903299E+005    ¤¤ ¤
¤ STANDARD ERROR          37.881875  ¤¤ ¤
¤ STANDARD DEVIATION     156.190973  ¤¤ ¤
¤ VARIANCE             24395.620032  ¤¤ ¤
¤ SKEWNESS                 1.505064  ¤¤ ¤
¤ KURTOSIS                 4.891833  ¤¤ ¥
äeeeeeeeeeeeeeeeeeeeeeeeeeeeeeeeeeeeeeeë
```

% Obscuration = 0.006%.

FREQUENCY

4.0 3.0 2.0 1.0 0.0

OBJECT AREA (Square microns)

0.0 63.0 126.0 189.0 252.0 315.0 378.0 441.0 504.0 567,630.0

EXHIBIT A-3

Sample B5

Test Date 6/19/89


```
¤ FILE:      jmcb5are.dat
¤ CREATED:   06-19-89
¤ QUANTITY:  OBJECT AREA
¤ UNITS:     Square microns
¤ DATA COUNT           41.0000000
¤ DATA SUM          16335.9285000
¤ MEAN               398.4372800
¤ MAXIMUM           1587.3000000
¤ MINIMUM             33.0687000
¤ RANGE             1554.2313000
¤ SUM OF SQUARES    6.510802E+006
¤ STANDARD ERROR      63.0079944
¤ STANDARD DEVIATION 403.447693
¤ VARIANCE          1.627700E+005
¤ SKEWNESS            1.5940062
¤ KURTOSIS            4.653101
```

% Obscuration = 0.038%.

FREQUENCY

OBJECT AREA (Square Microns)

EXHIBIT A-4

Sample B6

Test Date 6/19/89

```
éëéëéëéëéëéëéëéëéëéëéëéëéëéëéëéëéëéëéëéëéëéëéëéì
¤ FILE:          jmcb6are.dat
¤ CREATED:       06-19-89
¤ QUANTITY:      OBJECT AREA
¤ UNITS:         Square microns
aéëéëéëéëéëéëéëéëéëéëéëéëéëéëéëéëéëéëéëéëéëéëéë¿
¤ DATA COUNT                      601.000000
¤ DATA SUM              2.288686E+005
¤ MEAN                           380.812970
¤ MAXIMUM                       5158.730000
¤ MINIMUM                         33.068700
¤ RANGE                         5125.661300
¤ SUM OF SQUARES        1.627211E+008
¤ STANDARD ERROR                  21.242668
¤ STANDARD DEVIATION             520.770398
¤ VARIANCE              2.712018E+005
¤ SKEWNESS                         3.619717
¤ KURTOSIS                        22.327497
aéëéëéëéëéëéëéëéëéëéëéëéëéëéëéëéëéëéëéëéëéëéëéëé¥
```

% Obscuration = 0.534%.

OBJECT AREA (Square microns)

FREQUENCY

EXHIBIT A-5

Sample B7

```
FILE:              jmcb7are.dat
CREATED:           06-19-89
QUANTITY:          OBJECT AREA
UNITS:             Square microns
DATA COUNT              1035.000000
DATA SUM              2.688818E+005
MEAN                   259.789197
MAXIMUM               6812.160000
MINIMUM                 33.068700
RANGE                 6779.091300
SUM OF SQUARES        1.834781E+008
STANDARD ERROR          13.093679
STANDARD DEVIATION     421.242192
VARIANCE              1.774450E+005
SKEWNESS                 7.082590
KURTOSIS                87.898905
```
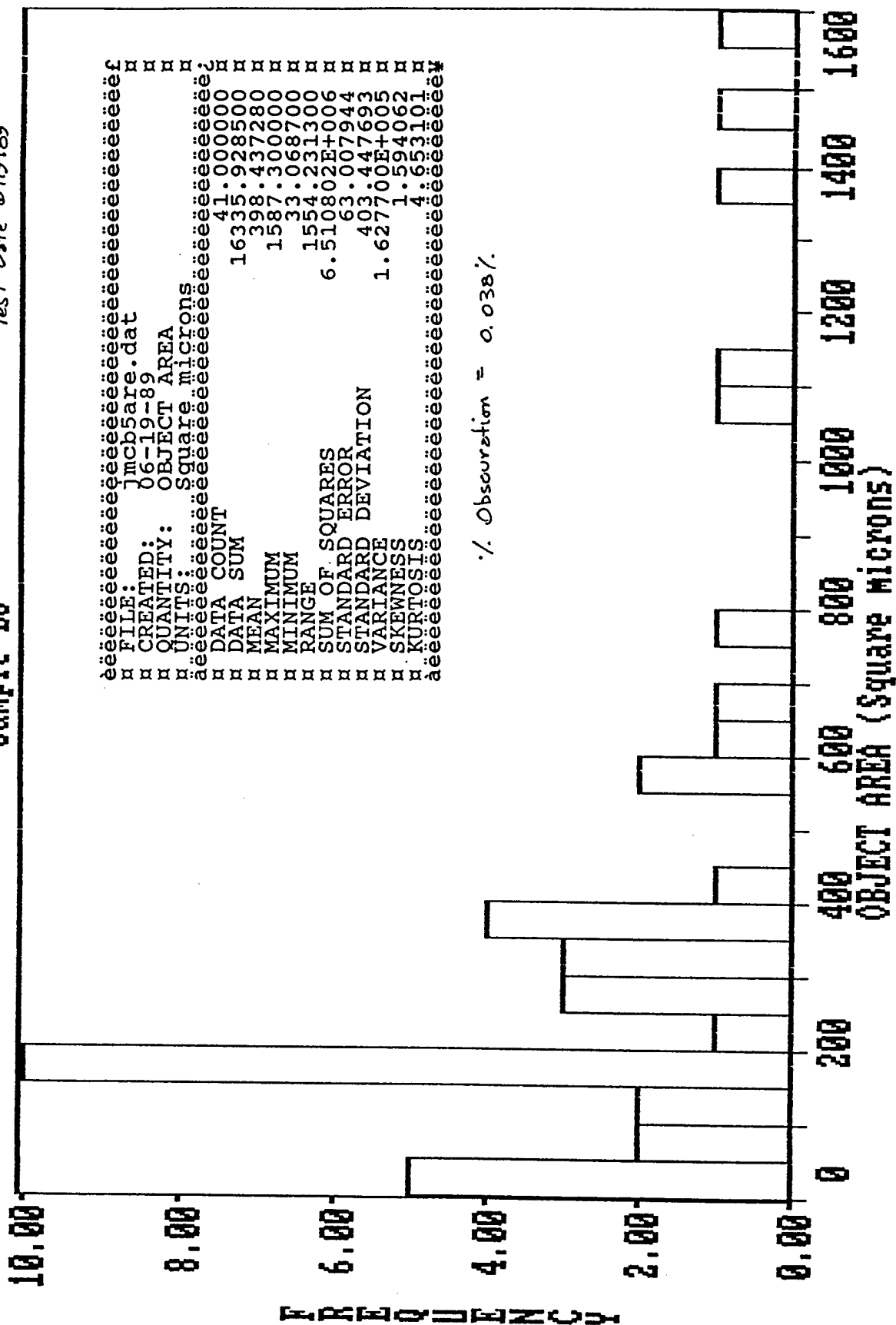
% Observation = .628%

OBJECT AREA (Square microns)

X-axis: 0 685 1370 2055 2740 3425 4110 4795 5480 6165 6850

FREQUENCY

Y-axis: 0 23 46 69 92 115 138 161 184 207 230 253

EXHIBIT A-6

Sample B8

Test Date 6/19/89

```
FILE:       jmcb8are.dat
CREATED:    06-19-89
QUANTITY:   OBJECT AREA
UNITS::     Square microns
DATA COUNT              2634.000000
DATA SUM           7.733452E+005
MEAN                293.601071
MAXIMUM            6746.030000
MINIMUM              33.0068700
RANGE              6712.961300
SUM OF SQUARES      4.601434E+008
STANDARD ERROR        8.145416
STANDARD DEVIATION  418.043210
VARIANCE           1.747601E+005
SKEWNESS              4.908082
KURTOSIS            48.325940
```

% Observation = 1.805%

FREQUENCY: 576 518 461 403 346 288 230 173 115 58 0

OBJECT AREA (Square microns): 0 675 1350 2025 2700 3375 4050 4725 5400 6075 6750

EXHIBIT A-7

1. Report No.	2. Government Accession No.	3. Recipient's Catalog No.
NASA CR-4293		

4. Title and Subtitle	5. Report Date
Optical Properties Monitor - Experiment Definition Phase	May 1990
	6. Performing Organization Code

7. Author(s)	8. Performing Organization Report No.
Donald R. Wilkes Russell A. Chipman Jean M. Bennett James B. Hadaway Leigh L. Hummer Larry Pezzaniti	NAS8-37755-FR
	10. Work Unit No.
	M-629

9. Performing Organization Name and Address	11. Contract or Grant No.
John M. Cockerham & Associates, Inc. 301 Randolph Avenue Huntsville, AL 35801	NAS8-37755
	13. Type of Report and Period Covered

12. Sponsoring Agency Name and Address	
National Aeronautics and Space Administration Washington, D. C. 20546-0001	Final Report Sep 16, 1988 - Sep 29, 1989
	14. Sponsoring Agency Code

15. Supplementary Notes

Contract Monitor: Mr. James M. Zwiener
NASA, Marshall Space Flight Center, MSFC, Alabama   35812

16. Abstract

The stability of materials used in the space environment will continue to be a
limiting technology for space missions. The Optical Properties Monitor (OPM)
Experiment provides a comprehensive space research program to study the effects
of the space environment--both natural and induced--on optical, thermal and space
power materials. The OPM Experiment was selected for definition under the NASA/
OAST In-Space Technology Experiment Program. This final report presents the
results of the OPM Definition Phase.

The OPM Experiment will expose selected materials to the space environment and
measure the effects with in-space optical measurements. In-space measurements
include total hemispherical reflectance total integrated scatter and VUV reflectance/
transmittance. The in-space measurements will be augmented with extensive pre- and
post-flight sample measurements to determine other optical, mechanical, electrical,
chemical or surface effects of space exposure. Environmental monitors will provide
the amount and time history of the sample exposure to solar irradiation, atomic
oxygen and molecular contamination.

17. Key Words (Suggested by Author(s))	18. Distribution Statement
Reflectance, Scatter, Space Environmental Effects, Flight Hardware, Materials Properties, Optical Properties, Thermal Control Surfaces, Optics	Unclassified - Unlimited Subject Category: 18

19. Security Classif. (of this report)	20. Security Classif. (of this page)	21. No. of pages	22. Price
Unclassified	Unclassified	148	A07

NASA FORM 1626 OCT 86